9-10-2008

Reduction of toxicity in the premature neonate addociated with aluminum as a contaminant of total parenteral nutrition solution

Sujittra Srisung
University of Missouri-St. Louis, ssk9d@studentmail.umsl.edu

Reduction of toxicity in the premature neonate associated with aluminum as a contaminant of total parenteral nutrition solution

By Sujittra Srisung

A dissertation submitted to the graduate school in partial fulfillment of the Requirements for the

DEGREE OF DOCTOR OF PHILOSOPHY

With a

Major in Chemistry

University of Missouri-St. Louis

Summer, 2007

Dr. Wesley R. Harris

Chairperson

Dr. Lawrence Barton

Dr. Keith J. Stine

Dr. Janet Braddock-Wilking

Abstract

Aluminum (Al) is the third most common element in the Earth's crust. It is widely consumed in water, foods, and drugs. However, in humans, the uptake of aluminum into the body and its deposition in tissues has been linked to conditions of medical concern, including many neurological disorders such as dialysis dementia, Alzheimer's disease, Parkinson's dementia and Down's syndrome. Premature neonates who receive intravenous feeding (TPN) are at a high risk for Al toxicity because the TPN solutions are contaminated with Al^{3+}, which is not excreted effectively due to poor kidney development in these patients. The FDA has recommended regulations to limit the Al^{3+} contaminant in TPN solutions, but the aluminum is very difficult to remove. Thus, the development of an immobilized hydroxamate chelator to remove the Al^{3+} from key components of TPN solutions is an important goal.

In this work, the complexation of Fe^{3+} and Al^{3+} by new ligands containing one, two and three hydroxamic acid groups has been studied by potentiometric titration and UV-vis spectroscopy to evaluate the metal-ligand complex stabilities of these new ligands. The binding of the divalent metal ions Cu^{2+}, Ni^{2+}, Zn^{2+}, Ca^{2+} and Mn^{2+} by these ligands has also been evaluated by potentiometric titration. The trihydroxamate ligand shows a high affinity for Al^{3+} and Fe^{3+} and high selectivity for trivalent ions over divalent ions. Because aqueous calcium gluconate is the component of TPN solutions that contributes most of the aluminum contamination, the stability constant of Al-gluconate was also determined by spectrophotometric competition.

We have immobilized the trihydroxamate ligand, 2,2,2-THA, on a polystyrene resin and studied the ability of this resin to remove Al^{3+} from solutions by spectrophotometric competition. The resin can easily remove Al^{3+} from buffered aqueous solutions. However, the Al-binding affinity of the resin-bound ligand is less than that of the free ligand. As a result, the resin is not very effective for the removal of Al^{3+} from gluconate solutions.

Acknowledgements

My first thanks goes to my advisor, Dr. Wes Harris, for the guidance and all the encouragement that he gave me over the past five years at UMSL. There are many things that I learned from him which will help me become the good chemist and good teacher. I will never hesitate to mention all these in future as well. I am thankful to him for being patient, especially, in the last few months for preparing this dissertation. Without all his guidance, this dissertation would have not been completed. I would like to thank Dr. Spilling and Dr. Praveen for helping me on the synthesis, and also Dr. Barton, Dr. Stine and Dr. Wilking for being my dissertation committee.

Then, I would like to express my gratitude to the Ministry of science and technology, Thailand government for giving me a chance to study abroad. Also, the officers at the office of the civil service commission and office of education affair, Royal Thai Embassy, Washington, D.C. for the entire document help before and after I came to US. I really like to thank everybody, especially, my former advisor, Dr. Supaluk Prachayasittikul, from the Department of chemistry, Faculty of science, Srinakharinwirot University, Bangkok, Thailand. They all gave me lots of support and I was happy to work with them.

It is my pleasure to thank my former and present lab mates, Dr. Satish, Dr. Claire, Dr. Peng, Rashmi K., Rashmi S. and all my foreign friends at UMSL for the fun and good time in the US. As with my Thai friends, who made me feel at home even though I was far away from my hometown. I would also like to thank the department of chemistry and biochemistry, UMSL, for giving me a chance to be teacher assistant on the last semester and Thrasher research foundation for funding on my research.

Finally, my highest gratitude goes to my parents, Sompit and Jintana Srisung, and also my brother, Tosapon Srisung, who have given me all the support to complete my studies in both Thailand and US. I know without them my dream would not be true.

Table of contests

List of Figures

List of Tables

Chapter 1

Introduction

1. Introduction

1.1 Aluminum in nature and humans

As the third most common element in the Earth's crust, aluminum (Al) is one of the most abundant metals in the environment, with 8% Al[1] compared to 5.0% by weight of iron (Figure1.1).[2] It is a silvery white metal in Group IIIA of the periodic table. Aluminum occurs in a variety of oxide minerals and aluminosilicate clays. These clays and soils from sediments have several functions, such as promoting the growth of roots, retaining trace elements and maintaining the soil pH balance.[3]

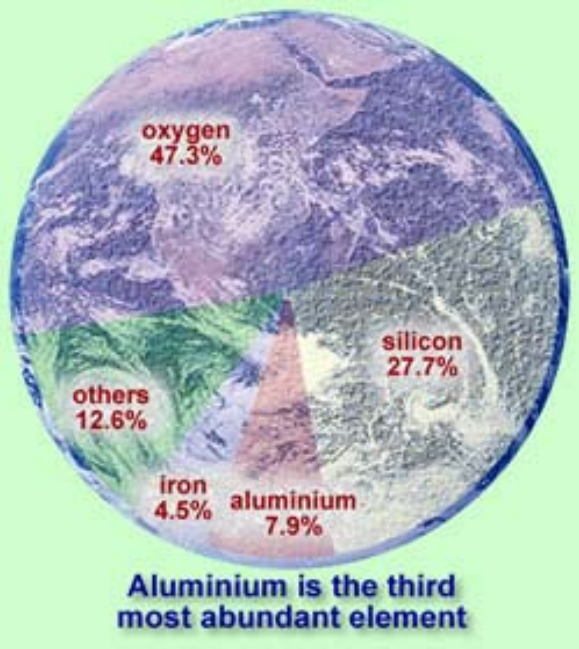

Figure 1.1 The abundance of the elements in the Earth's crust.[2]

Although Al^{3+} is more abundant in the human body than most trivalent metal ions, it is not an essential element in biological systems. Approximately 50% of the aluminum

is found in the lungs, 25% is in the soft tissues and 25% in bones, but it is found in small amounts in all mammals in the brain, liver, kidney, heart, and blood.[4] This greater abundance is due to the single +3 oxidation state of aluminum as opposed to most trivalent metal ions that readily undergo redox chemistry.

Aluminum may inhibit the action of enzymes such a succinic dehydrogenase and δ-aminolevulinate dehydrase, which are involved in porphyrin and hemoglobin synthesis.[5] It may also interfere with various metabolic processes, in which Ca^{2+}, Mg^{2+}, Fe^{3+} (in transferrin and ferritin) and Fe^{2+} (gastrointestinal absorption) are involved.[6] It is rarely a cause for concern because it is absorbed relatively poorly from the gastrointestinal tract and is normally rapidly excreted in the urine.[3]

Aluminum is widely consumed in drinking water, foods (especially herbs, tea, some baking powders, cake mixes, frozen dough, pancake mixes, self-rising flour, grains, processed cheeses and infant formula), drugs (antacids) and in various over-the-counter (OTC) mediations.[7] An examination of labels on consumer products will reveal that many of them contain the metal, and Al exposure also comes from sources such as beverage cans, aluminum foil in contact with food, and aluminum pots and pans. OTC products containing Al^{3+} also include deodorants, baby wipes, skin creams, suntan lotions and toothpaste.

There are a variety of drugs that contain aluminum. Aspirin is commonly buffered with aluminum hydroxide, aluminum glycinate and other aluminum compounds. Vaginal douches contain potassium aluminum sulfate, ammonium aluminum sulfate, and alum. Antacids contain aluminum hydroxide and aluminum oxide. Antidiarrheal drugs contain aluminum magnesium silicate and kaolin, an aluminum salt.[8]

The majority of the population in industrialized nations ingests a minimum of 30-50 mg of aluminum per day.[6] The GI tract provides efficient protection against Al^{3+} absorption. It is estimated that less than 1% of the Al^{3+} in the diet is absorbed, and in healthy individuals most of this is very quickly excreted by the kidneys.[7,9-11] The intake of Al^{3+} from antacids may occasionally amount to several grams per day, usually without toxic effects.[6,9] Typically, the concentration of Al^{3+} in water is approximately 70 μg/L. When multiplying the typical daily Al^{3+} exposure from water (100 μg) by the estimated percentage absorbed in humans (0.3%), the daily Al^{3+} absorbed is 0.005 μg/kg (Table1.1).[10]

Source	Al concentration	Daily Al Exposure	Estimated % Absorbed	Daily Al Absorbed (μg / Kg)
Water	~70 μg/L	100 μg	0.1	0.005
Food		5000-10,000 μg	0.1-0.3	0.08-0.5
Air-rural	0.2 μg/m^3	4 μg	1.5-2.0 from lungs 0.1-0.3 from GI tract	0.001 0.0001
Air-urban	1 μg/m^3	20 μg	1.5-2.0 from lungs 0.1-0.3 from GI tract	0.006 0.0006

Table 1.1 Common sources of aluminum.[10]

Al^{3+} in the blood can be transported by the iron transport protein serum transferrin,[12-16] a single-chain, approximately 80 kDa glycoprotein. Transferrin has two

structurally similar lobes, each of approximately 40 kDa, linked by a short connecting peptide, and each lobe contains an interdomain, high-affinity metal-binding site (Figure 1.2).[17] There is much interest in the functional differences between these sites, and numerous experiments have been reported in which attempts have been made to load metal ions into either the N-lobe or the C-lobe, or in both lobes.[18] Approximately 81% of plasma Al^{3+} is complexed by transferrin; while the remainder is associated with small-molecular-weight ligands. It has been calculated that 19% of plasma Al^{3+} is complexed to citrate, forming Al^{3+} citrate, the predominant low-molecular weight (LMW) Al^{3+} species in plasma.[19] Al^{3+} is complexed by two carboxylates and the alkoxy group of citrate, leaving a free carboxylate.[20-21] However, the mechanism by which Al^{3+} is absorbed, transported and excreted in vivo is largely unclear. Al^{3+}-induced alteration of cell membrane permeability may lead to facilitated transport of LMW or high molecular weight (HMW) Al^{3+}-complexes with suitable ligands across the membrane.[21]

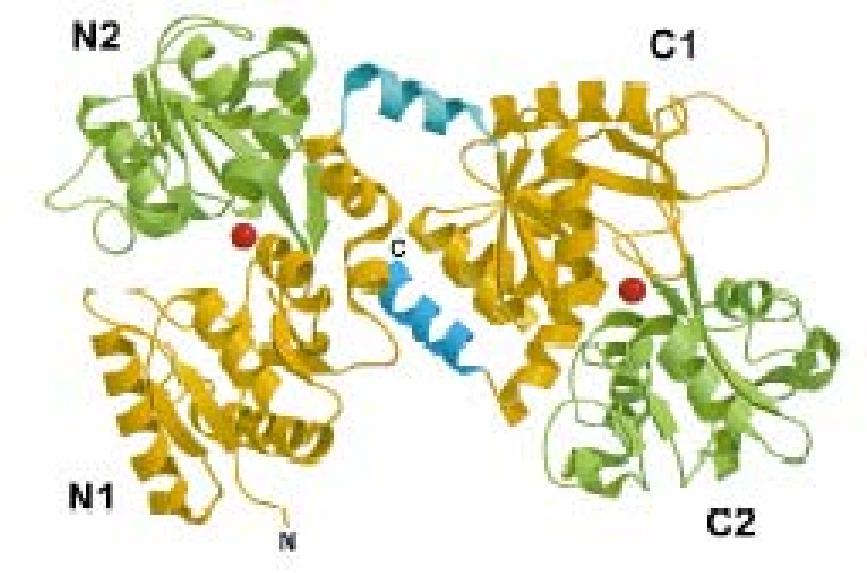

Figure 1.2 Structure of C and N lobes of transferrin with the binding of ferric ion.[17]

1.2 Aluminum in aqueous solution and its coordination chemistry

Different methods, such as UV-visible spectroscopy and NMR spectroscopy can be used to determine the coordination number of metal ions in aqueous solution. As shown in Table 1.2,[22-24] the coordination number is 6 for the aquo ions of Al^{3+} as well as other trivalent and divalent metal ions such as Fe^{3+}, Zn^{2+}, Ni^{2+}, Fe^{2+} and Mn^{2+}.

Ion	Np	N_T	R
Mn^{2+}	6		2.19
Fe^{2+}	6	10-13	2.11
Ni^{2+}	6	21	2.06
Zn^{2+}	6	10-13	1.09
Al^{3+}	6	13	1.88
Fe^{3+}	6		2.03

Table 1.2 Approximate numbers of water molecules in the primary coordination sphere (N_p), the approximate total numbers of waters in the primary and secondary coordination sphere (N_T), and the M-O distance (R).[22-24]

The properties of a metal ion can be described in terms of Hard-Soft Acid–Base Theory (HSAB). In the HSAB ideas of Pearson[25] or the A and B type acids of Schwarzenbach[26] or Ahrland et al.,[27] hard metal ions prefer to bind hard bases, and soft metal ions prefer to bind soft bases. Table 1.3 shows the classifications of metal ions in HSAB Theory.

	Hard	Borderline	Soft
Acids	H^+, Li^+, Na^+, K^+, Be^{2+}, Mg^+, Ca^{2+}, Cr^{2+}, Cr^{3+}, Al^{3+}, Fe^{3+}	Fe^{2+}, Co^{2+}, Ni^{2+}, Cu^{2+}, Zn^{2+}, Pb^{2+}	Cu^+, Ag^+, Au^+, Tl^+, Hg^+ Pd^{2+}, Cd^{2+}, Pt^{2+}, Hg^{2+}
Bases	F^-, HO^-, O^{2-}, CO_3^{2-}, NO_3^-, SO_4^{2-}, ClO_4^-, PO_4^{3-}, H_2O, NH_3	NO_2^-, SO_3^{2-}, Br^-, N_3^-, SCN^-	H^-, R^-, CN^-, I^-, S^{2-}, NCS^-, CO, R_3P, C_6H_6, R_2S

Table 1.3 Hard-Soft Acid-Base classifications of metal ions (acids) and bases.[28]

In aqueous solutions, metal ions hydrolyze to form $M(OH)_n$ complexes, and the solution becomes acidic. The acidity of a metal ion is controlled by its size and its charge and can be described in terms of log K (OH^-) as shown below.

$$M^{n+} + OH^- \rightleftharpoons M(OH^-)^{(n-1)+} \qquad \text{Eq 1.1}$$

$$\log K(OH^-) = \frac{M(OH^-)^{(n-1)+}}{[M^{n+}][OH^-]} \qquad \text{Eq 1.2}$$

If the metal ion is hard and strongly acidic (e.g., Ga^{3+}, Fe^{3+}, Pu^{4+}; log $K_1(OH^-)$ greater than 9.0), then complexation by very basic, negative oxygen donors such as phenols, catechols, hydroxamates, hydroxypyridinones or methylphosphonate is preferred.[28]

The Al^{3+} ion is a very small, hard metal ion, so that Al^{3+} ions have a high affinity for a variety of hard ligands, as shown in Table 1.4. In addition, the smaller ionic radius of Al^{3+} (0.54 Å) compared to Fe^{3+} (0.65 Å) leads to a preference for six membered chelate rings.[15] This shows that the chelate ring size is important in the overall stability of aluminum complexes. Al^{3+} is less acidic (log K_1 (OH^-) = 9.01) than Fe^{3+} (log K_1(OH^-) = 11.81),[39-41] and has a lower affinity for most hard basic donors than does Fe^{3+} (Table 1.4).

Ligand	Log β (Al^{3+})	Log β (Fe^{3+})
Desferrioxamine	24.50	30.99
Transferrin	13.72	21.44
EDTA	16.13	25.70
Oxalic acid	7.26	9.84
NTA	11.61	15.90
NH_3	0.80	3.80
Citric acid	7.98	11.21

Table 1.4 Formation constants for selected Al^{3+} and Fe^{3+} complexes.[29-39]

Aluminum is one of the most hydrolytic metal ions known in aqueous solution. The formation of $Al(OH)_n$ complexes from hydrolysis is shown in Figure 1.3.[42-43] The $[Al(H_2O)_6]^{3+}$ ion is presented in solution at pH < 3.5. The aqua hydroxycomplexes $[Al(OH)]^{2+}$ and $[Al(OH)]^{+}$ are formed above pH 3.5, and colloidal $Al(OH)_3$ forms at pH > 5.0. The $[Al(OH)_4]^-$ species begins to form in solution at pH > 7.0 and is dominant at

pH 8.0-9.0. Polynuclear hydroxo complexes are also created by the hydrolysis of Al^{3+} ions, and with increased Al^{3+} concentration they can convert to colloids.[43-44]

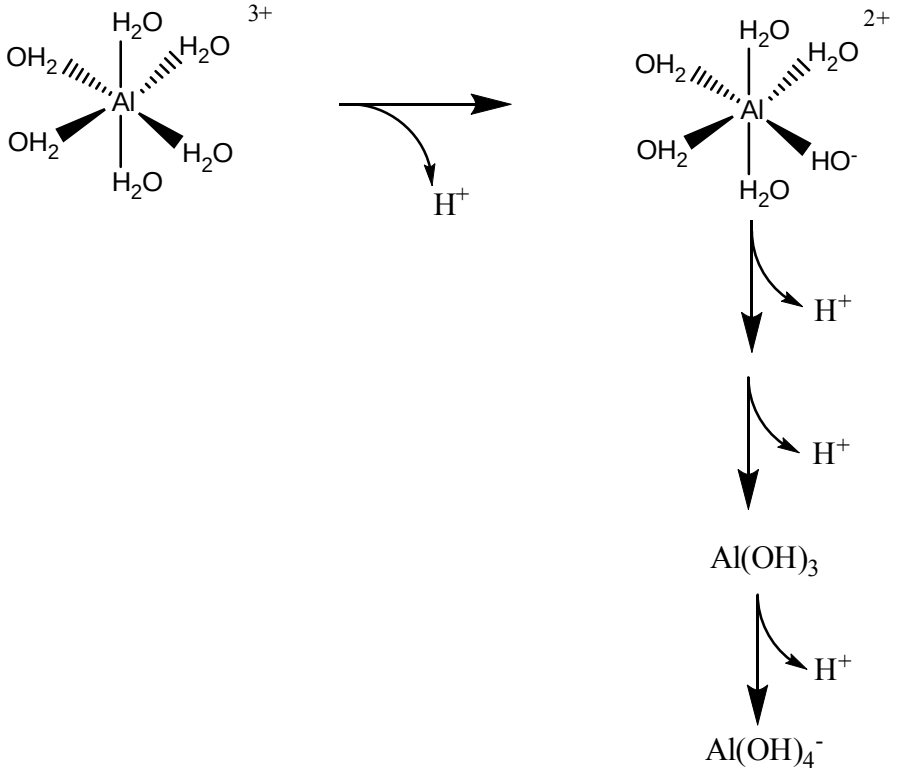

Figure 1.3 Aluminum hydrolysis reactions.

Equilibrium constants for the four mononuclear hydroxo complexes are described in Equations 1.3-1.6.[42]

$$\beta_1 = \frac{[Al(OH)][H]}{[Al]} = 10^{-5.40} \quad \text{Eq 1.3}$$

$$\beta_2 = \frac{[Al(OH)_2][H]^2}{[Al]} = 10^{-10.04} \quad \text{Eq 1.4}$$

$$\beta_3 = \frac{[Al(OH)_3][H]^3}{[Al]} = 10^{-15.74} \quad \text{Eq 1.5}$$

$$\beta_4 = \frac{[Al(OH)_4][H]^4}{[Al]} = 10^{-23.49} \quad \text{Eq 1.6}$$

1.3 Aluminum Toxicity

In spite of many efforts to establish an essential function for aluminum in humans, a specific, active pathway for its uptake and retention by healthy persons is still not clear. On the other hand, its toxicity is well-known, particularly in patients with renal failure. Therefore, an important clinical problem is how to eliminate aluminum that has accumulated in the body of uraemic patients.[45] In the 1970s, this was most clearly demonstrated by the appearance of severe neurological disorders among long-term dialysis patients (dialysis dementia).[46-47]

Aluminum overload has been linked with many neurological disorders[48] such as Alzheimer's disease (senile dementia),[49-50] Parkinson's dementia,[51] and Down's syndrome.[52] It also affects the bone marrow, thereby producing anemia. The toxicity of Al^{3+} has also been observed in infants, whose kidney function is not fully developed.[53-55] Premature neonates who receive intravenous feeding (TPN) solutions contaminated with

aluminum are at a high risk for impaired mental development and metabolic bone disease.[56] These risks arise from the demand for large amounts of calcium and phosphate solutions that are contaminated with Al^{3+}, which their immature kidneys cannot remove.[11]

Al^{3+} toxicity raises questions concerning the possible route of its absorption into the body and its binding modes after ingestion. Its toxicity is usually limited by a combination of poor intestinal absorption and effective renal clearance, but the abundance of Al^{3+} in food processing, pharmaceuticals and water supplies can still pose a serious thereat.[57] The growing awareness of the toxicity of Al^{3+} has generated a great deal of interest in the behavior of this element in serum.

1.3.1 Dialysis encephalopathy syndrome

Aluminum toxicity has been observed in patients with impaired renal function such as dialysis patients.[58] In 2003, more than 453,000 patients with end stage renal disease in the US were considered to be at high risk for Al^{3+} toxicity, and this number is increasing by ~100,000 patients per year.[59]

These patients are at high risk for aluminum overload not only because their kidneys do not function well, which leads to a high concentration of serum aluminum, but also because the dialysis solutions may be contaminated with aluminum. In the past, aluminum was a known contaminant of the water used to prepare dialysate for hemodialysis patients with end-stage renal disease.[60]

Aluminum accumulation in the brain causes dialysis dementia, and the increased concentration in bone appears to be responsible for one type of osteomalacia. Both

encephalophthy and osteomalacia are associated with long-term, intermittent hemodialysis.[61] There are now accepted standards for the Al^{3+} concentration in dialysate, and the control of Al^{3+} in the water has effectively reduced the cases of dementia.[62]

1.3.2 Alzheimer's disease

In 1982, it was suggested that aluminum might be related to Alzheimer's disease.[63] A study published in Lancet[64] involved an evaluation of the geographical relationship between the aluminum content of drinking water and the prevalence of Alzheimer's disease. The study reported a 50% increase in the risk of Alzheimer's disease in areas with high concentrations of aluminum. Even low concentrations of aluminum in drinking water had an effect. The risk of Alzheimer's was 1.5 times higher when the aluminum concentration exceeded 0.11 mg/L than in areas where the concentration was 0.01 mg/L. Although Al^{3+} has been implicated in senile and pre-senile dementia, it has not been proven to be the cause of this disease, and more recent studies cast doubt on an aluminum-Alzheimer's connection.[61]

1.4 Total parenteral nutrition (TPN) solutions

A high percentage of children born prematurely each year in the US require intravenous feeding after birth. Intravenous solutions contaminated with Al^{3+} cause Al^{3+} loading, which places premature infants at high risk of Al^{3+} toxicity. Preterm infants are more likely to accumulate aluminum because aluminum given intravenously bypasses the normal gastrointestinal barrier to absorption of this element. About 81% of the Al^{3+} in blood is bound to circulating plasma proteins, so that only 19% of circulating aluminum

is present as LMW complexes that are ultrafilterable by the kidneys.[65-66] The preterm infants have the additional burden of poor kidney function. There are some reports that even patients with normal renal function receiving long-term TPN demonstrated evidence of Al^{3+} loading.[67]

The variety of vitamins, electrolytes, sugars, minerals, lipids, and amino acids that are contained in total parenteral nutrition solutions is shown in Table 1.5.[68] A risk for adverse interactions can be found in the complexity of TPN formulas. Minerals may be needed for infants receiving long-term parenteral nutrition due to increased risk for bone demineralization and fractures. The importance of trace elements in the nutritional management of patients receiving TPN is now widely recognized.[69] Various trace elements, including zinc,[70] copper,[71] chromium,[72] and manganese,[73] are commonly added to TPN solutions and may also be present as contaminants.[71,74]

Component	Dose	Volume (mL)	Percent of volume (%)
Amino acid 10%	75 g	750	35
Dextrose 70%	1309 kcal	550	25.7
Water	200 mL	200	9.3
Lipid 10%	550 kcal	500	23.5
NaCl 23.4%	100 mmol	25	1.17
KCl	40 mmol	20	0.93
K phosphate	15 mmol	5	0.23
K acetate	40 mmol	20	0.93
$MgSO_4$	10 mmol	5	0.23
Ca gluconate	360 mg	40	1.87
$ZnSO_4$	3 mg	3	0.14
Se acid	20 µg	1	0.05
$MnSO_4$	100 µg	1	0.05
CuCl	300 µg	1	0.05
$CrCl_2$	16 µg	4	0.19
Vitamins	10 mL	12	0.56
Total		2137	100

Table 1.5 A typical daily TPN solution.[68]

TPN solutions are mixed with a compounder[75] such as that shown in Figure 1.4 that can be programmed to mix the appropriate amounts of the TPN ingredients (e.g. dextrose, water, amino acids, and fat). The pharmacist or the technician programs the compounder with the specific gravity and volume needed for each component.

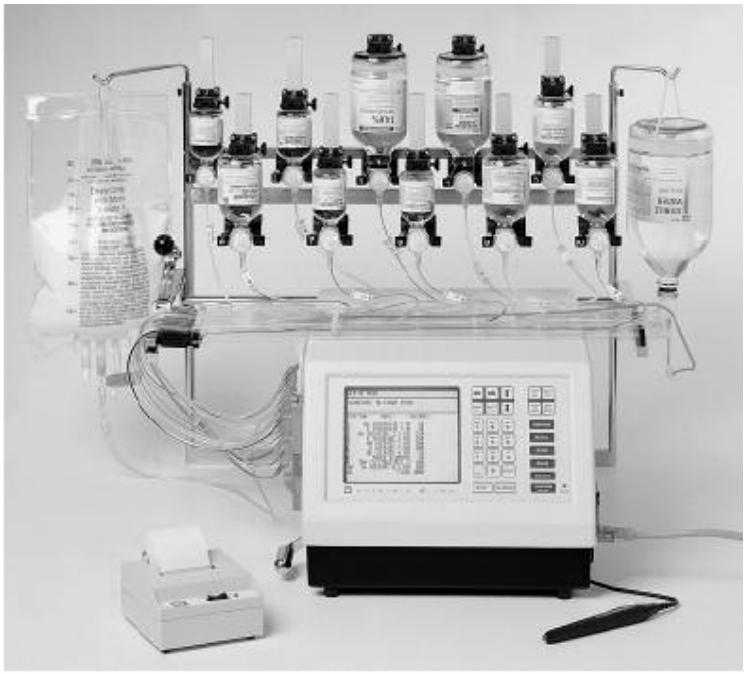

Nutrimix Micro TPN compounder. (Courtesy of Abbott Hospital Products Division.)

Figure 1.4 TPN compounder.

Aluminum loading is a problem due to Al^{3+} contamination of the commercial TPN component solutions, as shown in Table 1.6. Phosphates and calcium gluconate are the primary sources, and typically account for 80-90% of the aluminum contamination in the final TPN.[11]

Solution	Aluminum content (μg / L)
Potassium phosphate (3000 mmol / L)	16,598±1801
Sodium phosphate (3000 mmol / L)	5977
Calcium gluconate (10%)	5056±335
Heparin (1000 units / mL)	684±761
Normal serum albumin (25%)	1822±2503
Intralipid	195
Essential amino acids (28%)	72±59
5% Dextrose	72±1
Sodium Chloride (4000 mmol/L)	6±4
Potassium chloride (3000 mmol/L)	6

Table 1.6 Levels of aluminum in common components of TPN solutions.[14]

Table 1.7 compares the calculated daily intakes of selected ultratrace elements from TPN with the reported amounts absorbed from the gastrointestinal (GI) tract in normal subjects. The data are taken from studies utilizing different methodologies and diets and therefore must be interpreted cautiously. Nevertheless, the data in the table indicate that the intakes of the elements Mo, Ni, V, and Cd from TPN solutions are within the general range of that absorbed daily from the GI tract. The intake of B from TPN solution is much lower, whereas the intake of Al^{3+} is much higher.[59]

Element	Calculated intake of TPN (μg/day)	Estimated absorption in the GI tract (μg/day)	Reference
B	148	1800-3600	76
Mo	244	50-150	77
Ni	53	15-70	78
V	29	5-20	79
Al	450	25-50	79
Cd	22	2-20	80

Table 1.7 Comparison of intakes of ultra trace elements from TPN solution and from GI absorption from a normal diet.

Possible toxicity from Al^{3+} in products such as medications, foods and cosmetics has been of concern to the FDA. In 2000, the FDA recommended regulations for labeling the Al^{3+} content in the reagents used to prepare TPN solutions. The TPN solutions are prepared daily from large and small volume parenteral (LVP and SVP) solutions. The FDA recommends that the aluminum content of an average TPN solution should be limited to 25 μg/L and a safe level of exposure in TPN therapy is 5 μg/kg/day.[81] Manufacturers continue to work on reducing the aluminum content in their products.

Over the past two decades, the contamination of aluminum in SVP solutions has been steady, with the primary source of aluminum being calcium gluconate solutions. Although Ca^{2+} is necessary in TPN solutions, >50% of the Al^{3+} contamination in TPN solutions comes from the Ca-gluconate SVP solution.[74,82] Therefore, we have begun studies to produce an immobilized chelator as an in-line filter to remove Al^{3+} from Ca

gluconate and other small volume parenteral solutions used to prepare the final TPN solutions.

In 1997, Bishop et al.[56] reported on the potential neurotoxicity of TPN solutions contaminated with Al^{3+} in a prospective randomized study. Infants were randomized to receive TPN solution (total Al intake; 45 μg/kg/day) or Al^{3+}-depleted solutions (total Al^{3+} intake; 4-5 μg/kg/day). A detailed description of the sources of the Al^{3+} contamination is shown in Table 1.8. The Mental Scale of the Bayley Scales of Infant Development was used to evaluate neurologic development. Infants receiving the standard TPN solution had a lower mean Bayley Mental Development Index than infants receiving the Al^{3+}-depleted solution.

Solution	Standard solution		Aluminum-depleted solution	
	Volume (ml)	Aluminum content (μg)	Volume (ml)	Aluminum content (μg)
Vamin Infant	50	1.5	50	1.5
Intralipid 20%	15	0.1	15	0.1
Vitalipid	1	0.3	1	0.3
Solivito	1	<0.1	1	<0.1
Neotrace	1.6	1.2	1.6	1.2
Potassium acid phosphate	1.3	2.8	-	-
Polyfusor phosphate	-	-	14.4	0.3
Calcium gluconate	8.0	38.8	-	-
Calcium chloride	-	-	2.1	0.5
Dextrose, sodium, potassium	102	<1.0	102	<1.0
Total aluminum intake at 180 ml/ kg / day	45 μg / kg / day		4.0-5.0 μg / kg / day	

Table 1.8 Composition and aluminum content of the standard and aluminum-depleted intravenous feeding solutions.[56]

1.5 Desferrioxamine Therapy

The treatment usually applied for aluminum removal is basic chelation therapy using desferrioxamine (DFO), which is a chelator with a great capacity to decrease Al^{3+} body burden by increasing its excretion in the urine. Desferrioxamine is a naturally occurring hydroxamate siderophore that was first extracted from *Streptomyces pilosus.* The linear trihydroxamic acid is composed of alternating 1,5-diaminopentane and succinic acid residues as shown in Figure 1.5, giving a MW of 560 D.

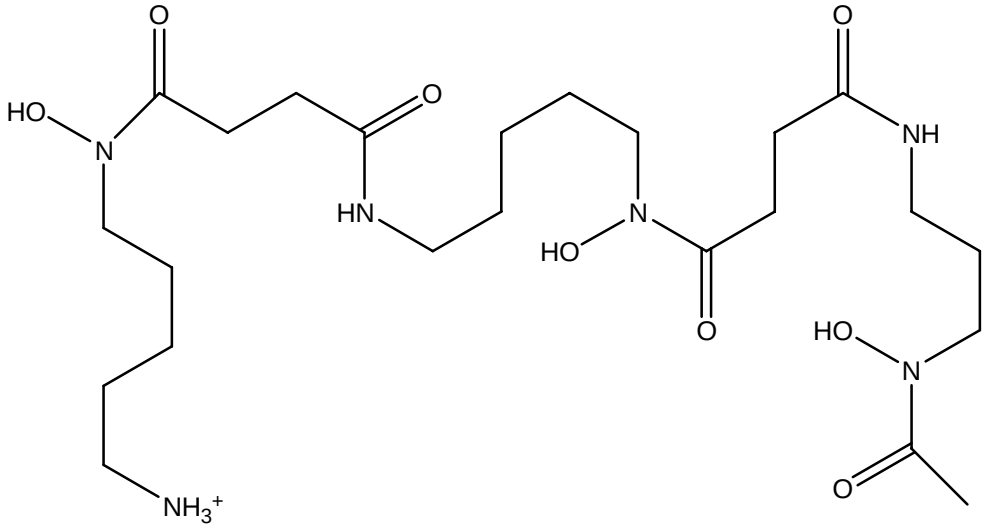

Figure 1.5 Structure of desferrioxamine (DFO).

The capability of DFO to form very stable complexes with hard metal ions suggested its potential use in the removal of these metal ions from organisms. It forms simple, stable 1:1 complexes of relatively low molecular mass that can be easily excreted.

The affinity of DFO for a particular metal ion is related to the acidity of the metal aquo ion. The acidity of a metal ion is related to its size and charge, and also to the degree of covalency in the M-O bond. Figure 1.6 shows the linear relationship between log K_1 for DFO and log K_1 (OH^-) for a series of metal ions. The most stable complexes with DFO occur with the most acidic metal ions.

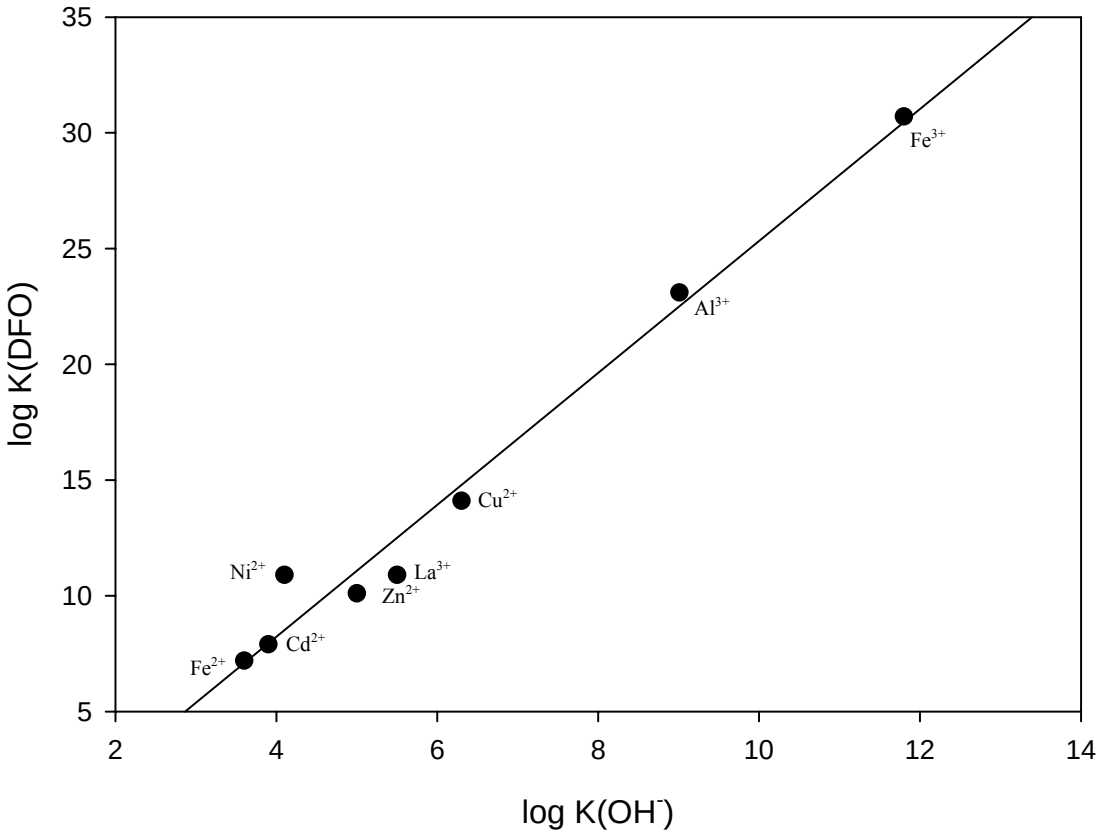

Figure 1.6 Correlation between the log K values for the polydentate ligand DFO and log K (OH^-).[39]

The first successful attempt to remove aluminum from patients with dialysis encephalophathy by using the chelating agent DFO was in 1979.[83] DFO is now used

extensively for the treatment of renal patients for aluminum-related conditions, such as dialysis encephalophathy, osteomalacia and microcytic anaemia. The drug operates by raising serum aluminum levels, while at the same time appearing to reduce aluminum toxicity. The increased aluminum concentration in serum during DFO treatment is clearly accompanied by changes in Al^{3+} speciation (the stable $Al(DFO)H^{+}$ complex is formed), and relatively large amounts of the element (up to ~95%) may be rapidly removed by dialysis.[84]

DFO is also used to treat iron overload, since there are chemical and physical similarities between aluminum and iron (charge, ionic radius and protein binding). Iron overload is most commonly associated with thalassemia. Thalassemic disorders are characterized by an abnormality in one or more of the globin genes, resulting in the inability to synthesize haemoglobin properly.[85] Thalassemic patients require regular blood transfusions to supplement their haemoglobin levels, but this results in a toxic buildup of iron in the body, and iron accumulation in the heart, liver and other vital organs ultimately results in death.

Unfortunately, DFO therapy is associated with undesirable side effects.[86] It is very expensive, and it is only efficient when administered intravenously or subcutaneously. Therefore, there has been an interest in the development of inexpensive, orally active compounds for the treatment of aluminum and iron overload. In particular, 1,2-dimethyl-3-hydroxypyridine-4-one, commercially available as Deferriprone, has been clinically used as an orally active iron chelating drug in thalassemic patients.

The selection of an appropriate ligand for aluminum complexation can be rationalized by classification of metals and ligands according to the concept of HSAB

theory. The affinity of the ligand for the target metal ion and the selectivity of the ligand for the target metal ion versus other essential metal ions are both very important. The stability of metal – ligand complexes is represented by stability constants or equilibrium constants. Conventional potentiometry and spectrophotometry are used to determine such constants.[4]

When a ligand is designed to remove a certain metal ion because it has reached toxic levels, it must be as selective as possible for that metal ion so as not to disturb the metals that are naturally present. Other factors that must be taken into consideration include the method of administration, bioavailability, toxicity, membrane permeability and rapid elimination of the ligand and its metal chelate without spreading the undesired metal to other organs throughout the body.

Definitions for metal-ligand complexation equilibria

The general expression for the formation of a metal ligand complex is

$$iM + jL + kH \rightleftharpoons [M_iL_jH_k] \qquad \text{Eq 1.7}$$

$$\beta_{ijk} = \frac{[M_iL_jH_k]}{[M]^i[L]^j[H]^k} \qquad \text{Eq 1.8}$$

where $M_iL_jH_k$ represents the complex formed, M represents the free unhydrolyzed hexaaquo metal ion, L represents the uncomplexed, totally deprotonated form of the ligand, H represent the free hydrogen ion, and β_{ijk} is the overall stability constant.

Much more informative of how a ligand will bind the metal at physiological pH is the pM value.[28,87] The pM value is defined in Equation 1.9 as the negative log of the concentration of the free metal ion.

$$pM = -\log [M] \qquad \text{Eq 1.9}$$

The value of pM is calculated for specific values of total metal, total ligand, and pH using the ligand protonation constants and the metal-ligand stability constants.

1.6 Hydroxamate ligands and immobilized hydroxamates

Over the past decades, the chemistry and biochemistry of hydroxamic acids and their derivatives have been considered because of their pharmacological, toxicological and pathological properties.[88] Hydroxamic acids are a group of naturally occurring and synthetic weak organic acids[89] of the general formula shown in Figure 1.7. They are much weaker acids than the structurally related carboxylic acids RC(=O)OH.[90]

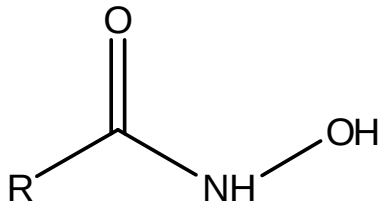

Figure 1.7 Structure of a hydroxamic acid.

Hydroxamates, including complex compounds, are common in the tissues of plants and as metabolites of bacteria and fungi. The biological importance of hydroxamic acids is well established.[91] They have antibacterial and anti-fungal properties and are inhibitors of enzymes such as prostaglandin H synthase, peroxidases, ureases, and matrix metalloproteinases (MMP), which degrade the barriers holding cells in place and are involved in tumor growth.[92-94] Their ability to inhibit enzymes makes them ideal as drug candidates- e.g. Marimastat is a hydroxamic acid that is an MMP inhibitor and is at an advanced stage of clinical development as an anticancer drug. Other medical applications of the hydroxamates which utilize their affinity for high charge density metal ions include the possible use of their metal complexes as imaging agents.[95]

Simple hydroxamic acids, including acetohydroxamic, benzohydroxamic and salicyhydroxamic acids, undergo a single deprotonation reaction to form a bidentate ligand as shown in Figure 1.8.[96] Desferrioxamine and many other siderophores utilize either two or three hydroxamate groups to form high-affinity multidentate ligands.

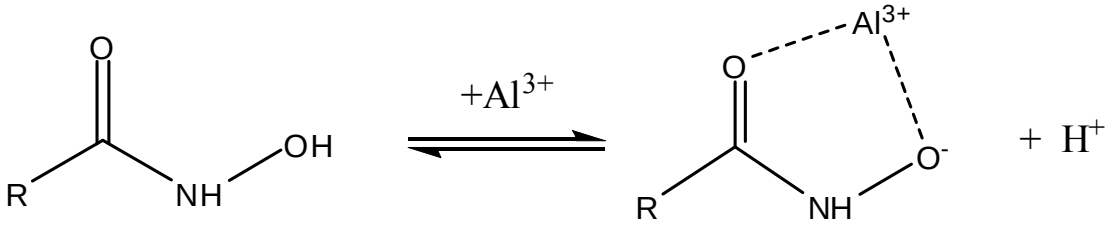

Figure 1.8 Aluminum coordination by a hydroxamic acid.

Hydroxamate ligands such as DFO has been investigated as Al^{3+} chelators.[29] The species distribution of Al^{3+} and DFO as a function of pH is shown in Figure 1.9.

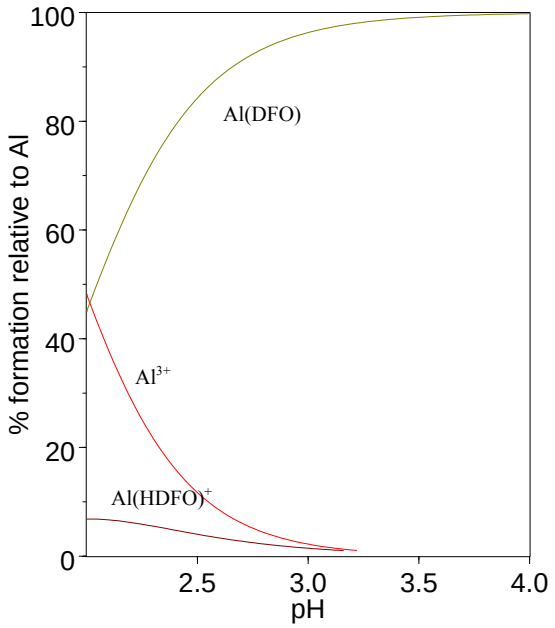

Figure 1.9 Species distribution diagram for 0.001 M Al^{3+} and DFO as a function of pH.

The results show the strong binding of Al^{3+} by DFO. The formation of the Al(DFO) complex starts at low pH and is predominant over a wide pH range, with a small amount of a protonated $Al(HDFO)^{+}$ forming below pH 3. In addition, a study of several dihydroxamic acids of the type $HONHCO(CH_2)_nCONHOH$ (n = 4, 6, 7 and 8) with Al^{3+} has been reported.[29] These studies show that the hydroxamate group is very effective for binding Al^{3+}. In the present study, the number and arrangement of hydroxamate groups have been varied to adjust the strength with which the chelator binds Al^{3+}.

A chelating resin is a solid organic polymer with ligands covalently bound to the polymer surface. The sorption of metal ions on chelating resins is mainly driven by the formation of complexes on the resin, which is the most important difference between

simple ion exchange resins and chelating resins.[97]

In the last few decades, chelating resins have been developed for different applications in analytical chemistry, metal processing and wastewater treatment.[98-100] A suitable resin improved with a metal-chelating agent for chemical and biological applications should possess a high capacity for, and a favorable selectively toward, the metal, combined with high stability and rapid exchange kinetics that will allow metal release and a regeneration process.

There are three basic units of a chelating resin as shown in Figure 1.10, each of which plays a critical role in the overall function of the resin.[101] One is the solid polymer that provides the core of the resin and helps to define its physical (mechanical) properties. The second is the linker or spacer unit that affects the reaction kinetics and helps to modify the interactions of the resin with solvent. The third is the functional end, which is responsible for the chemical reactivity and selectivity of the resin. Each unit must be carefully selected to suit the intended application of the resin.

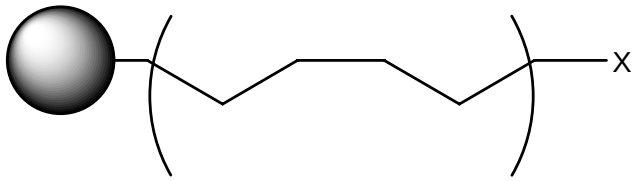

Figure 1.10 Three basic units of a chelating resin.

Polystyrene resins are commonly modified by aromatic electrophilic substitution of functional groups onto the phenyl rings. The Merrifield resin, a chloromethyl polystyrene shown in Figure 1.11, is the first and most frequently used resin for solid phase synthesis. However, TentaGel, a graft copolymer of cross-linked polystyrene and polyethyleneglycol (PEG), has also been used for solid phase organic synthesis.

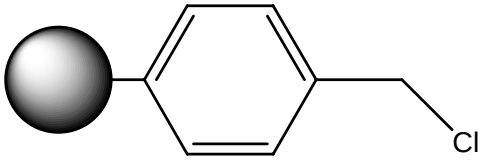

Merrifield resin

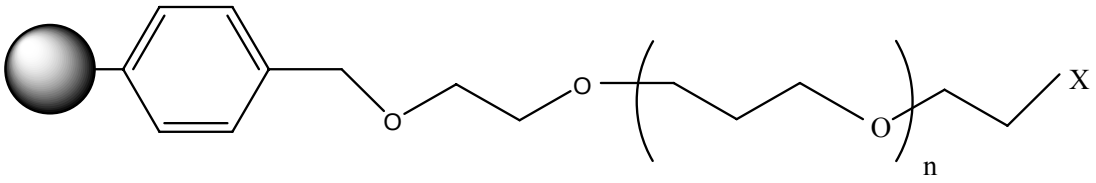

TentaGel resin

Figure 1.11 Polystyrene resins.

Chelex is a commonly-used resin in which the iminodiacetate chelating group is present on the surface as shown in Figure 1.12. Iminodiacetate chelating resins would be a poor choice for the proposed application of removing Al^{3+} from solutions with a high concentration of Ca^{2+} because they have poor selectivity for Al^{3+} over Ca^{2+} ($K_{Al} / K_{Ca} \approx$

100).[102] Thus, it is proposed to use resins with di- and trihydroxamate ligands, which are expected to have K_{Al} / K_{Ca} ratios[39] of 10^{11} and 10^{21}.

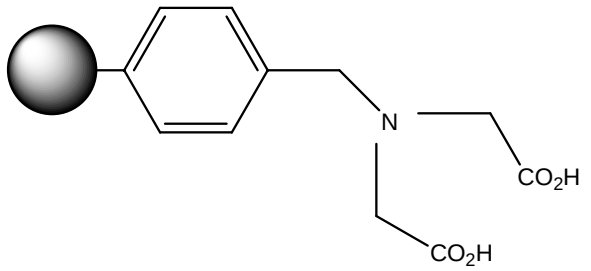

Chelex

Figure 1.12 Structure of Chelex.

The six coordination sites of an Al^{3+} ion can be filled by binding three bidentate hydroxamate ligands. Since the binding of a single hydroxamate group is unlikely to be strong enough to remove low concentrations of Al^{3+}, two or three hydroxamate groups such as the proposed di- and trihydroxamate resins shown in Figure 1.13 are preferred. The final quality of a chelating resin is dependent on the quality of the ligand functional group on the solid support, selection of the appropriate solid support, and optimization of the coupling conditions of ligands.

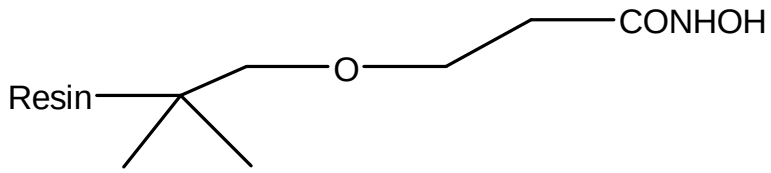

Monohydroxamate resin

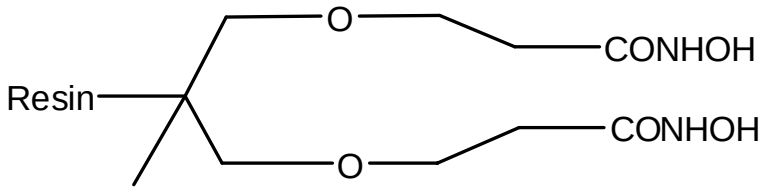

Dihydroxamate resin

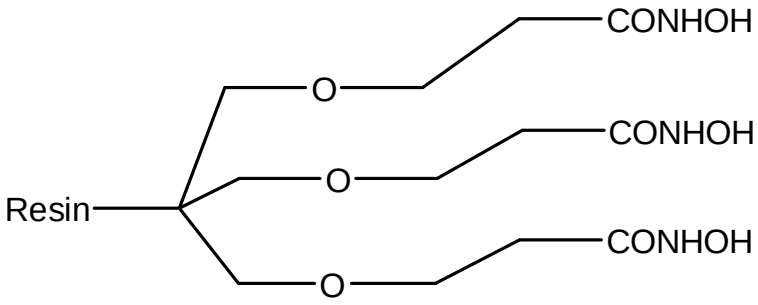

Trihydroxamate resin

Figure 1.13 Three proposed hydroxamate chelating resins.

Chelating resins have found use for removal of trace metal ions from reagents, biochemical and physiological fluids, and for separation and preconcentration in analytical chemistry. There have been studies with immobilized hydroxamates. A monohydroxamic acid was attached to an epoxy-activated Sepharose SB support.[103] This resin was loaded with Fe^{3+} and used in a procedure known as immobilized metal affinity

chromatography to separate proteins from human serum. In addition, immobilized desferrioxamine (DFO) has been used for the extracorporeal removal of aluminum from blood.[104] A conventional hemodialyzer was modified by the addition of a cartridge containing high-flux polysulfone F-60 hollow fibers in which just 0.3 g of DFO had been non-covalently imbedded. Use of the modified dialyzer for two-hour treatments of dialysis patients was found to be safe. Desferrioxamine would be prohibitively expensive for the proposed application, and thus the development of a new immobilized hydroxamate chelator to remove the Al^{3+} from the components of TPN solution is an important goal.

There are two reasons for evaluating ligands with a range of Al^{3+}-binding affinities. One is that a simpler, more easily synthesized ligand, although not the most powerful chelator, might be adequate to meet the clinical objectives and considerably cheaper to synthesize. In addition, it would be easier to regenerate the resin for reuse by eluting the bound Al^{3+} at low pH. This will be a critical factor in the possible use of the proposed resins on a large scale to produce commercial, Al^{3+}-free TPN solutions. A trihydroxamate ligand could bind the Al^{3+} so tightly that it is not feasible to regenerate the resin. One possible outcome of the proposed research is that a trihydroxamate resin might be used in the clinic in the form of a one-time, disposable cartridge to clean Al^{3+} from small volumes of TPN solutions, while a dihydroxamate resin might be more suitable for industrial use to prepare large batches of Al-free TPN solutions.

References

1. Douglas, B.; McDaniel, D.; Alexander, J.; *Concepts and models of inorganic chemistry*, New York, 1994, 888.

2. William, R. J. P. *J. Inorg. Biochem.* 1999, 76, 80.

3. Ganrot, P. O. *Environ. Health Perspect.* 1986, 65, 363.

4. Bowen, H. J. M. *Environment chemistry of elements*, Academic Press: New York, 1979.

5. Santos, M.A.; Gano, L.; Gama, S. *J. Inorg. Biochem.* 2005, 99, 1845.

6. http://www.trufax.org/general/aluminum.html, contamination with aluminum compounds, and effect on human neurophysiology and behavior.

7. Greger J. L.; Sutherland J. E. *Crit. Rev. Clin. Lab. Sci*. 1997, 34, 439.

8. Bettelheim, F. A.; March, J. *Acids and bases. Introduction to general, organic and biochemistry*, Saunders College Publishing: New York, 1991, 214.

9. http://www.eaa.net/eaa/downloads/envbody2.pdf Aluminum and health.

10. Yokel, R. A.; McNamara P. J. *Pharmacol. Toxicol*. 2001, 88, 159.

11. Sedman, A. B.; Klein, G. L.; Merritt, R. J.; Miller, N. L.; Weber, K. O.; Gill, W. L.; Anand, H.; Alfrey, A. C. *N. Engl. J. Med.* 1985, 312, 1337.

12. Kubal, G.; Mason, A.; Sadler, B. P.; Tucker, J. A.; Woodworth, R. C. *Biochem. J.* 1992, 285, 711.

13. Martin, R. B. *Metal Ions in Biological Systems*, Marcel Dekker, New York, 1988, vol. 24, 1.

14. Day, J. P.; Barker, J.; Evans, L. J. A.; Perks, J.; Seabright, P. J.; Ackrill, P.; Lilly, J.

S.; Drum, P. V.; Newtow, J. W. A. *Lancet* 1991, 337, 1345.

15. Harris, W. R.; Messori, L. *Coord. Chem. Rev.* 2002, 228, 237.

16. Harris, W. R.; Sheldon, *J. Inorg. Chem.* 1990, 29, 119.

17. Baker, E.; Rumball, S. V.; Anderson, B. F. *Trends Biochem. Sci.* 1987, 12, 350.

18. Harris, D. C.; Aisen, P. *Iron carriers and iron proteins*, VCH Pub. Inc, New York, 1989.

19. Harris, W. R. *Clin. Chem*. 1992, 38, 1809.

20. Yokel, R. A.; Ackrill, P.; Burgess, E.; Philip, D. J. *Tox. Environ. Health* 1996, 48, 667.

21. Ackley, A. C.; Yokel, R. A. *Toxicology* 127, 1998, 59.

22. Burgess, J. *Metal ions in solutions*, Ellis Horwood, Chichester, 1979.

23. Hunt, J. P.; Friedman, H. L. *Prog. Inorg. Chem.* 1983, 30, 359.

24. Marcus, Y. *Chem. Rev*. 1988, 88, 1475.

25. Pearson, R. G. *J. Am. Chem. Soc.* 1963, 85, 3533.

26. Schwarzenbach, G. *Adv. Inorg. Radiochem.* 1961, 3, 257.

27. Ahrland, S.; Chatt, J.; Davies, N.R. *Rev. Chem. Soc*. 1958, 12.

28. Martell, A. E.; Hancock, R. *Metal complexes in aqueous solution,* New York, 1996.

29. Evers, A.; Hancock, R.; Martell, A. E.; Motekaitis, R. J. *Inorg. Chem.* 1989, 28, 2189.

30. Harris, W. R.; Chen, Y.; Wein, K. *Inorg. Chem.* 1994, 33, 4991.

31. Ahmad, J.; Higginson, W. *J. Chem. Soc., Dalton Trans.* 1983, 1449.

32. Kolthuff, I.; Averbach, E. *J. Chem. Soc., Dalton Trans.* 1952, 74, 1452.

33. Babko, A.; Dubovendo. L. *Zhur. Neorg. Khim*. 1957, 2, 1294.

34. Babko, A.; Dubovendo. L. *Zhur. Neorg. Khim*. 1956, 660, 992.

35. Motekaitis, R. J.; Martell, A. E. *Inorg. Chem.* 1984, 23, 18.

36. Field, T.; McCoort, J.; McBryde, W. *Can. J. Chem.* 1974, 52, 3119.

37. Khan, M.; Hussian, A. *Indian J. Chem.* 1980, 19a, 44, 50.

38. Motekaitis, R. J.; Martell, A. E. *J. Coord. Chem.* 1994, 31, 67.

39. Martell, A. E.; Smith, R. M. *Critical stability Constants,* Plenum, New York, 1988, vol 6.

40. Hancock, R. D.; Marsicano, F. *Inorg. Chem*. 1978, 17, 560.

41. Hancock, R. D.; Marsicano F. *Inorg. Chem*. 1980, 19, 2709.

42. Base, C. F.; Mesmer, R. E. *The hydrolysis of cations,* Wiley and Sons, New York, 1967.

43. Martin, R. B. *Bioinorganic chemistry of magnesium*; *Metal ions in biological systems*, 1990, 26, 1.

44. Matue, P.; Kubova, J. *J. Inorg. Biochem.* 2005, 99, 1769.

45. Wróbel, K.; González, E.B.; Wróbel, K. A. *Analyst* 1995, 120, 809.

46. Alfrey, A. C. *Contrib. Nephrol*. 1993, 102, 110.

47. McDermott, J. R.; Smith, A. I.; Parkinson, I. S. *Lancet* 1978, 1, 901.

48. McLachlan, D. R. C.; Lukiw, W.J.; Kruck, T. P. A. *Can. J. Neur. Sci*. 1989, 16, 490.

49. Good, P. F.; Perl, D. P.; Bierer L. M.; Schmeidler J. *Ann. Neurol*. 1992, 31, 286.

50. Yokel, R. A. *Neurotoxicology* 2000, 21, 813.

51. Perl, D. P.; Gajfusek, D. C.; Garruto, R. M.; Yanagihara, R. T.; Gibbs, C. J. *Science* 1982, 217, 1053.

52. Heston, L. L.; Ann, N. Y. *Acad. Sci.* 1982, 396, 29.

53. Hawkins, N. M.; Coffey, S.; Lawson, M. S.; Delves, H. T. *J. Pediatr. Gastroenterol.*

Nutr. 1994, 19, 377.

54. Klein, G. L. *Am. J. Clin. Nutr.* 1995, 61, 449.

55. Freundlich, M.; Zilleruelo, G.; Abitbol, C.; Strauss, J. *Lancet* 1985, 527.

56. Bishop, N. J.; Morley, R.; Day, J. P.; Lucus A. *N. Engl. J. Med.* 1997, 336, 1557.

57. Fulton, B.; Jeffrey, E. G. *Appl. Toxicol*. 1990, 14, 788.

58. Koo, W.W.K.; Kaplan, L. A. *J. Am. College Nutr.* 1988, 7, 199.

59. NKUDIC – National Kidney and Urologic Diseases Clearinghouse, National Institute of Diabetes and Digestive and Kidney Diseases, Kidney and Urologic Diseases Statistics for the United States, http://kidney.niddk.nih.gov/kudiseases/pupb/kustats/index.htm

60. Klein, G. L.; Herndon, D. N.; Rutan, T. C.; Miller, N. L.; Alfrey, A. C. *J. Burn Care Rehabil.* 1990, 11, 526.

61. Wills, M. R.; Savory, J. *Lancet* 1983, 2, 29.

62. King, S. W.; Savory, J.; Wills, M. R. *Ann. Clin. Lab. Sci.* 1982, 12, 143.

63. Perl, D. P.; Munoz-Garcia, D.; Good, P. F.; Pendlebury, W. W. *Science* 1982, 217, 1053.

64. Martyn, C. N.; Barker, D. J.; Osmond, C.; Harris, E. C.; Edwardson, J. A.; Lacey, R. F. *Lancet* 1989, 1, 59.

65. Klein, G. L.; Ott, S. M.; Alfrey, A. C.; Sherrard, D. J.; Hazlet, T. K.; Miller, N. L.; Maloney, N. A.; Berquist, W. E.; Ament, M. E.; Coburn, J. W. *Trans. Assoc. Am. Phys.* 1982, 95, 155.

66. Trapp, G. A. *Kidney Int.* 1986, 19, S12.

67. Ott, S. M.; Maloney, N. A.; Klein, G. L.; Alfrey, A. C.; Ament, M. E.; Coburn, J. W.; Sherrard, D. J. *Ann. Intern. Med.* 1983, 98, 910.

68. Berner, Y. N.; Shuler, T. R.; Nielsen, F. H.; Flombaum, C.; Farkouh, S. A.; Shike, M. *Am. J. Clin. Nutr.* 1989, 50, 1079.

69. Wolman, S. L.; Anderson, G. H.; Marliss, E. B.; Jeejeebhoy, K. N. *Gastroenterology* l979, 76, 458.

70. Shike, M.; Roulet, M.; Kurian, R.; Whitwell, J.; Stewart, S.; Jeejeebhoy, K. N. *Gastroenterology* 198l, 81, 290.

71. Jeejeebhoy K. N.; Chu R. C.; Marliss E. B. *Am. J. Clin. Nutr.* 1977, 30, 531.

72. Shike, M.; Ritchie, M.; Shils, M. E.; Alcock, N.; Flombaum, C. *Clin. Res.* l986, 34, 804A(abstr).

73. Hauer, E. C.; Mitchell, B. S.; Kaminski, M. V. Jr. *Am. J. Clin. Nutr.* l978, 3l, 264.

74. Mouser, J. F.; Wu, A. H.; Herson, V. C. *Am. J. Health-System Pharm.* 1998, 55, 1071.

75. http://connection.lww.com/Products/maryemohr/documents/PDF/Ch18.pdf

76. Boron, F. H.; Mertz, W. *Trace elements in human and animal nutrition*, 5th ed.,Vol 2. San Diego: Academic Press. 1986, 420.

77. Tsongas, T. A.; Melfen, R. R.; Walravens, P. A.; Chapell, W. R. *Am. J. Clin. Nutr.* 1980, 33, 1103.

78. Myron, D. R.; Zimmerman, T. J.; Shuler, T. R.; Klevay, L. M.; Lee, D. E.; Nielsen, F. H. *Am. J. Clin. Nutr.* 1978, 31, 527.

79. Ihle, B. V.; Becker, G. J. *Am. J. Kidney Dis.* 1985, 5, 302.

80. Flanagan, P. R.; McLellan, J. S.; Haist, J.; Cherian, M. G.; Chamberlain, M. J.; Valberg, L. S. *Gastroenterology* 1978, 74, 841.

81. US Dept Health and Human Services. Food and Drug Administration. Aluminum in

large and small volume parenterals used in total parenteral nutrition. Washington, DC: US Dept Health and Human Services 2000. Federal Register 90N-0056.65:4103-4111.

82. Koo, W. W. K.; Kaplan, L. A.; Horn, J.; Tsang, R. C.; Steichen, J. J. *J. Parenteral Enteral Nutr.* 1986, 10, 591.

83. Ackrill, P.; Ralston, A. J.; Day, J. P.; Hodge, K. C. *Lancet* 1980, 27, 692.

84. Day, J. P. *Aluminum and other trace elements in renal disease,* (Ed. A. Taylor), Baliere Tindell, Eastbourne , 1986, 184.

85. Lo, L.; Singer, S. T. *Pediatr. Clin. North Am.* 2002, 49, 1165.

86. Porter, J. B. *Clin. Hematol*. 1989, 2, 459.

87. Martell, A. E.; Calvin, M. *Chemistry of metal chelate compounds*, Prentice-Hall, Englewood Cliffs, N. J. 1952, 472.

88. Wahlroos, O.; Virtanen, A. L. *Acta Chem. Scand*. 13, 1906, 1959.

89. Bauer, L.; Exner, O. *Angew. Chem. Int. Ed. Engl*. 1974, 13, 376.

90. Bagno, A.; Comuzzi, C.; Scorrano, G. *J. Am. Chem. Soc.* 1994, 116, 916.

91. Kehl, H. *Chemistry and biology of hydroxamic acids*, Karger, New York, 1982.

92. Nishino, N.; Powers, J. C. *Biochemistry* 1979, 18, 4340.

93. Petrillo, E. W.; Ondetti, M. A. *Res. Rev*. 1982, 2, 1.

94. Rockwell, A.; Melden, M.; Copeland, R. A.; Hardman, K.; Decicco, C. P.; DeGrado, W. F. *J. Am. Chem. Soc.* 1996, 118, 10337.

95. Miller, M. J.; Malouin, F.; Bergeron, R. J.; Brittenham, G. M. In: *The development of iron chelators for clinical use, Elsevier, New York,* 1994.

96. Dessi, A.; Micera, G.; Sanna, D.; Erre, L. S. *J. Inorg. Biochem*. 1992, 48, 279.

97. Pesavento, M.; Biesuz, R. *React. and Funct. Polym*. 1998, 36, 135.

98. Compano, R.; Ferrer, R.; Guiteras, J.; Part, M. D. *Analyst* 1994, 119, 1225.

99. Kantipuly, C.; Karagadda, S.; Chow, A.; Gesser, H. D. *Talanta* 1990, 37, 491.

100. Lancaster, H. L.; Marshall, G. D.; Gonzalo, E. R.; Ruzicka, J.; Christian, G. D. *Analyst* 1994, 119, 1459.

101. Hermkems, P. H. H.; Ottenheijm, H. C. J.; Ree, D. *Tetrahedron* 1996, 52, 4527.

102. Zachariou, M.; Hearn, M. T. *Biochemistry* 1996, 35, 202.

103. Ramadan, N.; Porath, J. *J. Chromatog*. 1985, 321, 81.

104. Anthone, S.; Ambrus, C. M.; Kohli, R.; Min, I.; Anthone, R.; Stadler, A.; Stadler, I.; Viadutiv, A. *J. Am. Soc. Nephrol*. 1995, 6, 1271.

Chapter 2

Materials and Methods

2. Materials and Methods

2.1 Standard acid and base solutions

Standard carbonate-free KOH solutions were prepared from Baker Dilut-IT ampoules of concentrated KOH using Millipore water in the reservoir of a Metrohm model 655 autoburette. The Millipore water was generated in the Harris lab by passing deionized water through a 4-bowel Millipore purification system that removed both organic and inorganic contaminants. The KOH in the storage reservoir was protected from atmospheric CO_2 by an ascarite scrubber. A Gran's plot analysis[1] (Figure 2.1) was used to check for carbonate contamination of the standard aqueous KOH using Equation 2.1, where V_{acid} and V_{base} refer to the x-intercept of the plots of $V_{Total}.10^{-pH}$ and $V_{Total}.10^{-pOH}$ vs V_{KOH}. The results consistently revealed less than 1.0 % carbonate.

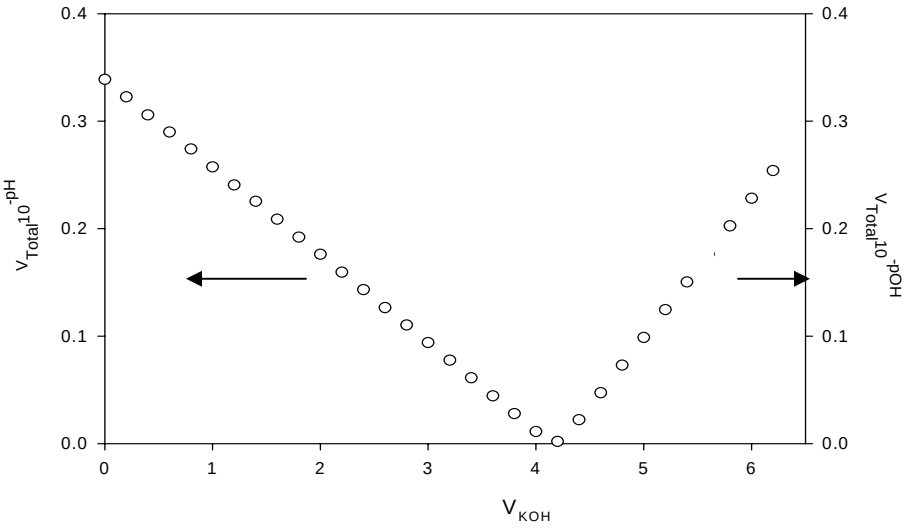

Figure 2.1 Gran's Plot.[1]

$$\%CO_3^{2-} = \frac{V_{base} - V_{acid}}{2V_{acid}} x100\% \qquad \text{Eq 2.1}$$

The KOH solutions were standardized by titration of dried, primary standard potassium hydrogen phthalate (KHP) purchased from Fisher Chemical Co. to a phenolphthalein end point. The indicator solution of 0.2% phenolphthalein in 90% ethanol was prepared from reagent grade phenolphthalein. The end point was detected as a color change of the solution from colorless to faint pink.

A ~0.1 M HCl solution was prepared by dilution of reagent grade concentrated HCl solution (12.4 M) that was purchased from Fisher Chemical Co. The standardized KOH solution and primary standard tris(hydroxymethyl)aminomethane were used to determine the acid concentration.

2.2 Buffer and electrolyte solutions

Reagent grade N-2-hydroxyethlypiperazine-N'-2-ethanesulfonic acid, HEPES, from Sigma was used to prepare 0.1 M buffer solutions at pH 8. The solid was added to Millipore water and the pH was adjusted with concentrated NaOH. MES buffers were prepared in the same way as HEPES buffers by use of reagent grade, 99.5%, morpholine-N-ethanesulfonic acid (MES) and adjusted to pH 6 with NaOH.

Acetate buffers (50 mM) were prepared by dissolving solid sodium acetate in Millipore water and adjusting the pH to 5 by adding hydrochloric acid. Solutions of 1.0 M potassium nitrate and potassium chloride were prepared by dissolving solid potassium nitrate and potassium chloride purchased from Fisher in Millipore water. They were used to adjust samples to 0.1 M ionic strength in the potentiometric and spectrophotometric titrations.

2.3 EDTA, DFO, AHA, and HEDTA solutions

Reagent grade, 99%, disodium ethylenediaminetetraacetic acid (EDTA) was purchased from Fisher, dried at 80°C, and used to prepare 0.1 M EDTA solutions in Millipore water. Desferrioxamine mesylate (DFO) from Sigma was used to prepare a 0.002 M stock DFO solution in MES buffer at pH 6. To prepare a 0.005 M acetohydroxamic acid (AHA) solution, solid AHA from Sigma was dissolved in Millipore water. The N-(2-hydroxyethyl)ethylenediaminetriacetic acid (HEDTA) solution was prepared by dissolving reagent grade HEDTA purchased from Sigma in Millipore water.

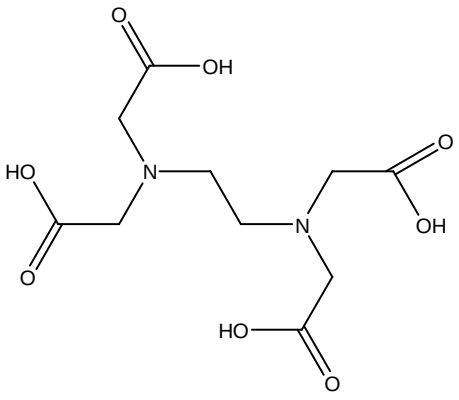

EDTA

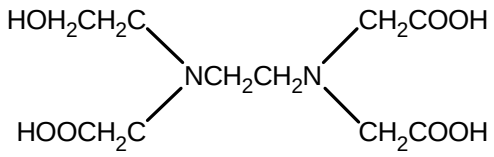

HEDTA

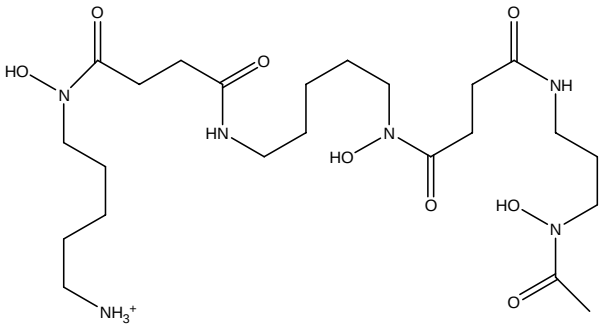

DFO

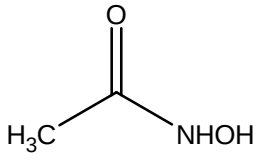

AHA

Figure 2.2 Structures of the ligands EDTA, HEDTA, DFO and AHA.

2.4 Calcein, gluconic acid and ferron solutions

The fluorescence probe calcein was purchased from Invitrogen and used to prepare ~500 μM calcein solutions in Millipore water. Analytical grade gluconic acid, 45-50% w/w, was purchased from Aldrich and used to prepare a ~0.1 M stock gluconic acid solution in Millipore water. The solution was standardized by titration with standard KOH solution. A 0.025 M solution of the chelating agent ferron, 7-iodo-8-hydroxyquinoline-5-sulfonic acid, was prepared by dissolving solid ferron in Millipore water and adjusting the pH to 5 by adding aliquots of a sodium hydroxide solution.

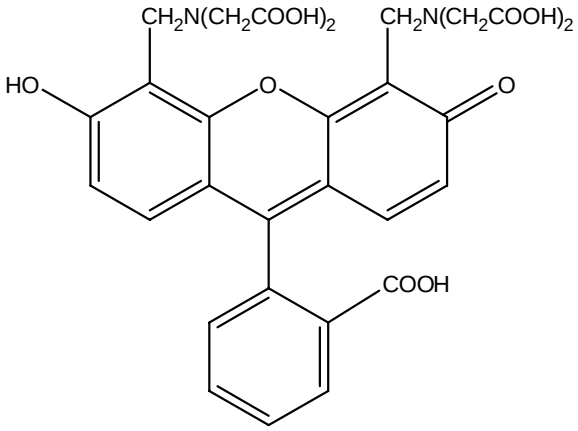

Calcein

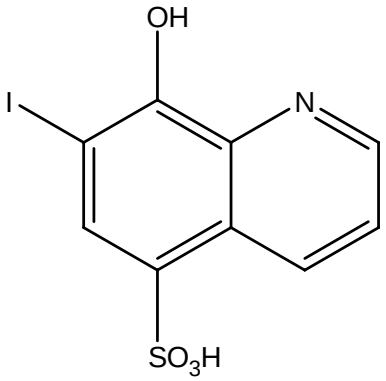

Ferron

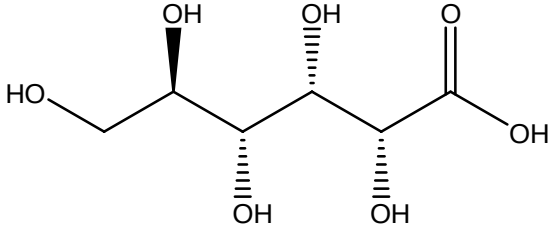

Gluconic acid

Figure 2.3 Structures of calcein, ferron and gluconic acid.

2.5 Metal solutions

2.5.1 Aluminum stock solution

A stock solution of aluminum was prepared by dissolving reagent grade aluminum chloride in 0.1 M HCl solution to prevent metal hydrolysis. Two methods were used to determine the molarity of the aluminum solution. In one method, a known volume of the aluminum stock solution was added to a column of the strong cation exchange resin DOWEX 50W (50-100 dry mesh, 2% cross-linking). The entire Al^{3+} sample solution was eluted from the column into a small beaker. Passage through the column replaced each Al^{3+} with three H^+ ions. The eluted sample was then titrated with standard KOH to a phenolphthalein end point to determine the total mmoles of H^+. The total mmoles of H^+ was the sum of the mmoles of HCl in the original Al^{3+} stock solution plus the mmoles of H^+ liberated from the cation exchange column.[2] Since the mmoles of H^+ from the HCl was known, the mmoles of Al^{3+} could be calculated.

In addition to the first method, a zinc back titration was used to standardize the Al^{3+} stock solution. A known excess of primary standard EDTA was added to an aluminum solution. This solution was back titrated with a standard zinc solution using 0.059% xylenol orange as the indicator.[3] The results from the two methods were consistent.

2.5.2 Iron stock solutions

Solid ferric chloride from Sigma was dissolved in 0.1 M HCl or in 0.1 HNO_3 to prevent the hydrolysis of the metal ion. The concentrations of the stock solutions were determined by two methods: direct titration with EDTA using standard methods[3] and

atomic absorption spectrophotometry.[4] The results obtained from the two methods were consistent.

A sample of ferric ion was also titrated with KOH in the presence of an excess of EDTA. There is an inflection in the titration curve that occurs when the added KOH has neutralized all the strong acid from the metal ion stock solution as well as the two protons that are released from the EDTA by the complexation of Fe^{3+}. This result serves to double-check the internal consistency of the acid and ferric ion concentrations. In addition, a 0.1 M Fe^{2+} solution was prepared by dissolving ferrous ammonium sulfate in 10 mM HCl for use in Fe-DFO studies.

2.5.3 Zinc, manganese, copper, calcium and nickel stock solutions

Standard zinc solution was prepared from reagent grade zinc nitrate in 10 mM HCl to prevent hydrolysis of the metal ion. Two methods were used to determinate the zinc concentration: cation exchange resin[2] and direct titration[3] with primary standard EDTA using Eriochrome Black T as the indicator. There was good agreement between the results of the two methods. Stock manganese solution was prepared from solid manganese nitrate purchased from Fisher and standardized in the same way as the zinc stock solution.

The copper, calcium and nickel stock solutions were prepared in 10 mM HCl from reagent grade copper nitrate and calcium chloride purchased from Fisher and nickel chloride purchased from Alfa. The solutions were standardized as described above for the aluminum stock solution.

2.6 Hydroxamate and immobilized hydroxamate

All hydroxamate ligands and chelating resins were synthesized in the Spilling lab at the University of Missouri-St Louis. The ligands were characterized using ^{1}H, ^{13}C, and ^{31}P NMR, mass spectrometry and elemental analysis. Sample solutions for potentiometric titrations were prepared by dissolving the solid ligands in 0.1 M KNO_3. Stock solutions containing 0.002 M concentrations of the trihydroxamate and monohydroxamate ligands were prepared in Millipore water for use in spectrophotometric studies.

2.7 Potentiometric titrations

The details of the methods employed have been previously described.[5] Measurements were made at 25.00 ± 0.05 °C in a sealed, water–jacketed glass vessel with a Teflon cap. The solution was maintained under an inert atmosphere of argon throughout the titration to avoid absorption of atmospheric CO_2. The typical sample volume was 50 mL. The hydrogen ion concentration was measured directly by use of an Accumet model 25 pH meter connected to a combination pH electrode. The ionic strength of each solution was initially adjusted to 0.100 M by the addition of the appropriate amount of 1.0 M KNO_3.

A computer-controlled autotitrator with operating software written at UM-St Louis was used to deliver the titrant and collect the potentiometric data. A Metrohm Dosimate 665 autoburet was used for titrant delivery. The titrator monitored the solution pH versus time. When the pH drift fell below a pre-set maximum, typically 0.001 pH/min, the pH and volume of titrant were recorded, and then the next aliquot of titrant was added. If equilibration was not reached in 10 minutes, the titrator recorded the pH

and proceeded with the addition of titrant. The data from unequilibrated solutions were excluded from any subsequent calculations of stability constants. The titrant in the potentiometric titrations was either KOH (referred to as a "forward" titration) or HCl (referred to as a "back" titration).

Before each sample titration, a titration of HCl with KOH was conducted to calibrate the pH electrode to give –log $[H^+]$ instead of –log a_{H^+}. The observed pH was plotted against the calculated p$[H^+]$ as shown in Figure 2.4 to give the linear calibration equation shown in Equation 2.2 that was used to convert the observed pH to –log $[H^+]$.

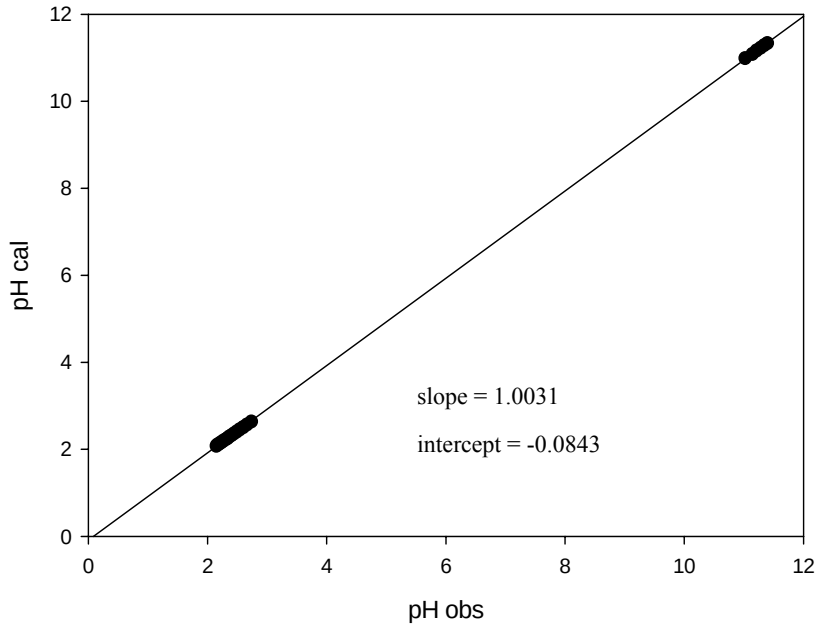

Figure 2.4 The observed pH and calculated p$[H^+]$ for an acid-base titration of HCl with KOH.

$$p[H] = \text{slope}\ (pH_{obs}) + \text{intercept} \qquad \text{Eq 2.2}$$

2.8 Calculations of protonation and stability constants

The various equilibria involving the protonation of the ligand and the formation of metal-ligand complexes can be described as overall stability constants by the general expressions shown in Equations 2.3 and 2.4, where the three basic components of metal ion, ligand and hydrogen ion are represented as M, L and H. Charges are omitted for simplicity.

$$iM + jL + kH \rightleftharpoons M_iL_jH_k \qquad \text{Eq 2.3}$$

$$\beta_{ijk} = \frac{[M_iL_jH_k]}{[M]^i[L]^j[H]^k} \qquad \text{Eq 2.4}$$

M is the hexaaquo metal ion, and L represents the fully deprotonated form of the ligand. The i, j and k values indicate the stoichiometric coefficients for metal, ligand and hydrogen ion in the complex.

Ligand protonation constants can be described as overall constants in terms of Equation 2.4, where the absence of a metal ion is represented by i = 0 as shown in Equations 2.5 and 2.6.

$$L^{n-} + kH^+ \rightleftharpoons H_kL^{(n-k)-} \qquad \text{Eq 2.5}$$

$$\beta_{01k} = \frac{[LH_k]}{[L]\,[H]^k} \qquad \text{Eq 2.6}$$

The hydrolysis of a metal ion is described by the reaction

$$M \overset{H_2O}{\rightleftharpoons} M(OH) + H^+ \qquad \text{Eq 2.7}$$

The equilibrium constants for these reactions can also be expressed using the formalism in Equation 2.4 by setting the stoichiometric coefficient of the ligand to j = 0, and assigning a negative coefficient to the hydrogen ion because it is a reaction product in Equation 2.7 and appears in the numerator rather than the denominator of the equilibrium expression in Equation 2.8.

$$\beta_{10\text{-}k} = \frac{[M(OH)_k[H]^k}{[M]} \qquad \text{Eq 2.8}$$

The potentiometric titration data were analyzed by the non-linear least squares program BETA to calculate ligand protonation constants and metal-ligand stability constants.[6] The program sets up mass balance equations for the total concentration of each component. As an example, consider a solution that contains Al^{3+} and the monoprotic ligand acetohydroxamic acid (HL). The mass balance equations for such a system would be

$$[Al]_{tot} = [Al^{3+}] + [Al(OH)^{2+}] + [Al(OH)_2^+] + [Al(OH)_3] + [Al(OH)_4^-] + [Al(L)^{2+}] + [Al(L)_2^+] + [Al(L)_3] \qquad \text{Eq 2.9}$$

$$[L]_{tot} = [L^-] + [HL] + [Al(L)^{2+}] + 2[Al(L)_2^+] + 3[Al(L)_3] \qquad \text{Eq 2.10}$$

$$[H]_{tot} = n[L]_{tot} + \text{added strong acid} + \text{added titrant}$$

$$= [H^+] - [OH^-] + [HL] - [Al(OH)^{2+}] - 2[Al(OH)_2^+] - 3[Al(OH)_3] - 4[Al(OH)_4] \qquad \text{Eq 2.11}$$

To begin a calculation, the operator provides values for all the β_{ijk} constants in the system. Some of these, such as the metal ion hydrolysis constants, are known and are input as fixed values. Others, such as the metal-ligand stability constants, are initial guesses that will be varied during the least squares refinement. The assignment of β_{ijk} values allows Equations 2.9–2.11 to be rewritten as

$$[\mathrm{M}]_{tot} = [Al] + \frac{\beta_{10-1}[Al]}{[H]} + \frac{\beta_{10-2}[Al]}{[H]^2} + \frac{\beta_{10-3}[Al]}{[H]^3} + \frac{\beta_{10-4}[Al]}{[H]^4} + \beta_{110}[Al][L] + \beta_{120}[Al][L]^2 + \beta_{130}[Al][L]^3 \quad \text{Eq 2.12}$$

$$[\mathrm{L}]_{tot} = [L] + \beta_{011}[L][H] + \beta_{110}[Al][L] + 2\beta_{120}[Al][L]^2 + 3\beta_{130}[Al][L]^3 \quad \text{Eq 2.13}$$

$$[\mathrm{H}]_{tot} = [H] - [OH] + \beta_{011}[H][L] - \frac{\beta_{10-1}[Al]}{[H]} - 2\frac{\beta_{10-2}[Al]}{[H]^2} - 3\frac{\beta_{10-3}[Al]}{[H]^3} - 4\frac{\beta_{10-4}[Al]}{[H]^4} \quad \text{Eq 2.14}$$

Thus we have a series of three simultaneous equations with three unknowns, the free component concentrations [Al], [L], and [H]. The program solves these simultaneous equations for each point in the potentiometric titration, and in doing so generates a value of pH_{calc} for each data point. After completing such a cycle of calculation, the program adjusts the values of the selected β_{ijk} values to reduce the sum of the squares of the residuals between the observed and calculated pH values. The program then returns to the beginning of the potentiometric data and uses these new values of β_{ijk}

to calculate a new set of pH_{calc} values. This calculation cycle is repeated until the variable β_{ijk} parameters converge to a consistent set of values. The quality of the final fit of the data is given by the goodness-of-fit parameter (GOF), which is defined as shown in Equation 2.15,

$$GOF = \sqrt{\frac{(pH_{obs} - pH_{calc})^2}{N_o - N_v}} \qquad \text{Eq 2.15}$$

where pH_{obs} and pH_{calc} are the observed and calculate pH, respectively, N_{obs} is the number of observations, and N_v is the number of adjustable parameters. The data were weighted by a factor related to the inverse of the slope of the titration curve at each point. This avoided giving undue weight to the large deviations in pH that occur near steep inflections in the titrations. For most calculations, the best model gave a GOF of less than 0.01. Metal hydrolysis constants[7] were included in all calculations of metal-ligand stability constants.

2.9 Potentiometric titration of hydroxamate resins

The loading of the resin-bound chelating groups was determined by potentiometric titration. An aqueous suspension of 20-25 mg of the resin was titrated as described above. The titration curve reflected the total protons that were titrated with KOH. This included the hydroxamate groups of the immobilized ligand, any HCl added to the sample, any free sulfonic acid groups ($-SO_3H$) remaining on the resin, and any carboxylate groups from the reaction intermediate that were not successfully converted to hydroxamic acids during the preparation of the resin. From the titration curve, the mmole

of ligand/gram resin was calculated by using the non-linear least squares program BETA to fit the titration data past the steep inflection to three protonation constants representing the immobilized hydroxamic acid. An elemental analysis of the resin to determine the percentage of nitrogen was also used to determine mmole of ligand/gram resin, since the immobilized ligand was the only source of nitrogen in the sample.

2.10 Spectrophotometric titration and pH dependence of Fe^{3+} complexes

The visible and ultraviolet absorption spectra of the ligand and the metal complexes were measured in 1.00 cm matched quartz cells using a Cary Model 100 recording spectrophotometer equipped with a cell holder maintained at 25.0 $\pm$ 0.1 C°. The 200 μM sample solution was prepared from stock solutions of the metal and ligand in 0.1 M KCl solution to maintain a constant 0.1 M ionic strength.

The investigation consisted of a series of spectrophotometric titrations that covered a pH range from 0.3 to 7.0. The pH of the sample was adjusted by using HCl or NaOH, the solution was allowed to equilibrate, and the absorbance spectrum was recorded. For the very low pH values, the pH was calculated directly from the known molarity of strong acid added to the sample, since experimental pH readings at extremely low pH are not accurate. The total Fe^{3+} concentration used in the spectrophotometric measurements was ~200 μM, and the Fe-ligand ratios were adjusted in the range 1:1.12 to 1:2.

Stability constants were calculated from the spectrophotometric data by the use of the commercial software SPECFIT. This program is used to analyze families of spectra to determine equilibrium constants. As with the non-linear least squares program BETA, the

program sets up appropriate mass balance equations for total metal and total ligand. For each spectrum, the program calculates the concentrations of all the metal complexes based on the experimental pH and a set of initial guesses for the binding constants. It then uses these concentrations and the absorbance spectrum of each individual complex to calculate an absorbance spectrum for the sample. The absorbance spectrum of each individual complex can either be measured independently and input as a fixed value, or it can treated as an adjustable parameter in the least squares fit.

SPECFIT uses a set of initial parameters to calculate an absorbance spectrum corresponding to each member of a family of spectra. It then uses non-linear least squares to adjust the values for any adjustable β_{ijk} values and any adjustable spectra for specific complexes to minimize the sum of the squares of the residuals between the observed and calculated absorbance values at all wavelengths. This cycle of parameter adjustment continues until the calculation converges on a consistent set of parameters.

2.11 Spectrophotometric studies of Al^{3+} binding by calcein

The direct titration of calcein was monitored by difference spectroscopy. Equal volumes of a solution of ~7.5 μM calcein in HEPES buffer at pH 8 was loaded into both sample and reference cuvettes, and a spectrophotometric baseline was recorded. Aliquots of 50 μM Al^{3+} were then added to the sample cuvette, while an equal volume of water was added to the reference cuvette. After each addition, the solution was allowed to equilibrate for 1 hr, after which the difference spectrum, which represented the perturbations caused by the binding of Al to calcein, was recorded.

In these studies, the Al-calcein complex formed in competition with the formation

of the $Al(OH)_4^-$ complex from hydrolysis. Binding constants for Al-calcein were calculated using SPECFIT based on the known β_{10-4} value for $Al(OH)_4^-$. In this type of experiment, SPECFIT adjusted the analytical value for $[M]_{tot}$ in the mass balance equations to account for the varying amounts of Al^{3+} that have been added at each point in the titration. Since all the data are collected at one pH, one calculates an effective binding constant for the Al-calcein complex that is valid only at the experimental pH.

2.12 Spectrophotometric competition of Al^{3+} and calcein with HEDTA

An effective binding constant for Al-calcein at pH 8.0 was also determined by spectrophotometric competition with the well-characterized chelating agent HEDTA. The spectrophotometric baseline was set with equal volumes of 25 μM calcein in the sample and reference cuvettes. A total of 5 μM Al^{3+} was added to the sample cuvette, and the total volume of the reference cuvette was adjusted by adding distilled water. The sample was allowed to equilibrate for one hour. The Al-calcein sample was then titrated with 0.005 M HEDTA in HEPES buffer at pH 8, while equal volumes of the HEPES buffer were added to the reference cuvette. The absorbance spectrum of the sample was recorded after each addition of HEDTA.

In a second series of experiments, an equilibrated solution of Al-calcein was placed in both sample and reference cuvettes to set the baseline. The sample cuvette was then titrated with HEDTA, while equal volumes of HEPES buffer were added to the reference cuvette.

2.13 Spectrophotometric competition of Al^{3+} and calcein with gluconic acid

In these studies gluconic acid was used as a competitive ligand versus Al-calcein. The concentration of Al^{3+} used in the spectrophotometric measurements was ~2.5 μM with a 1:10 ratio of Al^{3+}:calcein. In these experiments, calcein was used in both cuvettes to set the spectrophotometric baseline. Aluminum was added to the sample cuvette and allowed to equilibrate for 1 hr before the sample cuvette was titrated with 0.05 M gluconate solution in HEPES buffer at pH 8.

2.14 Spectrophotometric assays of Al^{3+} binding to the chelating resin

Solutions containing 150 μM concentrations of Al^{3+} and the chelating agent ferron, 7-iodo-8-hydroxyquinoline-5-sulfonic acid , in a 50 mM pH 5 acetate buffer were prepared in a 1 cm quartz cuvette. The absorbance spectrum of the resulting mixture of Al-ferron complexes was recorded using a Hewlett Packard Model 8254A diode array spectrophotometer equipped with a thermostated sample chamber connected to a circulating water bath. A weighed sample of the solid chelating resin was added to the cuvette. As the Al^{3+} was removed from the ferron and bound by the resin, the absorbance was monitored. There was a decrease in the absorbance of the Al-ferron complexes and an increase in the absorbance of free ferron. Control experiments were run using EDTA to remove the Al^{3+} from ferron.

References

1. Rossotti, F. J. C.; Rossotti, H. *J. Chem. Ed*. 1965, 42, 375.

2. Harris, W. R.; Sheldon, J. *Inorg. Chem.* 1990, 29, 119.

3. Welcher, T. J. *The analytical use of ethylenediamine tetraacetic acid,* Van Nostrand, Princeton, 1958.

4. Athanasopulos, N. *Flame methods manual for atomic absorption*, GBC Scientific Equipment Pty Ltd., Victoria, Australia.

5. Martell, A. E.; Motekaitis, R.J. *Determination and use of stability constants,* VCH Publishers, New York, 1988.

6. Harris, W. R.; Carrano, C. J.; Cooper, S. R.; Sofen, S. R.; Avdeef, A. E.; McArdle, J. V.; Raymond, K. N. *J. Am. Chem. Soc.* 1979, 101, 6097.

7. Bases, C. F.; Mesmer, R. E. *The hydrolysis of cations,* New York: Wiley and Sons, 1967.

8. Martell, A. E.; Smith, R. M. NIST *Critical stability constants of metal complexes*, NIST Standard Reference Database 46, Version 5.0, 1998

Chapter 3

Stability constants of hydroxamate ligands with trivalent metal ions

3.1 Introduction

There is presently a need in several areas for a rational approach toward ligand design for the selective complexation of metal ions in solution. Potential applications include iron removal in the treatment of thalassemia[1] and the treatment of Al^{3+} toxicity.[2] In general, there are several factors that are considered in the design of new ligands, including high selectivity toward the target metal ion, low toxicity, high oral bioavailability, and low cost. Therefore, there has been considerable interest in the development of inexpensive, orally active compounds for the treatment of metal toxicity. Effective chelation therapy has been studied with different types of donor groups with a high affinity for trivalent metal ions (e.g. Fe^{3+}, Al^{3+}) such as catecholates,[3] phenolates,[4] phosphonates[5] and hydroxamates.[6]

Hydroxamic acids have been shown to possess diverse biological activities and commonly form strong complexes with trivalent metal ions, such as Al^{3+}, La^{3+}, Fe^{3+} and In^{3+}.[7] There is a strong correlation between the affinity of metals ions for OH^- and the affinity for hydroxamate ligands. The affinity for OH^- is expressed by $K_1(OH^-)$, which it defined as

$$M^{n+} + OH^- \rightleftharpoons M(OH^-)^{n-1} \qquad \text{Eq 3.1}$$

As shown in Figure 3.1, there is a good linear relationship between log $K_1(OH^-)$ and log K_1 for the monohydroxamate ligand, acetohydroxamic acid (AHA), log K_1 for the dihydroxamate ligand, C_8DHA, and log K_1 for the trihydroxamate ligand, N,N′,N″-tris[2-(N-hydroxycarbamoyl)ethyl]-1,3,5-benzenetricarboxamide (BAMTPH). The binding affinity and selectivity for trivalent metal ions increases with the number of hydroxamate groups in the ligand.

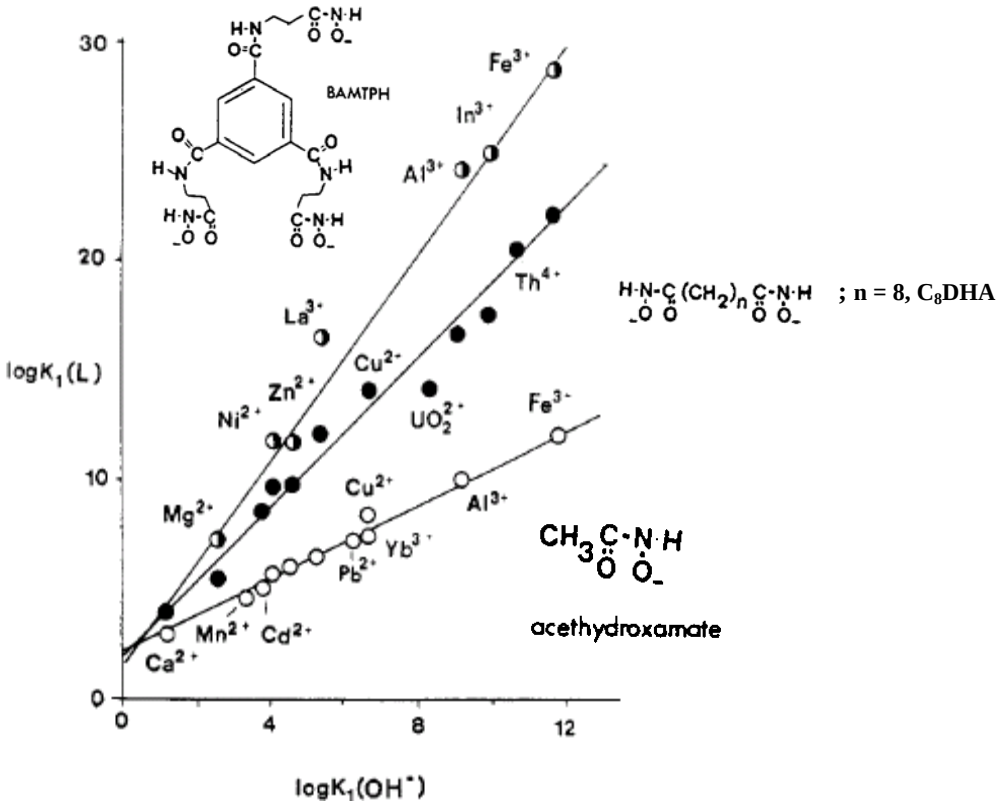

Figure 3.1 Correlation between log K_1 (OH^-) values and the stability constants for hydroxamic acid ligands.[7]

The natural linear trihydroxamic acid desferrioxamine shown in Figure 3.2 has been widely used in chelation therapy to remove excess iron in patients suffering from

iron overload associated with thalassamia[8-10] and to remove Al^{3+} from patients who must undergo permanent hemodialysis.[9-12] Therefore, complexation studies of new hydroxamic acid ligands with Al^{3+} and Fe^{3+} are of interest in the development of new chelation therapy agents.

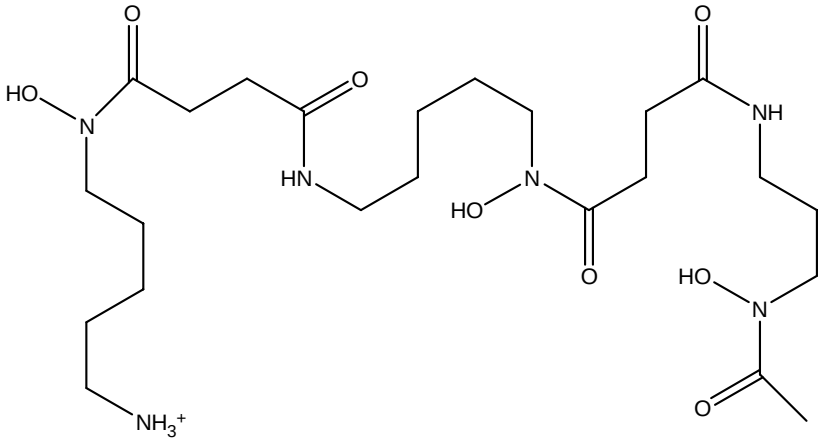

Figure 3.2 Structure of DFO.

In this chapter, equilibrium studies have been performed on the Al^{3+} and Fe^{3+} complexes of series of new ligands containing one, two and three hydroxamic acid groups.

Result and Discussion

3.2 Ligand properties

3.2.1 Acid-base properties of the trihydroxamate ligand, 2,2,2-THA

The fully protonated form of 2,2,2-THA is shown in Figure 3.3.

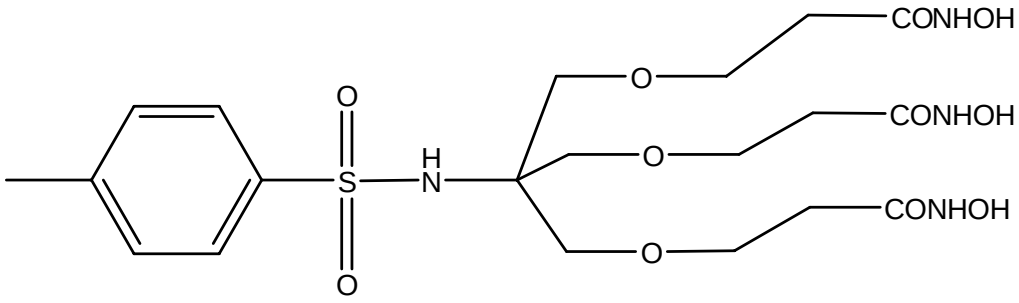

Figure 3.3 Structural formula of 2,2,2-THA.

The ligand contains three hydroxamic acid groups, all of which would be deprotonated over the pH range of typical potentiometric titrations. For this reason, we described the ligand as H_3L. The compound 2,2,2-THA is not very soluble at low pH, but it readily dissolves above pH 5. A potentiometric titration of the completely protonated ligand with potassium hydroxide revealed that three protons are released in the pH range 5-11.4. The potentiometric equilibrium curve of the free ligand is shown in Figure 3.4. These titration data were used to calculate the three ligand protonation constants listed in Table 3.1. The least squares fit was very good with GOF = 0.0075.

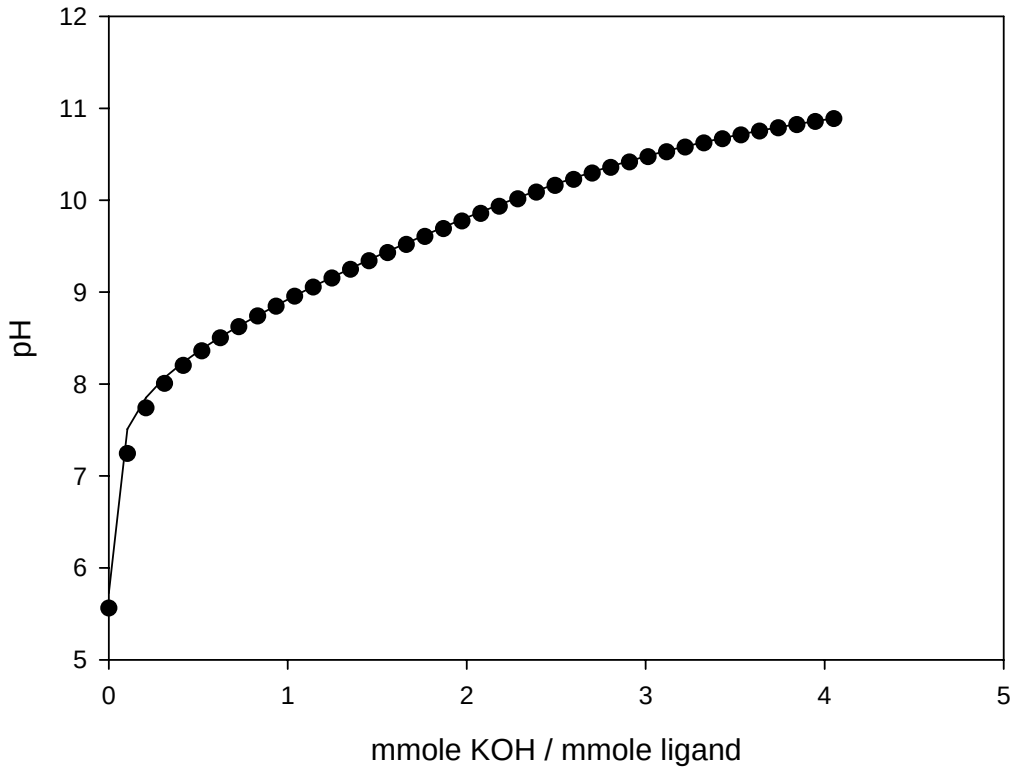

Figure 3.4 Potentiometric titration curve of 2,2,2-THA. The symbols represent the observed data points while the line represents the least squares fit based on the ligand protonation constants, listed in Table 3.1.

The stepwise protonation constants are describes as shown in Equation 3.2.

$$H^+ + H_{n-1}L \xrightarrow{\text{Log } K_n} H_nL \qquad \text{Eq 3.2}$$

The three protonation constants for 2,2,2-THA fall in the normal range for hydroxamic acids.[13-15] The values are slightly higher than the protonation constants for desferrioxamine B, as shown in Table 3.1. The absence of the cationic $-NH_3^+$ group in 2,2,2-THA probably decreases the acidic character of the OH groups compared to DFO.[16]

log K_n	DFO	2,2,2-THA	Δ log K for DFO B	Δ log K for 2,2,2-THA
log K_1	9.55	10.26 ± 0.08	-	-
log K_2	8.96	9.42 ± 0.11	0.59	0.84
log K_3	8.32	8.47 ± 0.16	0.64	0.95

Table 3.1 Stepwise protonation constants (log K_n) of the hydroxamic acid groups in 2,2,2-THA and desferrioxamine as H_3L ligands.[17]

In general, for any ligand containing three identical functional groups, one might expect the protonation constants of each functional group to be identical. However, the protonation constants are macroscopic constants that represent the total ligand, not a single functional group. The protonation constants are affected by statistical factors based on the number of functional groups in the ligand.[8] For any H_3L ligand with three identical, non-interacting functional groups, the statistical factor would lead to a separation of 0.48 log units between successive stepwise protonation constants. If a ligand has Δ log K values larger than 0.48, this indicates that the functional groups are interacting with one another. As shown in Table 3.1, the Δ log K values for 2,2,2-THA are significantly greater than the statistical factor of 0.48. Thus the deprotonation of one hydroxamic acid group of 2,2,2-THA affects the acidity of the other hydroxamic acids groups. This likely reflects a combination of long-range electrostatic effects as well as intramolecular hydrogen bonding as shown in Figure 3.5.

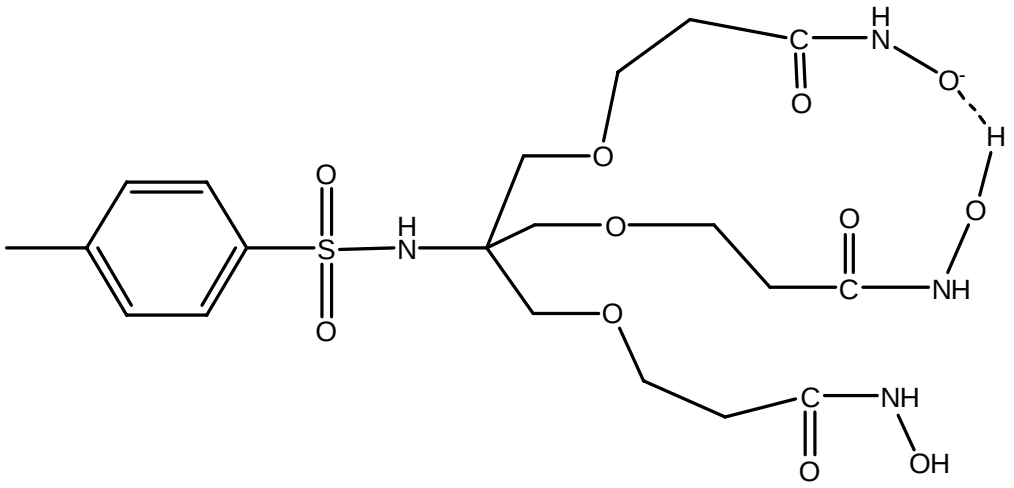

Figure 3.5 Possible intramolecular hydrogen bonding for partially deprotonated 2,2,2-THA.

3.2.2 Acid-base properties of di- and monohydroxamate ligands, 2,2-DHA and 2-HA

The structures of 2,2-DHA and 2-HA are shown in Figure 3.6 along with the structures of the known dihydroxamate ligand, rhodotorulic acid (RA) and the monohydroxamate ligand acetohydroxamic acid (AHA). The protonation constants of 2,2-DHA and 2-HA ligands have been determined by potentiometric titration. 2,2-DHA and 2-HA are, respectively, diprotic (H_2L) and monoprotic (HL) acids.

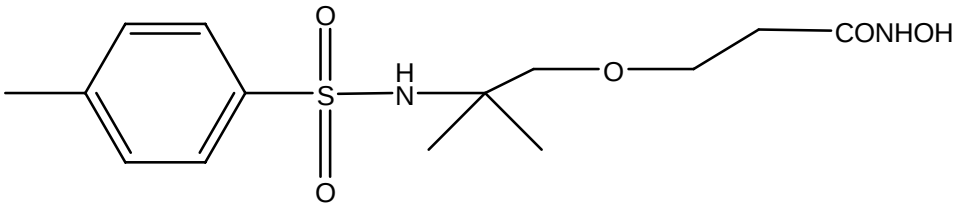

2-HA

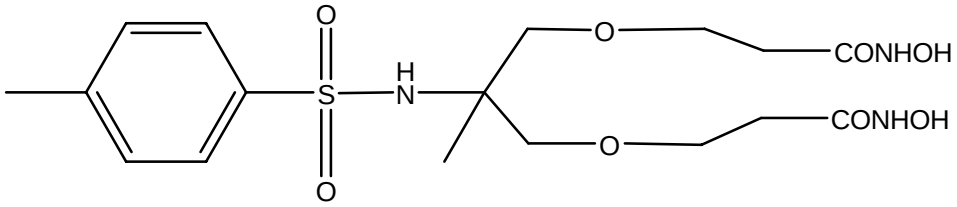

2,2-DHA

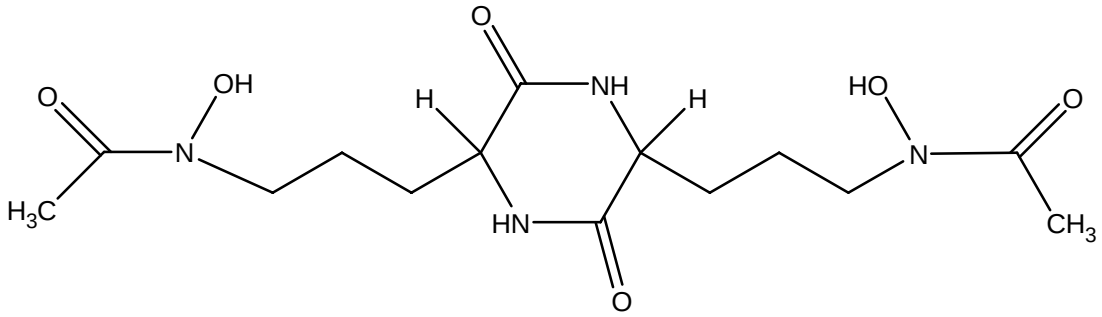

Rhodotorulic acid (RA)

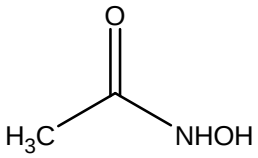

Acetohydroxamic acid (AHA)

Figure 3.6 Structures of 2,2-DHA , 2-HA, rhodotorulic acid (RA) and acetohydroxamic acid (AHA).

Titration curves for the free ligands, 2,2-DHA and 2-HA, are shown in Figure 3.7. The protonation constants of 2,2-DHA and 2-HA are listed in Table 3.2. This table also lists protonation constants for rhodotorulic acid (RA), and acetohydroxamic acid (AHA). The protonation constants for 2,2-DHA and 2-HA are consistent with the reported values for RA and AHA.[19-21]

The statistical considerations discussed above for the 2,2,2-THA ligand also apply to 2,2-DHA. For a molecule with two identical and noninteracting acid sites, the statistical factor leads to a difference in the two stepwise protonation constants of 0.60 log units.[18] The two log K values for 2,2-DHA differ by 1.1 log units, which indicates that the hydroxamate groups of 2,2-DHA are interacting to each other.

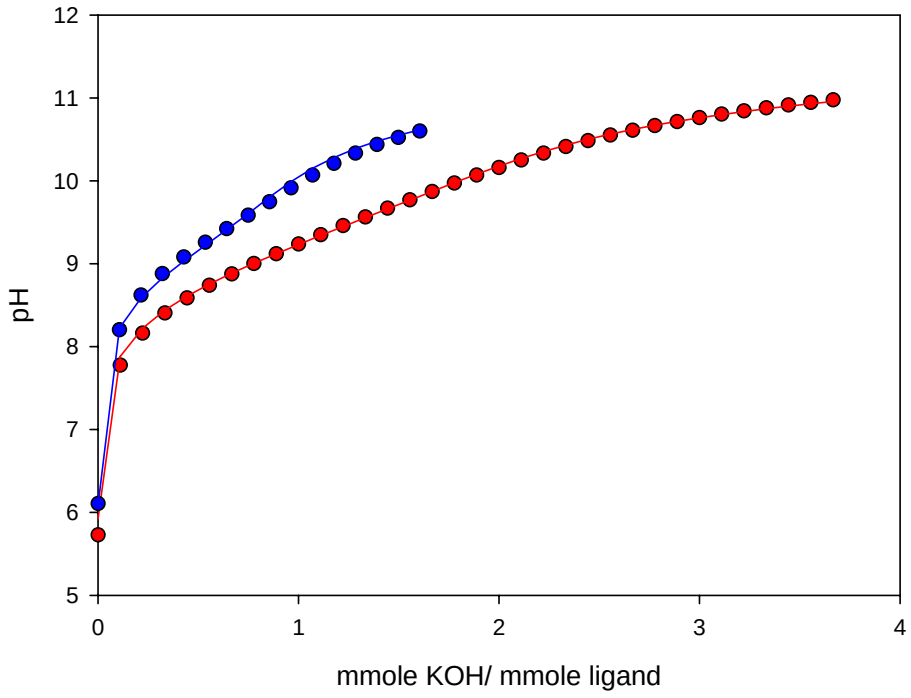

Figure 3.7 Potentiometric titration curves of 2,2-DHA (red) and 2-HA (blue). The symbols represent the observed data points while the lines represents the least squares fit based on the ligand protonation constants listed in Table 3.2.

	AHA	2-HA	RA	2,2-DHA
Log K_1	9.35	9.26 $\pm$ 0.06	9.44	9.80 $\pm$ 0.06
Log K_2	-	-	8.49	8.69 $\pm$ 0.05

Table 3.2 Stepwise protonation constants (log K_n) of the hydroxamic acid groups in 2,2-DHA, 2-HA, RA[19] and AHA.[20]

3.3 Metal complexation equilibria for Al^{3+}

3.3.1 Binding of Al^{3+} by 2,2,2,-THA, 2,2-DHA and 2-HA

The potentiometric titration curve for a 1:1 solution of Al^{3+} and 2,2,2-THA from pH 2 to 4.8 is shown by the red symbols in Figure 3.8. There is a sharp inflection at 2.0 equiv of base, indicating the liberation of two protons upon complexation of Al^{3+}. Since the ligand contains three hydroxamate groups, the release of only two protons upon the binding of Al^{3+} indicates that the Al^{3+} is coordinating to only two of the three hydroxamate groups, and one group is remaining as a non-coordinated, protonated hydroxamic acid. This low-pH complex is designated as $AlLH^+$. For convenience, complexes will often be identified in terms of the stoichiometric coefficients for Al^{3+}, ligand, and protons. For example, the $AlLH^+$ species would also be designated as the 111 complex of 2,2,2-THA.

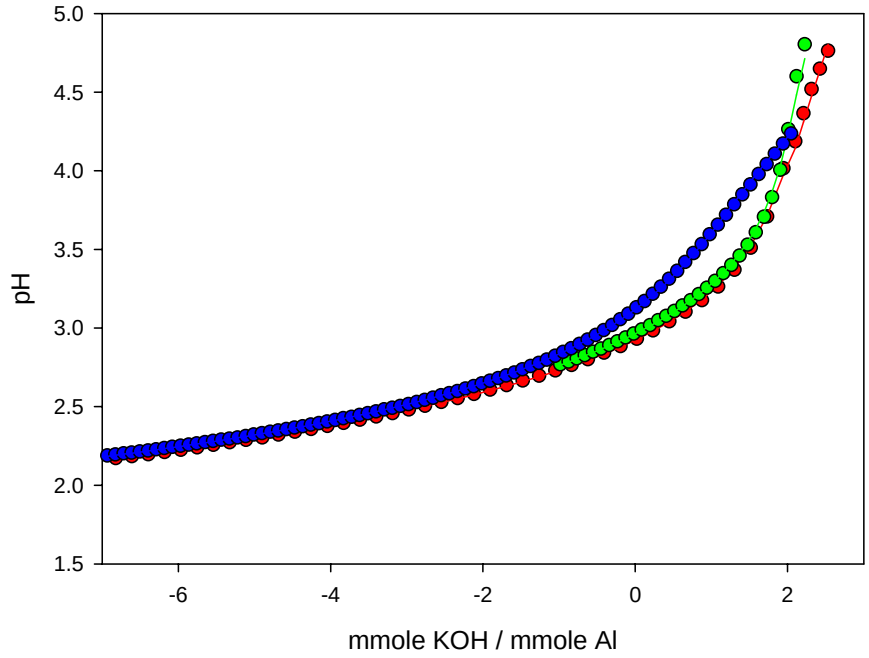

Figure 3.8 Potentiometric titration curves of Al^{3+} with 2,2,2-THA (red), 2,2-DHA (green) and 2-HA (blue). The symbols represent the observed data points while the lines represent the least squares fit based on the ligand protonation constants, the Al^{3+} hydrolysis constants and the stability constants listed in Tables 3.3 and 3.4.

The further addition of base beyond two equiv leads to the release of additional protons. However, the titration is terminated at ~2.5 equiv by precipitation. The IR spectrum of the precipitate was compared to a precipitate of $Al(OH)_3$. The spectra showed that the precipitate in the presence of 2,2,2-THA is not $Al(OH)_3$. Instead, the precipitate is presumed to be the neutral complex AlL (the 110 complex).

The data from several titrations of Al^{3+} with 2,2,2-THA were analyzed by non-linear least squares. The calculations included the ligand protonation constants and aluminum hydrolysis constants from Table 3.3 as fixed parameters. The binding

constants for Al^{3+} with 2,2,2-THA were treated as adjustable parameters in the minimization of the sum of the squares of the residuals between the observed and calculated pH values in the titration curve. Various combinations of β_{112}, β_{111} and β_{110} were tested. The best fit was obtained for the combination of β_{111} and β_{110}, which resulted in a very low GOF of 0.006. The final values of β_{111} and β_{110} are shown in Table 3.3, and the proposed structures of the 110 and 111 complexes are shown in Figure 3.9.

System	i	j	k	reaction	log β_{ijk}	σ
2,2,2-THA	0	1	1	$L^{3-} + H^{+} \rightleftharpoons HL^{2-}$	10.26	
	0	1	2	$L^{3-} + 2H^{+} \rightleftharpoons H_2L^{-}$	19.68	
	0	1	3	$L^{3-} + 3H^{+} \rightleftharpoons H_3L$	28.15	
2,2-DHA	0	1	1	$L^{2-} + H^{+} \rightleftharpoons HL^{-}$	9.80	
	0	1	2	$L^{2-} + 2H^{+} \rightleftharpoons H_2L$	18.49	
2-HA	0	1	1	$L^{-} + H^{+} \rightleftharpoons HL$	9.26	
Al-OH^{-}	1	0	-1	$Al^{3+} \rightleftharpoons AlOH^{2+} + H^{+}$	-5.24	
	1	0	-2	$Al^{3+} \rightleftharpoons Al(OH)_2^{+} + 2H^{+}$	-10.54	
	1	0	-3	$Al^{3+} \rightleftharpoons Al(OH)_3 + 3H^{+}$	-15.74	
	1	0	-4	$Al^{3+} \rightleftharpoons Al(OH)_4^{-} + 4H^{+}$	-23.49	
Al-2,2,2-THA	1	1	1	$Al^{3+} + L^{3-} + H^{+} \rightleftharpoons AlLH^{+}$	26.27 *	0.02
	1	1	0	$Al^{3+} + L^{3-} \rightleftharpoons AlL$	21.44 *	0.06
Al-2,2-DHA	1	1	-1	$Al^{3+} + L^{2-} \rightleftharpoons AlLOH + H^{+}$	11.06*	0.13
	1	1	0	$Al^{3+} + L^{2-} \rightleftharpoons AlL^{+}$	16.07*	0.09

Table 3.3 Variable (*) and fixed parameters for the least squares refinement of the potentiometric titration data for Al-2,2,2-THA and Al-2,2-DHA.

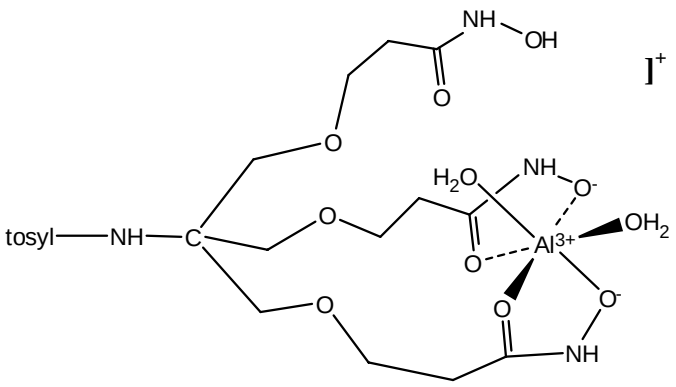

111 complex

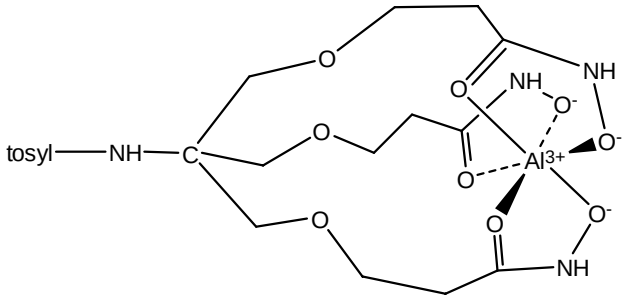

110 complex

Figure 3.9 Proposed structures of the 110 and 111 complexes of Al^{3+} and 2,2,2-THA.

The titration of Al^{3+} with 2,2-DHA is shown in Figure 3.8. The curve for a 1:1 ratio of Al^{3+} with 2,2-DHA shows the complete formation of the fully deprotonated complex AlL^{+} at 2 equiv of base. Precipitation occurs as the pH increases above 4.8. As with 2,2,2-THA, different models were used to fit the data. The best model included β_{110} and $\beta_{11\text{-}1}$ as the adjustable parameters, with a GOF of 0.007. Values for β_{110} and $\beta_{11\text{-}1}$ are listed in Table 3.3 and the proposed structures of the 110 and 11-1 complexes of Al^{3+} with 2,2-DHA are shown in Figure 3.10.

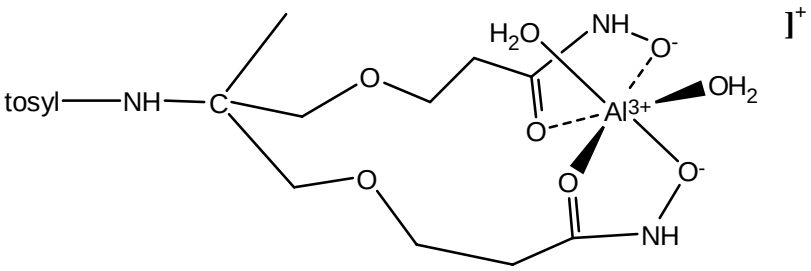

110 complex

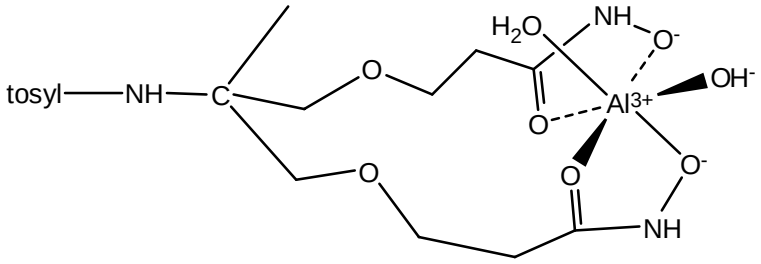

11-1 complex

Figure 3.10 Proposed structures of the 110 and 11-1 complexes of Al^{3+} with 2,2-DHA.

The potentiometric titration curve of a 3:1 ratio of 2-HA and Al^{3+} is shown in Figure 3.8. An inflection is observed at 2.0 equiv of base, with precipitation observed above pH 4.3. In general, the release of two protons upon complexation by this mono-hydroxamate ligand reflects the formation of the 110 and 120 complexes in the solution. Therefore, the titration data were initially fit with a model that contained the 110 and 120 complexes. The ligand protonation constants and the aluminum hydrolysis constants were used as fixed parameters in the least squares fit. However, this model had a large GOF as shown for model 1 in Table 3.4.

Because of the poor fit to the first model, the additional metal-ligand complexes 11-1, 11-2 and 12-1 were also considered. The 11-1 complex and the 120 complex both involve the release of 2 protons per metal ion, and we found that we could not include both these complexes in the same model because there was always a very high correlation between log β_{120} and log $\beta_{11\text{-}1}$. The 120 species was retained in the models and the 11-1 species was eliminated.

Two models were found to give equally good fits of the data. Model 2 included the complexes 110, 120, and 11-2. Model 3 consisted of the complexes 110, 120, and 12-1. As shown in Table 3.4, the GOF values and the correlation coefficients are similar for these two models. A previous study on Al^{3+} complexation by AHA reported a 12-1 complex,[22] but there appears to be no literature reports of a 11-2 complex. Therefore, model 3 in Table 3.4 is considered to be the best description of Al^{3+} binding by 2-HA.

Species	Model 1	Model 2	Model 3
110	8.54 ± 0.12	8.80 ± 0.02	8.76 ± 0.03
120	16.87 ± 0.10	16.53 ± 0.06	16.47 ± 0.02
11-2		0.10 ± 0.02	
12-1			12.30 ± 0.06
GOF	0.0357	0.004	0.004
Correlation coefficient	0.5806	-0.8167	-0.8286

Table 3.4 Various equilibrium models for Al^{3+} and 2-HA.

The calculated binding constants from Tables 3.3 and 3.4 have been used to calculate the distribution of species as a function of pH for a solution of 10 µM Al^{3+} with 10 µM 2,2,2-THA, 10 µM 2,2-DHA and 30 µM 2-HA. These dilute concentrations are representative of physiological conditions. The metal hydroxo species were included in the speciation models. The results are shown in Figures 3.11-3.13.

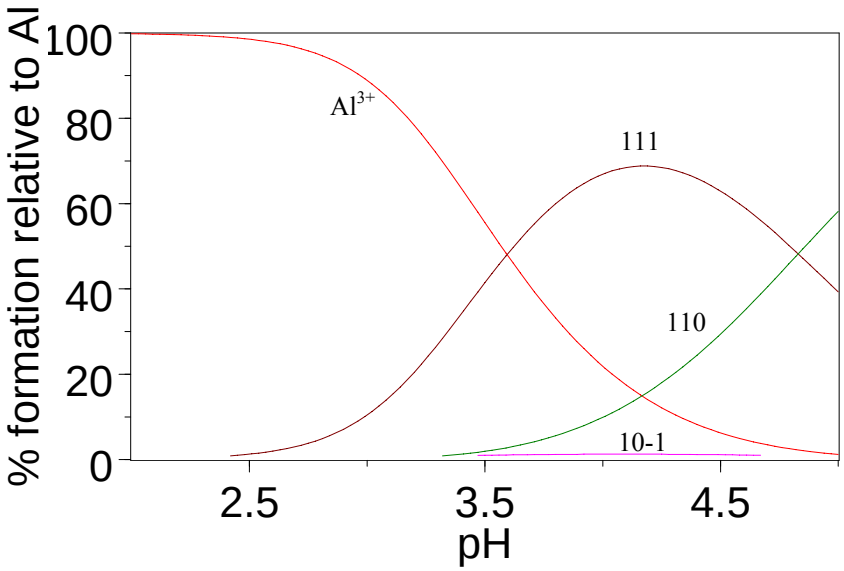

Figure 3.11 Species distribution diagram for 10 µM Al^{3+} and 10 µM 2,2,2-THA as a function of pH.

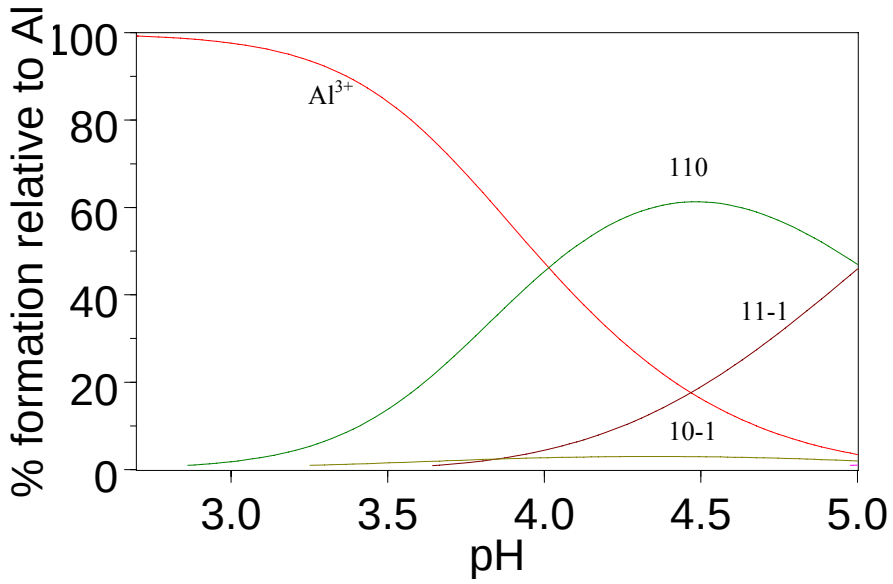

Figure 3.12 Species distribution diagram for 10 µM Al^{3+} and 10 µM 2,2-DHA as a function of pH.

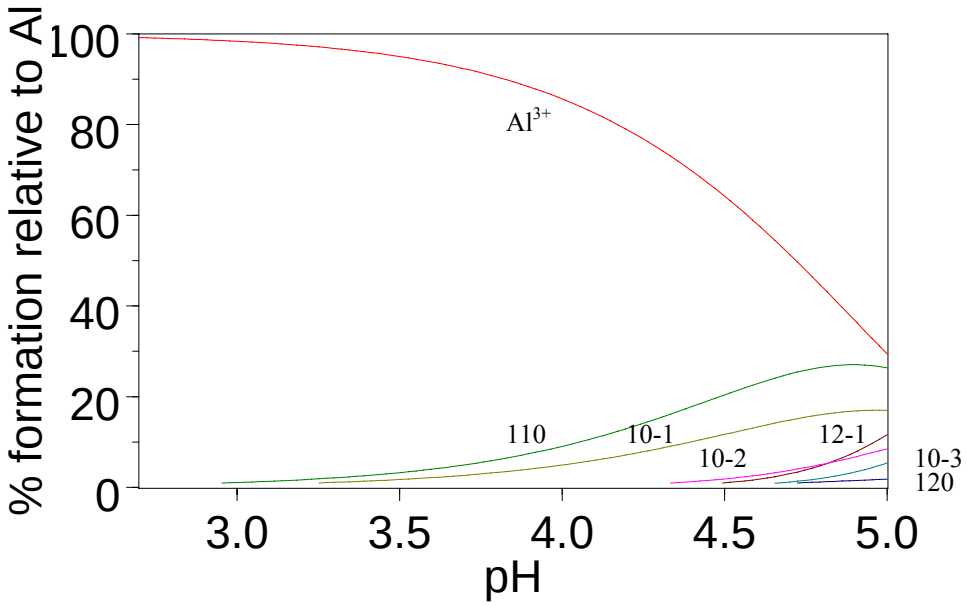

Figure 3.13 Species distribution diagram for 10 µM Al^{3+} and 30 µM 2-HA as a function of pH.

In the case of Al-2,2,2-THA (Figure 3.11), the dominating species between pH 3.2-4.7 is the 111 complex, which accumulates to a maximum of 70% of the total Al^{3+} at pH 4.2. As the pH increases above 4.2, the 111 complex deprotonates to form the 110 complex. For 2,2-DHA, the speciation calculation indicates that the 110 complex predominates between pH 4 and 5. The deprotonated species 11-1 was found at pH above 4.0 (Figure 3.12).

The species distribution diagram of the Al-2-HA system at a 1:3 ratio of metal:ligand is shown in Figure 3.13. There are six species, 110, 12-1, 120, 10-1, 10-2 and 10-3, present in the pH range 4 to 5. The 110 complex reaches a maximum of 25% of the total Al^{3+} at pH 4.8 with a mixture of the remaining species.

3.4 Metal complexation equilibria for Fe^{3+}

3.4.1 Complexation of Fe^{3+} by 2,2,2-THA

The complexation of Fe^{3+} by 2,2,2-THA was studied by potentiometry as with Al^{3+}. The potentiometric titration curve of a 1:1 mixture of Fe^{3+} and 2,2,2-THA with excess acid added to the solution is shown in Figure 3.14. The initial pH is quite low and remains low as base is added, indicating the formation of a strong complex. The pH increases rapidly at 3.0 equiv of base, and the titration is terminated by precipitation at pH 5.

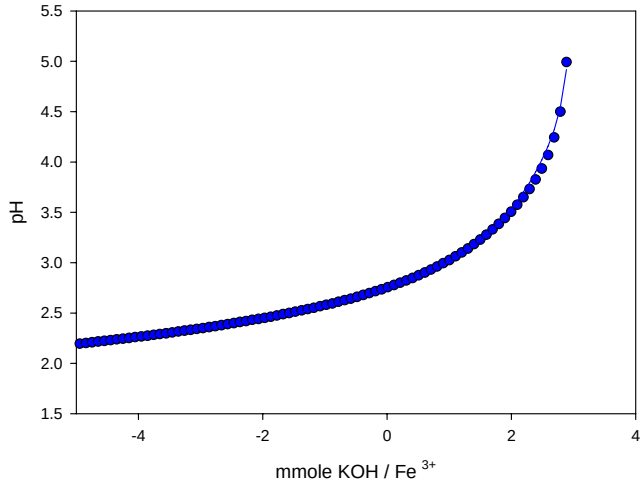

Figure 3.14 Potentiometric titration curve of Fe^{3+} with 2,2,2-THA. The symbols represent the observed data points while the line represents the least squares fit based on the ligand protonation constants, the Fe^{3+} hydrolysis constants and the stability constants listed in Table 3.5.

System	i	j	k	reaction	log β_{ijk}
2,2,2-THA	0	1	1	$L^{3-} + H^{+} \rightleftharpoons HL^{2-}$	10.26
	0	1	2	$L^{3-} + 2H^{+} \rightleftharpoons H_2L^{-}$	19.68
	0	1	3	$L^{3-} + 3H^{+} \rightleftharpoons H_3L$	28.15
$Fe\text{-}OH^{-}$	1	0	-1	$Fe^{3+} \rightleftharpoons FeOH^{2+} + H^{+}$	-2.68
	1	0	-2	$Fe^{3+} \rightleftharpoons Fe(OH)_2^{+} + 2H^{+}$	-6.41
	1	0	-3	$Fe^{3+} \rightleftharpoons Fe(OH)_3 + 3H^{+}$	-12.74
	1	0	-4	$Fe^{3+} \rightleftharpoons Fe(OH)_4^{-} + 4H^{+}$	-22.09
Fe-2,2,2-THA	1	1	1	$Fe^{3+} + L^{3-} + H^{+} \rightleftharpoons FeL^{+}$	27.60*
	1	1	0	$Fe^{3+} + L^{3-} \rightleftharpoons FeL$	23.78*

Table 3.5 Variable (*) and fixed parameters for least squares refinement of the potentiometric titration data for Fe-2,2,2-THA.

The data in Figure 3.14 were fit using the Fe^{3+} hydrolysis constants and ligand protonation constants as fixed parameters. Various equilibrium models were tested. The model with β_{110} and β_{111} as adjustable parameters gave the best fit with a GOF of 0.005. However, there was a high correlation between the values of β_{110} and β_{111}. Inspection of the calculations indicated that this was due to a very low concentration of free Fe^{3+} at all experimental pH values. Under these conditions, the potentiometric results give the chelate protonation constant for the protonation of the 110 complex to give the 111 complex, but we cannot get a reliable calculation of the absolute value of β_{110}.

Due to this limitation of the potentiometric method, a spectrophotometric titration was used to determine the binding constants of the Fe-2,2,2-THA complexes. The absorption spectra represent a ligand-to-metal charge transfer band for the hydroxamate groups coordinated to Fe^{3+}. One advantage of the spectrophotometric method is that the system can be studied at very low pH, where there is sufficient dissociation of free Fe^{3+}. In addition, the λ_{max} for the charge transfer band provides an indication of the number of hydroxamate groups coordinated to Fe^{3+} at any given pH.

3.4.2 Spectrophotometric studies of mono- bis- and trishydroxamate complexes of Fe^{3+}.

3.4.2.1 Metal-binding properties of iron with 2,2,2-THA and DFO

In order to evaluate the Fe^{3+} binding properties of 2,2,2-THA, the binding of DFO with Fe^{3+} was studied to establish the λ_{max} value for the charge transfer band when three hydroxamate groups are bound to Fe^{3+}. UV-vis spectrophometric titrations were initially performed by adding aliquots of Fe^{3+} to DFO solution. However, to avoid long

equilibration time, these titrations were repeated using ferrous ion. In the presence of DFO, there is rapid air oxidation and binding of the added ferrous ion as Fe^{3+}.

The addition of sequential aliquots of iron solution to DFO produced a single absorbance band at 430 nm as shown in Figure 3.15. This value of λ_{max} is indicative of the coordination of three hydroxamate groups.

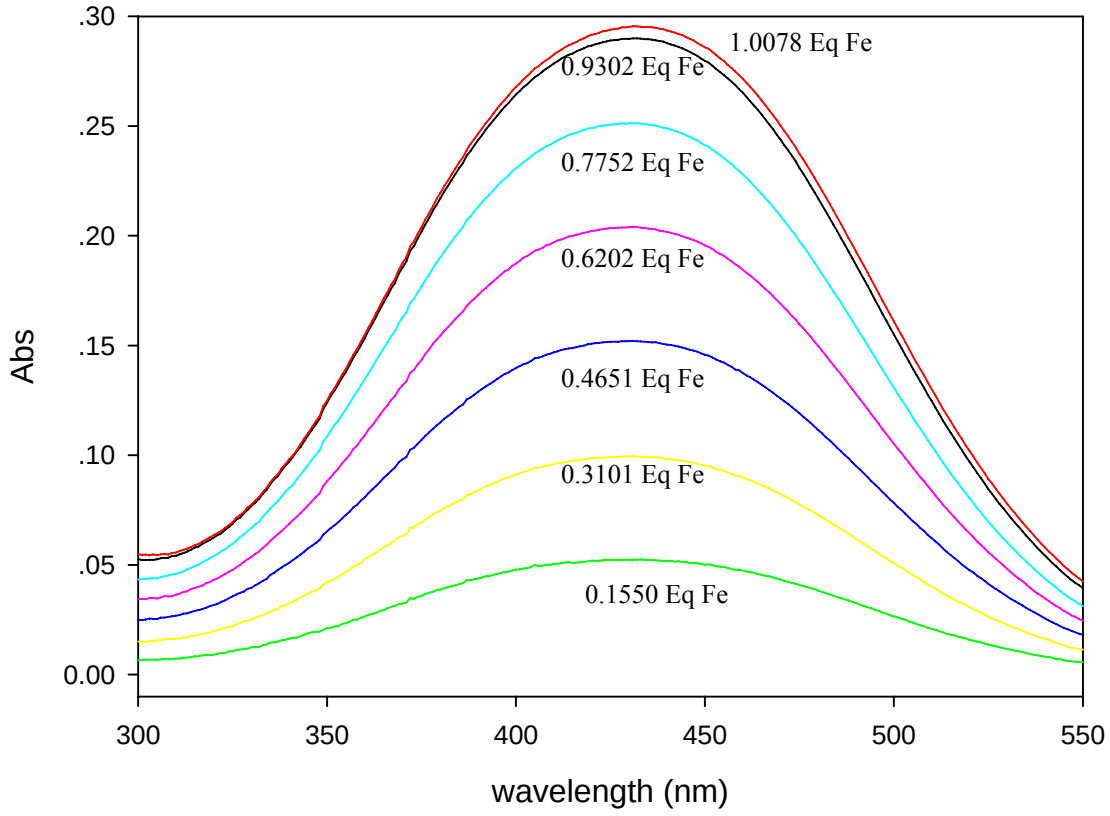

Figure 3.15 Titration of DFO with iron at pH 6.

A solution of 2,2,2-THA was also titrated with Fe^{2+} as described above for DFO. The spectra show the ligand-to-metal charge transfer band at 430 nm, as shown in Figure 3.16, indicating that 2,2,2-THA also binds iron through all three hydroxamate groups at pH 6.

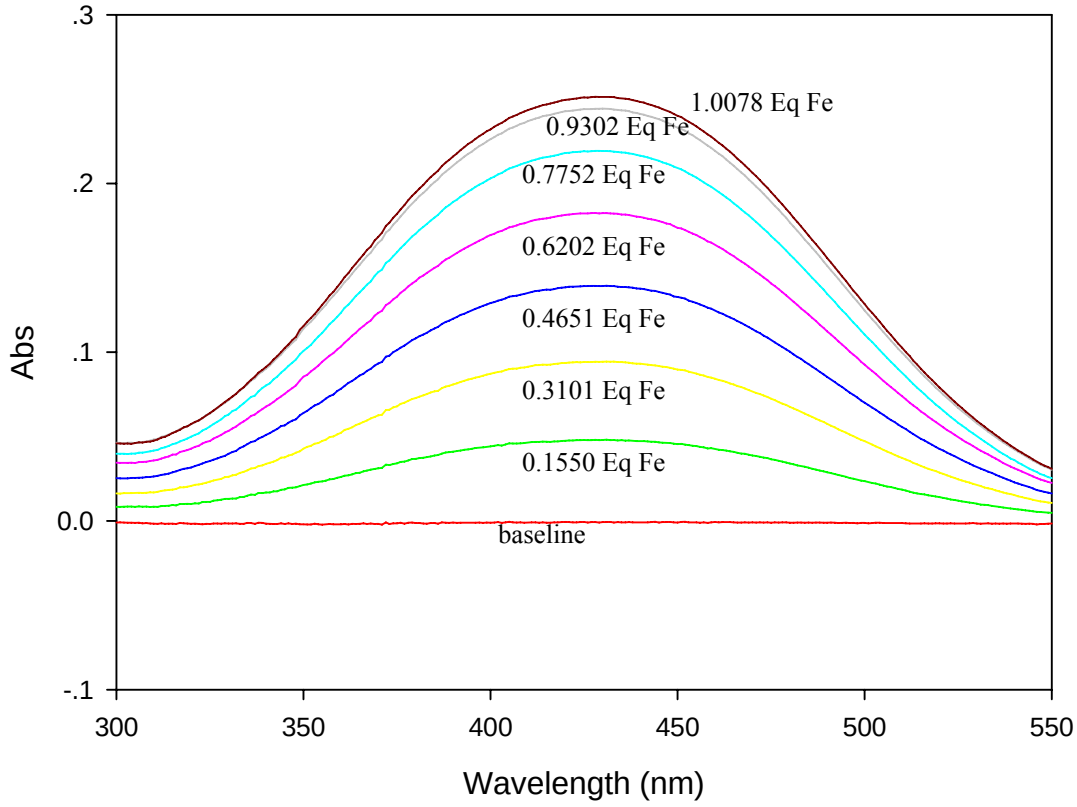

Figure 3.16 Titration of 2,2,2-THA with iron at pH 6.

Plots of absorbance versus equivalents of Fe were used to confirm the metal-ligand stoichiometry of the complexes of DFO and 2,2,2-THA. As shown in Figure 3.17, the intensity of the LMCT band increases until a 1:1 ratio of Fe to DFO is reached. The same result was observed for 2,2,2-THA. Therefore, it was confirmed that both ligands form 1:1 ferric complexes involving the coordination of all three hydroxamate groups of the ligand, with a λ_{max} at 430 nm.

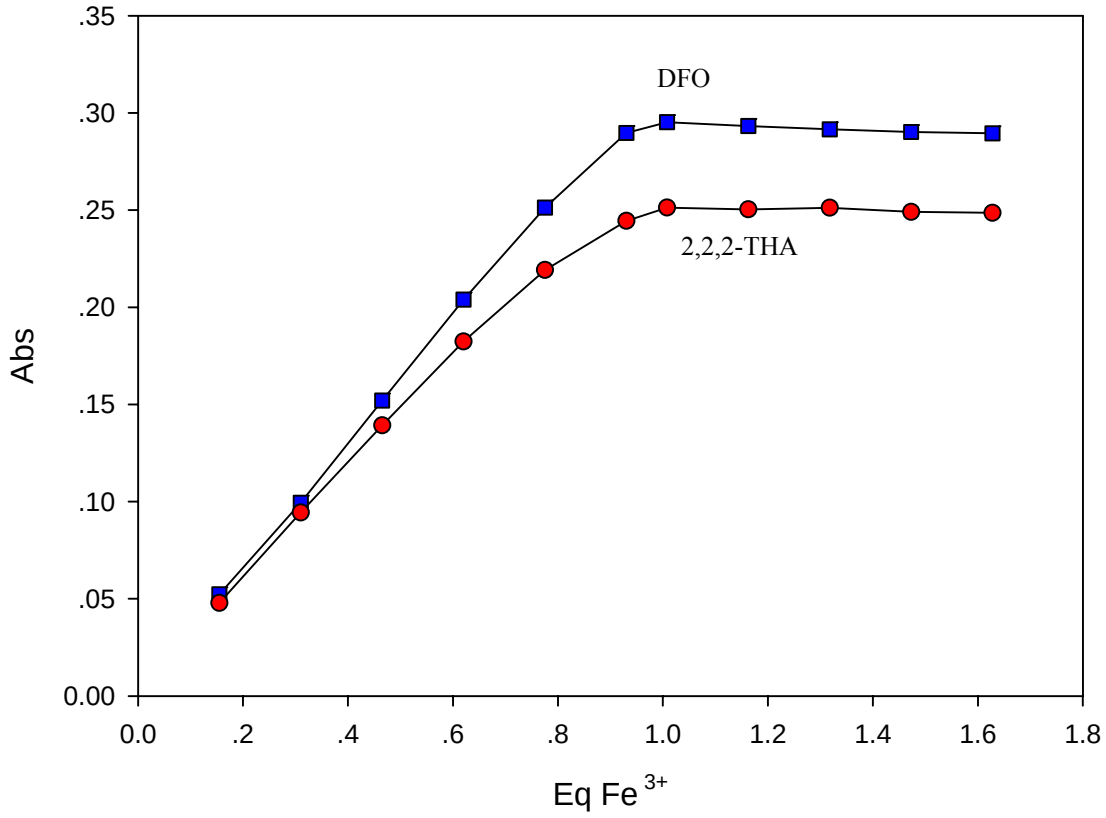

Figure 3.17 Absorbance at 430 nm vs equivalents of Fe for DFO (blue) and 2,2,2-THA (red).

3.4.2.2 Spectrophotometric pH titration of Fe^{3+} with AHA

Spectrophotometric studies were conducted to confirm the λ_{max} values for the mono and bis complexes of Fe^{3+} with AHA. The spectra of a 1:1 solution of Fe^{3+} and AHA as a function of pH are shown in Figure 3.18. As the pH increases from 2.1 to 3.5, the formation of the 1:1 $Fe(AHA)^{2+}$ complex was observed, with a λ_{max} at ~490 nm. Upon increasing the pH to 4.7, the LMCT band of Fe-hydroxamate disappears because of the hydrolysis of Fe^{3+} to $Fe(OH)_3$.

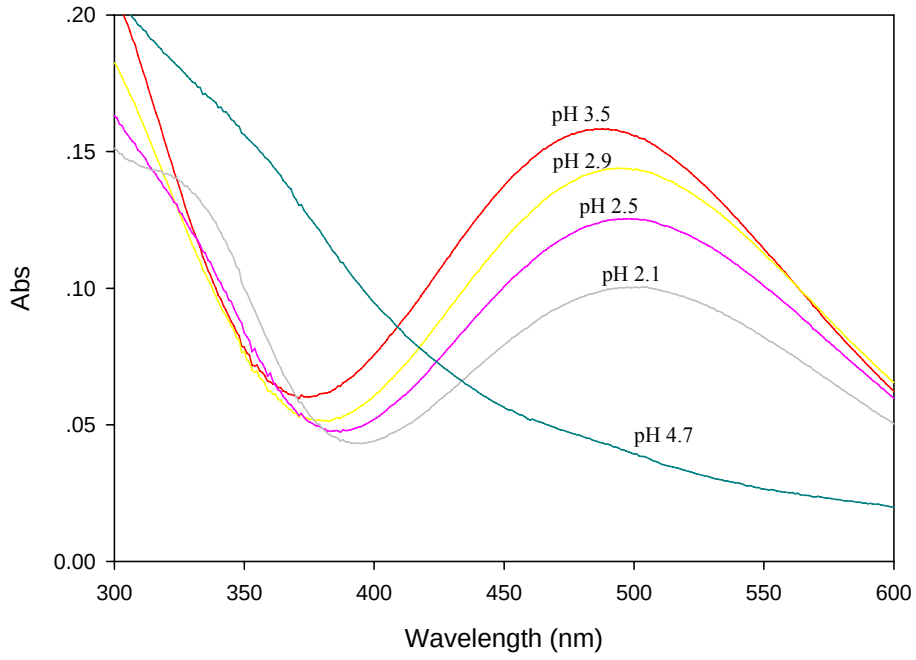

Figure 3.18 pH titration spectra of a 1:1 ratio Fe^{3+} with AHA.

Figure 3.19 shows the spectra of a 1:2 solution of Fe^{3+} with AHA as a function of pH. At pH 2.5 the λ_{max} corresponds to the 1:1 complex. As the pH increases from pH 2.5 to 3.5, the λ_{max} shifts to ~470 nm. This is consistent with previous reports that the λ_{max} for bis(hydroxamate) complexes is approximately 465 nm.[23,24] Above pH 4.2, the $Fe(OH)_3$ was formed as in the case of the 1:1 Fe-AHA system. Thus we have confirmed that mono-, bis-, and tris(hydroxamate) complexes of Fe^{3+} have λ_{max} values of 490 , 470 and 430 nm, respectively.

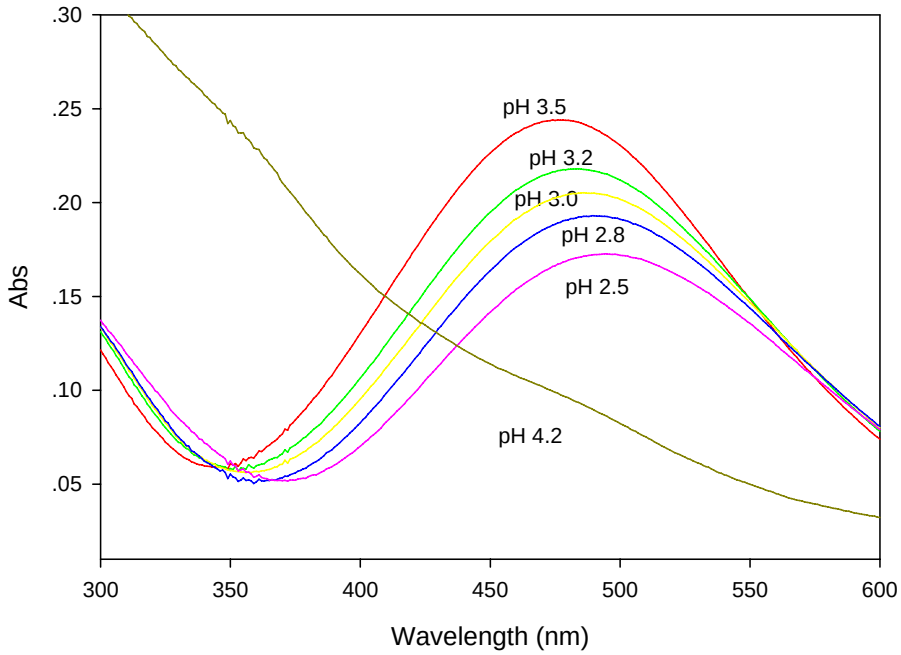

Figure 3.19 pH titration spectra of a 1:2 ratio of Fe^{3+} with AHA.

3.4.3 Spectrophotometric titration of Fe-2,2,2-THA as a function of pH

Visible spectra of solutions of Fe^{3+} and 2,2,2-THA were recorded over the pH range 0.3 to 7.6. We initially used a slight excess of ligand (1:1.12) in the spectrophotometric titration. The resulting family of spectra is shown in Figure 3.20. At lower pH, the λ_{max} is at 460 nm. This absorbance band increases up to pH 3.4. Between pH 3.4 to 4.4, there is no significant change in $\lambda_{max,}$ but the absorbance decreases slightly. This suggested that there was some hydrolysis of the Fe^{3+}. To prevent this phenomenon, we switched to a 2:1 ratio of ligand: Fe^{3+}. The visible spectra of a 2:1 mixture of 2,2,2-THA with Fe^{3+} as a function of pH between 0.3 and 7.0 are shown in Figure 3.21.

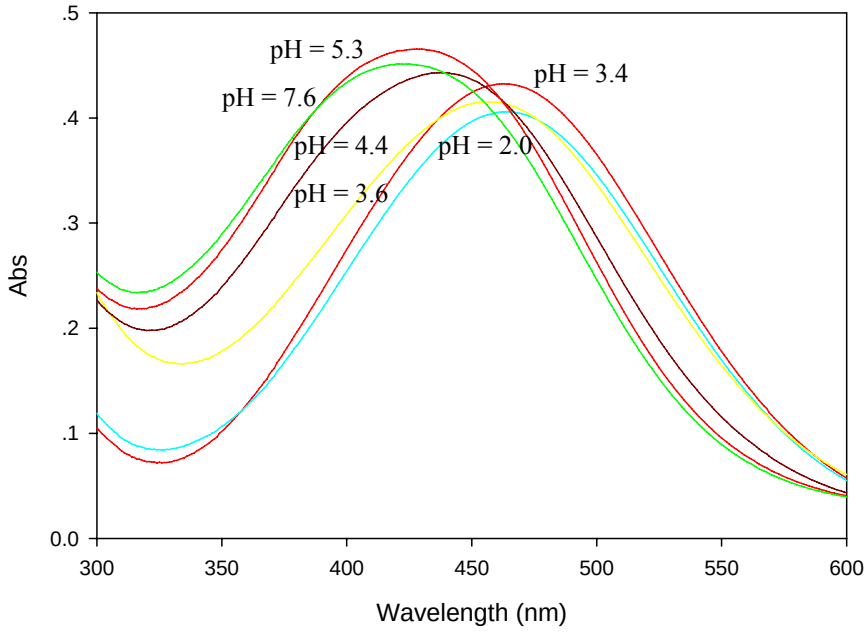

Figure 3.20 pH titration spectra of a 1:1.12 ratio of Fe^{3+} with 2,2,2-THA.

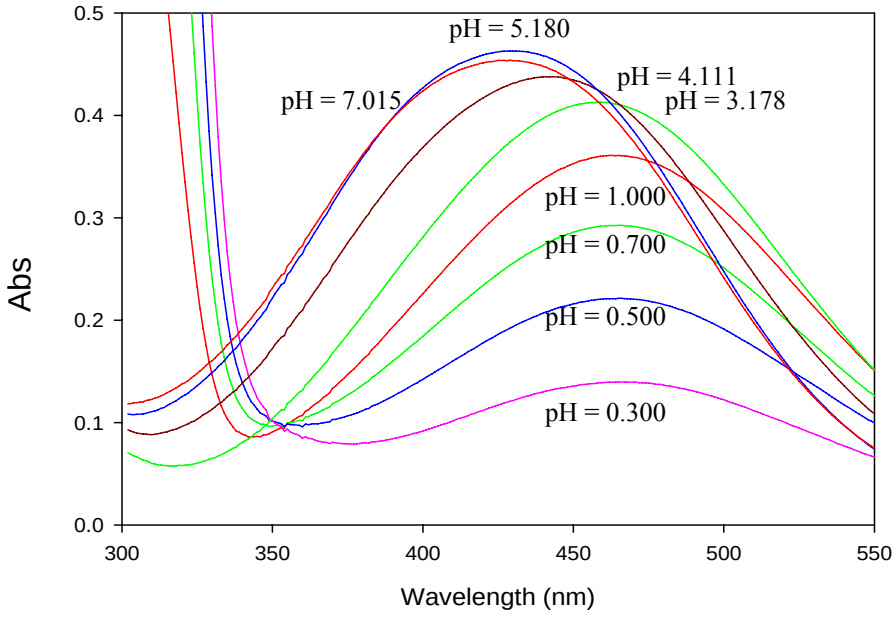

Figure 3.21 pH titration spectra of a 1:2 ratio of Fe^{3+} with 2,2,2-THA.

A more detailed set of spectra collected between pH 0.3 and 3.2 is shown in Figure 3.22. The absorbance band at 465 nm increases with increasing pH. At pH 3.2, the bis(hydroxamate) complex 111 is completely formed, with a molar extinction coefficient of ε = 2,024 M^{-1} cm^{-1}. In the 111 complex, two of the hydroxamate groups of 2,2,2-THA are coordinated to the Fe^{3+}, while the third hydroxamic acid group remains protonated and uncoordinated to Fe^{3+}.

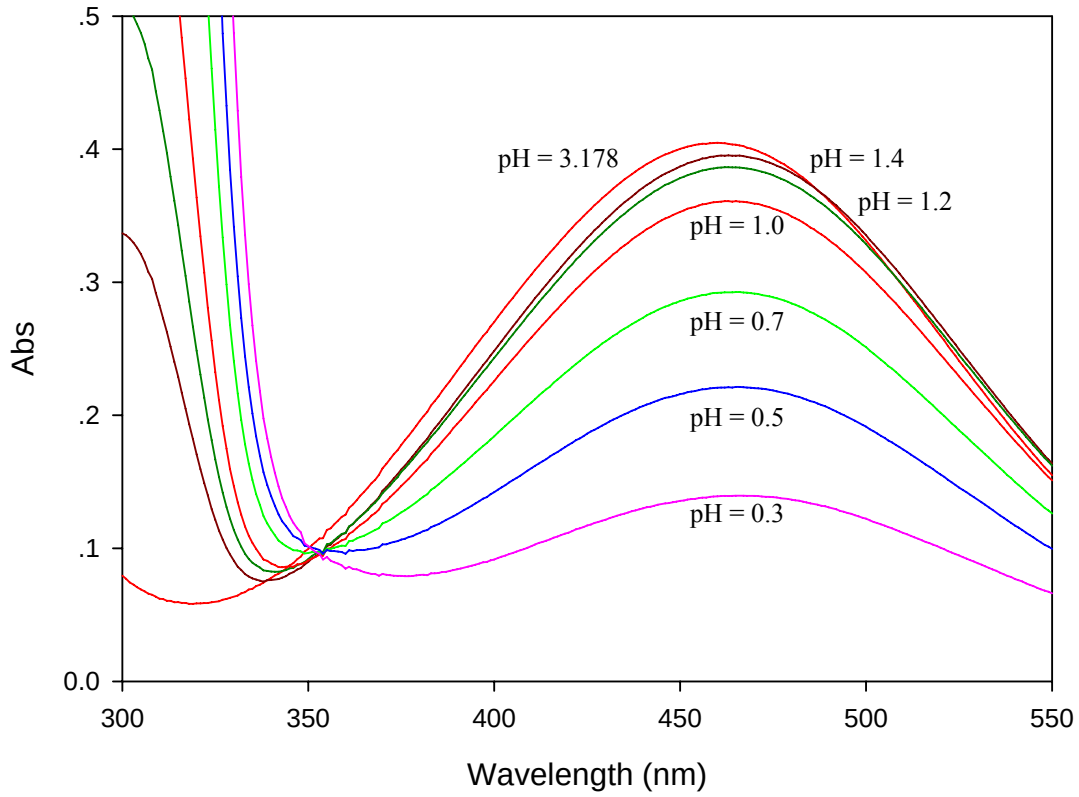

Figure 3.22 Spectra of a 1:2 ratio of Fe^{3+}: 2,2,2-THA at low pH.

The spectra from Figure 3.22 were used to calculate the stability constant of the FeHL complex using SPECFIT. SPECFIT is a sophisticated, multivariate data analysis program for modeling and fitting spectra to a variety of kinetics and equilibrium models.

Typically, the data set consists of absorbance spectra recorded as a function of an independent variable like time, pH or [titrant].

The spectra were analyzed with the ligand protonation constants and the Fe^{3+} hydrolysis constants input as fixed parameters, while the stability constant and the spectrum of the 111 complex were treated as variable parameters. The result was a value of $\log \beta_{111} = 30.80 \pm 0.02$.

When the pH of a solution with a 1:2 ratio of Fe^{3+}: 2,2,2-THA is increased from pH 3.2 to pH 5.2, the absorbance band at 460 nm shifts to 430 nm and the intensity increases to 2,515 $M^{-1}cm^{-1}$ as shown in Figure 3.23. These changes are consistent with the formation of a tris(hydroxamate) 110 complex. The visible spectrum of the FeL species is very similar to those corresponding to the tris(hydroxamate) complexes of Fe^{3+} with acetohydroxamic acid and other model compounds.[23-24] However, at pH 7, the absorbance at 430 nm decreases. This was attributed to partial hydrolysis of the 110 complex, yielding $Fe(OH)_3$ and the anion of 2,2,2-THA, with a decrease in the characteristic LMCT band.

It has been reported[25] that the molar absorptivity of a Fe^{3+}-hydroxamate complex is about 1000n M^{-1} cm^{-1}, n being the number of hydroxamate groups bonded per ferric ion. The observed molar absorptivities of the FeHL and FeL complexes with 2,2,2-THA are consistent with the literature data.

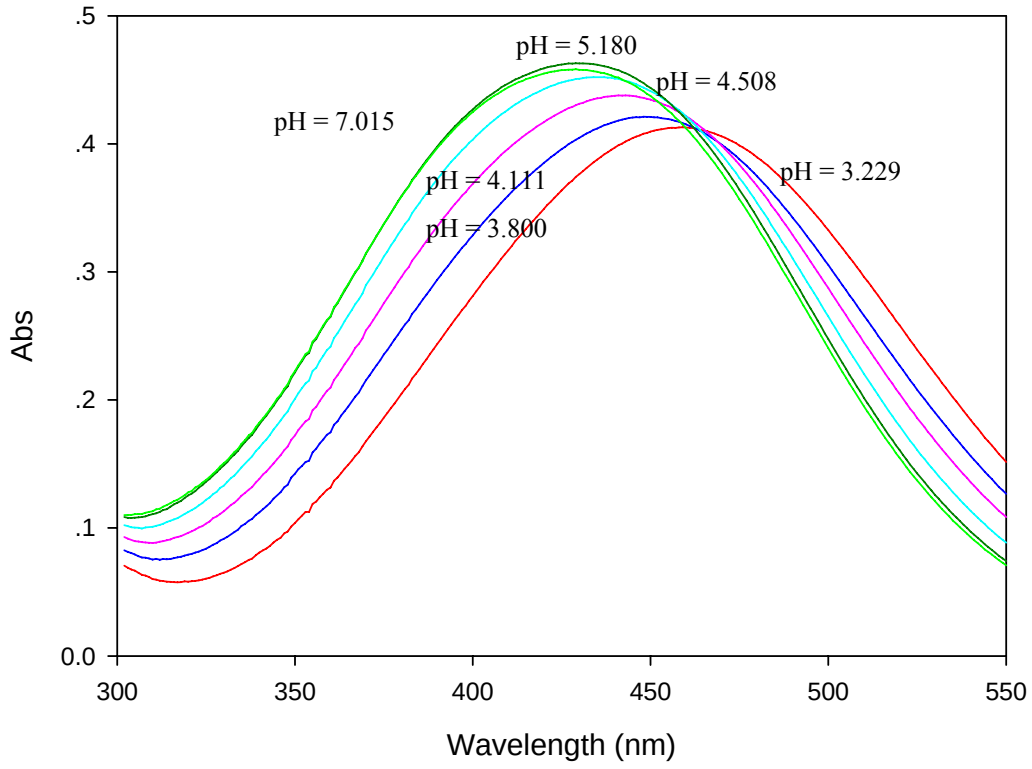

Figure 3.23 Spectra of a 1:2 ratio of Fe^{3+}: 2,2,2-THA at higher pH.

The spectra in Figure 3.23 show an isosbestic point at 460 nm, which indicates that there is a simple equilibrium between only two light-absorbing species. This equilibrium is the deprotonation of the 111 complex, as show below.

$$FeHL \underset{}{\overset{K}{\rightleftharpoons}} FeL + H \qquad \text{Eq 3.3}$$

$$K = \frac{[FeL][H]}{[FeHL]} \qquad \text{Eq 3.4}$$

The overall spectrophotometric pH titration data of Fe^{3+} with 2,2,2-THA between pH 0.3 and 5.2 were fitted with SPECFIT. The spectrum and stability constant for the 111 complex determined from the low pH data were input as fixed parameters, while log β_{110} and the spectrum of the 110 complex were treated as adjustable parameters. The results are shown in Table 3.6. The fit of the spectra was very good, as indicated by the small standard deviations in the log β values. The values of β_{111} and β_{110} were used to calculate the chelate protonation constant of the Fe-2,2,2-THA complex listed in Table 3.6.

	Stability constant (log β)	Chelate protonation constant (log K)
FeL (110)	26.75 ± 0.05	-
FeHL (111)	30.80 ± 0.01	4.05

Table 3.6 Stability constants of FeL and FeHL complexes of 2,2,2-THA and the chelate protonation constant.

By using the stability constants obtained from SPECFIT listed in Table 3.6, the species distribution for a 1:2 ratio of Fe^{3+} and 2,2,2-THA was calculated as a function of pH, as shown in Figure 3.24. It is seen that the FeHL complex predominates from pH 1 to 4. Above pH 4, the FeL complex becomes the major species in the solution. There is a 50:50 mixture of the complexes at about pH 4, which corresponds to the chelate protonation constant obtained from the SPECFIT.

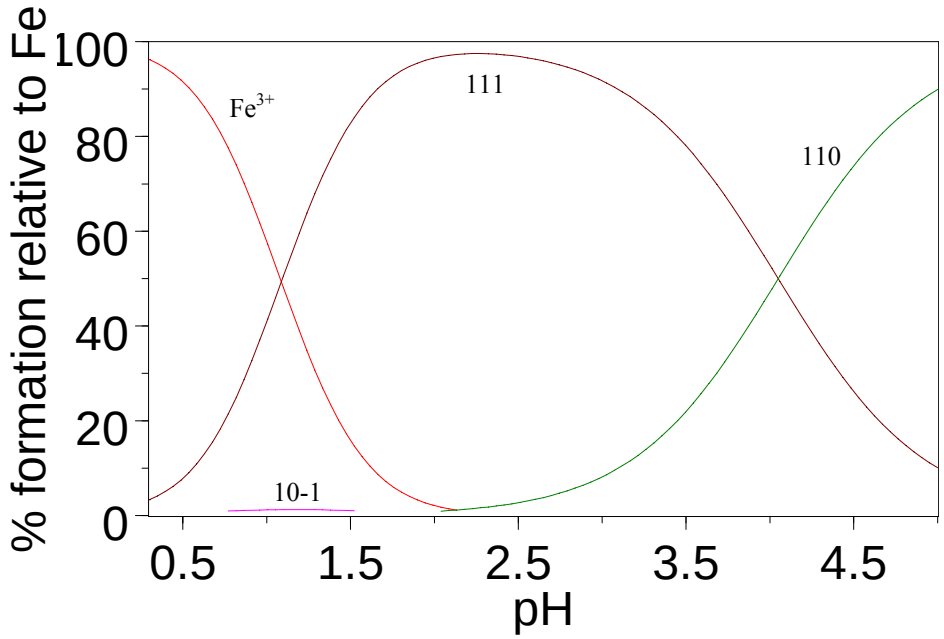

Figure 3.24 Species distribution diagram for 10 μM of Fe^{3+} and 20 μM of 2,2,2-THA as a function of pH.

We have mentioned that only the chelate protonation constant could be determined accurately from the potentiometric titration data because of the lack of free Fe^{3+}, even at pH 2 at the beginning of the titration. The results from fitting the potentiometric data using both β_{110} and β_{111} as variable parameters are shown as model 1 in Table 3.7. The chelate protonation constant agrees with the spectrophotometric value listed in Table 3.6. However, the absolute values of β_{111} and β_{110} do not agree with the spectrophotometric values.

The results from the spectrophotometic pH titration were incorporated into the fitting of the potentiometric titration data. We evaluated two additional models for the potentiometric data. In one case, we input the spectrophotometric value for β_{111} as a

fixed constant and calculated β_{110} (model 2). In the last case we set β_{110} at the spectrophotometric value and refined a value for β_{111}. All the results are shown in Table 3.7. The chelate protonation constant is log K = 3.8 in all three potentiometric models, which is in good agreement with the value of log K = 4.0 obtained from the spectrophotometric pH titration. In addition, the results from the potentiometric data when one of the metal stability constants is fixed are consistent with the spectrophotometric values for the stability constants of the 110 and 111 complexes.

Ligand	Reaction	Stability constants (log β)		
		Model 1	Model 2	Model 3
2,2,2-THA	$Fe^{3+} + L^{3-} + H^{+} \rightleftharpoons FeLH^{+}$	27.60	30.80*	30.59
	$Fe^{3+} + L^{3-} \rightleftharpoons FeL$	23.78	26.94	26.75*
	GOF	0.005	0.017	0.017
	$FeL + H \rightleftharpoons FeHL$	3.82	3.86	3.84

*Value fixed at the spectrophotometric value from Table 3.6

Table 3.7 The chelate protonation constant and the stability constants of the Fe-2,2,2-THA from a combination of potentiometric and spectrophotometric data.

3.4.4 Fe^{3+} titration with 2,2-DHA

When a solution containing a 1:1 ratio of 2,2-DHA to Fe^{3+} is titrated with base, there is an inflection at 2 equiv, as shown in Figure 3.25. The constants β_{110} and β_{111} were used as adjustable parameters in the least squares refinement of the potentiometric data. It

appears that the 110 complex is the only species in the solution. Precipitation is still a problem for these systems above pH 4.9. The stability constant of the 110 complex was 18.70 $\pm$ 0.10 with a GOF of 0.01. Table 3.8 shows the equilibrium model used to fit the data for 2,2-DHA with Fe^{3+}.

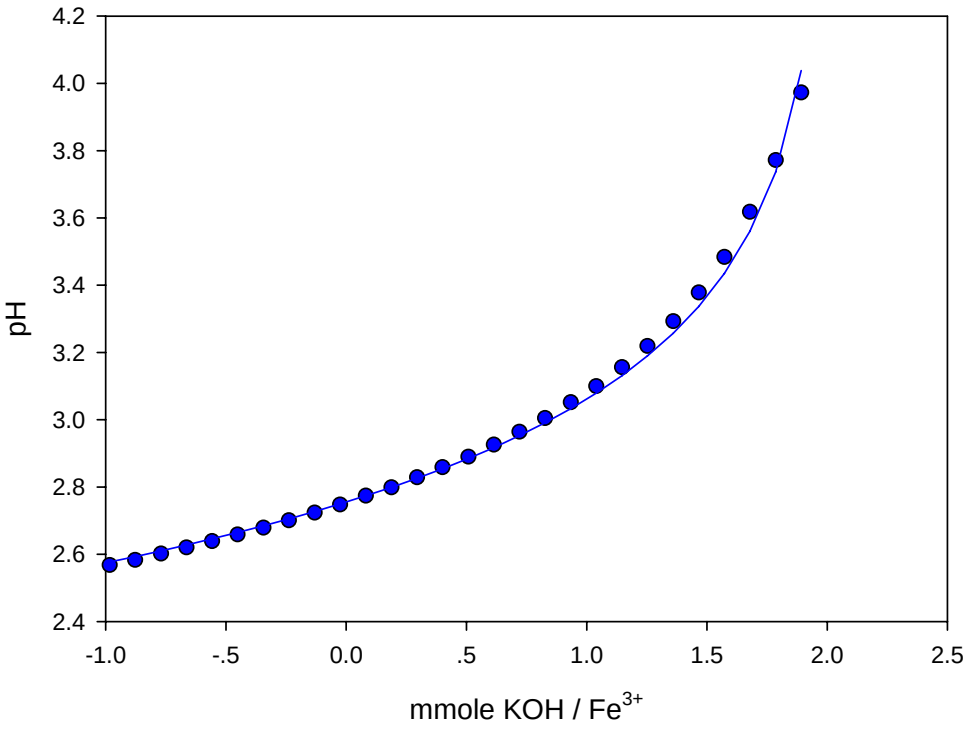

Figure 3.25 Potentiometric titration curve of Fe^{3+} with 2,2-DHA. The symbols represent the observed data points while the line represents the least squares fit based on the ligand protonation constants, the Fe^{3+} hydrolysis constants and the stability constants listed in Table 3.8.

System	i	j	k	reaction	log β_{ijk}	σ
2,2-DHA	0	1	1	$L^{2-} + H^{+} \rightleftharpoons HL^{-}$	9.80	
	0	1	2	$L^{2-} + 2H^{+} \rightleftharpoons H_2L$	18.49	
Fe-OH^{-}	1	0	-1	$Fe^{3+} \rightleftharpoons FeOH^{2+} + H^{+}$	-2.68	
	1	0	-2	$Fe^{3+} \rightleftharpoons Fe(OH)_2^{+} + 2H^{+}$	-6.41	
	1	0	-3	$Fe^{3+} \rightleftharpoons Fe(OH)_3 + 3H^{+}$	-12.74	
	1	0	-4	$Fe^{3+} \rightleftharpoons Fe(OH)_4^{-} + 4H^{+}$	-22.09	
Fe-2,2-DHA	1	1	0	$Fe^{3+} + L^{2-} \rightleftharpoons FeL^{+}$	18.70*	0.10

Table 3.8 Variable (*) and fixed parameters for the least squares refinement of the potentiometric titration data for Fe-2,2-DHA.

3.5 Comparison between the stability constants of Al^{3+} and Fe^{3+} with 2,2,2-THA, 2,2-DHA or 2-HA with those of known mono-, di- and trihydroxamate ligands

The stability constants of the trivalent metal ions Al^{3+} and Fe^{3+} have been determined by a combination of potentiometric and spectrophotometric titrations. There is usually a strong correlation between the stability constants for these two metal ions. This is illustrated by the linear free energy relationship (LFER) between log β (Al^{3+}) and log β (Fe^{3+}) shown in Figure 3.26. The LFER was constructed from literature data on the ligands AHA, C_4DHA, C_6DHA, C_8DHA and DFO, which are shown by the filled circles in Figure 3.26. The experimental results reported here for the Al^{3+} and Fe^{3+} complexes with 2,2,2-THA and 2,2-DHA, shown by the red diamonds in the figure, are in good agreement with the LFER. The graph shows that 2,2-DHA binds Al^{3+} slightly better than

the other dihydroxamate ligands. However, the binding constants for 2,2,2-THA for both Fe^{3+} and Al^{3+} are considerably smaller than those for the trihydroxamate DFO. This is presumed to reflect unfavorable steric strain associated with complexation by all three arms of 2,2,2-THA.

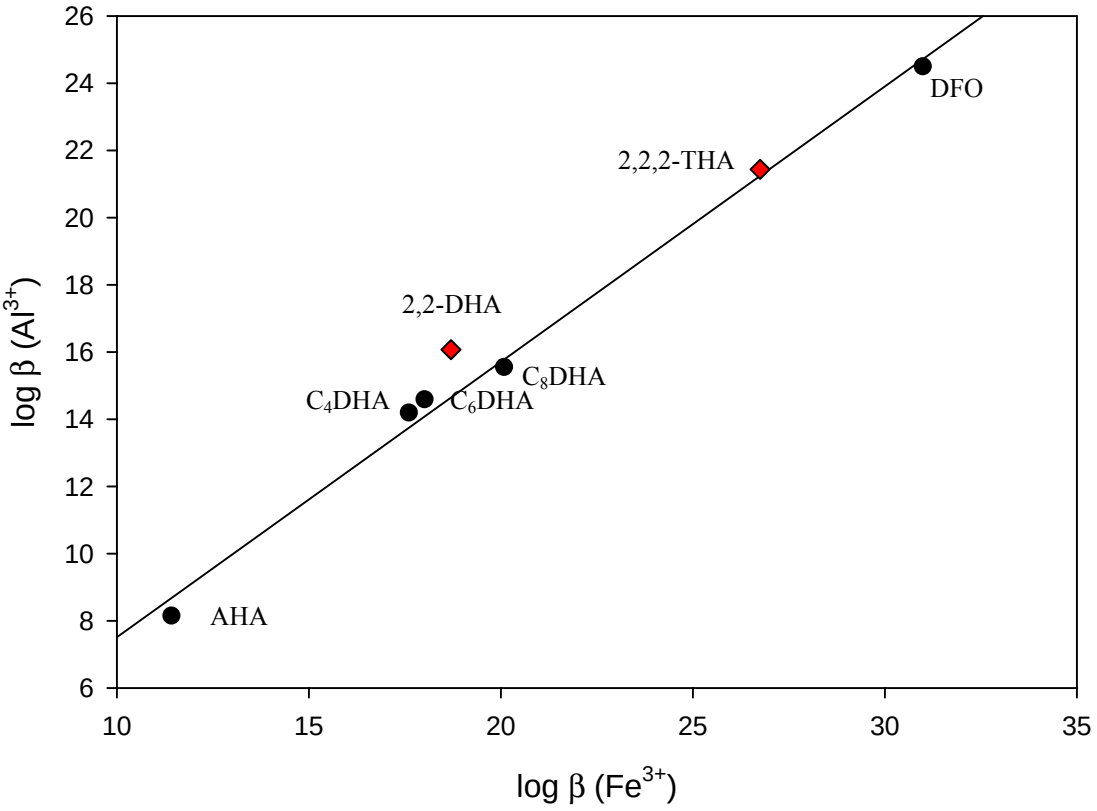

Figure 3.26 Linear free energy relationships (LFER) for the complexation of Al^{3+} and Fe^{3+} by hydroxamic acids.

References

1. Martell, A. E.; Anderson, W. F.; Badman, D. G. *Development of iron chelators for clinical use*, Elsevier, New York, 1981.

2. McLachlan, D. R. C.; Farnell, B.; Gallin, H.; Karlik, S.; Eichorn, G.; DeBoni, U. *Biological aspects of metals and metal-related diseases*, Raven Press, New York, 1983.

3. Raymond, K. N.; Freeman, G. E.; Kappel, M. J. *Inorg. Chim. Acta* 1984, 94, 193.

4. Harris, W. R.; Martell, A. E. *Inorg. Chem*. 1976, 15, 713.

5. Sun, Y.; Martell, A. E., Motekaitis, R. J. *Inorg. Chem*. 1985, 24, 4343.

6. McMillan, D. T.; Murase, I.; Motekaitis, R. J.; Martell, A. E. *Inorg. Chem*. 1975, 14, 468.

7. Evers, A.; Hancock, R. D.; Martell, A. E.; Motekaitis, R. J. *Inorg. Chem.* 1989, 28, 2189.

8. Weatherall, D. J.; Pippard, M. J.; Callender, S. J. *N. Engl. J. Med*. 1983, 305, 456.

9. Peter, H. H. *Proteins of iron storage and transport*, Elsevier: Amsterdam, 1985, 293.

10. Mallucke, H. H.; Smith, A. J.; Abreo, K.; Faugere, M. C. *N. Engl. J. Med*. 1984, 311, 140.

11. Akrill, P.; Ralston, A. J.; Day, J. P.; Hodge, K. C. *Lancet* 1980, 2, 692.

12. Brown, D. J.; Ham, K. N.; Dawborn, J. K. *Lancet* 1982, 2, 343.

13. Brink, C. P.; Crumbliss, A. L. *J. Org. Chem*. 1982, 47, 1171.

14. Brink, C. P.; Fish, L. L.; Crumbliss, A. L. *J. Org. Chem*. 1985, 50, 2277.

15. Monzyk, B.; Crumbliss, A. L. *J. Org. Chem*. 1980, 45, 4670.

16. Hernlem, B. J.; Vane, L. M.; Sayles, G. D. *Inorg. Chim. Acta* 1996, 244, 179.

17. Leporati, E., *J. Chem. Soc., Dalton Trans.* 1987, 1409.

18. Adams, E. Q. *J. Am. Chem. Soc*. 1916, 38, 1503.

19. Carrano, C. J.; Cooper, S. R.; Raymond, K. N. *J. Am. Chem. Soc.* 1979, 101, 599.

20. Anderegg, G.; L'Eplattenier, F. L.; Schwarzenbach, G. *Helv. Chim. Acta* 1963, 156, 1409.

21. Konetschny-Rapp, S.; Jung, G.; Raymond, K. N.; Meiwes, J. *J. Am. Chem. Soc.* 1992, 114, 2224.

22. Farkas, E.; Kozma, E.; Kiss, T.; Toth, I.; Kurzak B. *J. Chem. Soc., Dalton Trans.* 1995, 477.

23. Albrecht-Gary, A. M.; Crumbliss, A. L. *Metal ions in biological systems*, Sigel, A., Sigel, H., Eds.; Marcel Dekker : New York, 1998, vol 35, 239.

24. Crumbliss, A. L. *Handbood of microbial iron chelates,* Winkelmann, G., Ed.; CRC Press, Boca Raton, FL. 1991, 177.

25. Santos, M. A.; Esteves, M. A.; Vaz, M. C. T.; Simões-Goncalves, M. L. S. *J. Chem. Soc., Dalton Trans.* 1993, 927.

Chapter 4

Potentiometric studies of the binding of divalent metal ions by hydroxamic acids

4.1 Introduction

Hydroxamic acids play an important role as bioligands in living systems. They represent the largest class of siderophores for iron(III).[1-2] One siderophore, DFO is the current drug of choice for iron-overload chelation therapy.[3] Hydroxamates also inhibit enzymes such as peroxidases,[4] and show hypotensive,[5] anti-cancer, anti-tuberculous and anti-fungal activity.[6] Hydroxamic acids have also been broadly studied as metal complexing agents in the sphere of zinc and nickel metalloenzyme inhibition, i.e. as inhibitors of matrix metalloproteinase (MMP)[7-9] and urease,[10-12] respectively.

The binding of the hydroxamate group of trifluoroacetohydroxamate to Zn^{2+} in human carbonic anhydrase II has been investigated. The ligand is monodentate, binding through the hydroxamate nitrogen only, but shows the presence of a weak Zn–F bond.[13] The variety of hydroxamate coordination structures is further enriched by the presence of additional coordinating sites in the Cu^{2+} complexes of the isomeric aminophenyl-hydroxamic acids.[14]

In the previous chapter, we have described the high binding affinity of a series of hydroxamate ligands for Al^{3+} and Fe^{3+}. The selectivity of these ligands for trivalent metal ions is also an important factor. Thus, it is important to investigate the binding of divalent metals by these hydroxamate ligands.

Divalent metal ions such as Cu^{2+}, Ni^{2+} and Zn^{2+} from the first row transition elements are intermediate metal ions in hard-soft-acid-base (HSAB) theory, while Mn^{2+} is a hard metal ion.[15] The ionic radii of these metal ions are Cu^{2+}, 0.73 Å ; Ni^{2+}, 0.69 Å; Mn^{2+}, 0.83 Å and Zn^{2+}, 0.74 Å.[16-17] The most common coordination number for Ni^{2+}, Mn^{2+} and Zn^{2+} is six, although coordination numbers 4 and 5 sometimes occur. For Cu^{2+}

Jahn-Teller effects favor square planar complexes.

The stability constants of the well-known trihydroxamic acid, DFO, with trivalent metal ions were mentioned in the previous chapter. A comparison of the stability constants of DFO with several divalent metal ions with those for Al^{3+} and Fe^{3+} is shown in Table 4.1. In this chapter, potentiometric studies on the solution equilibria and the stability constants of divalent metal ions with the series of hydroxamate ligands 2,2,2-THA, 2,2-DHA and 2-HA are described.

	Al^{3+}	Fe^{3+}	Ni^{2+}	Cu^{2+}	Zn^{2+}
$\log \beta_{110}$	24.1	30.6	10.9	13.73	11.1

Table 4.1 The stability constants for the complexes of DFO with trivalent and divalent metal ions.[17-19]

Result and Discussion

4.2 Divalent metal ions with 2,2,2-THA

The coordinating tendencies of 2,2,2-THA toward Ni^{2+}, Zn^{2+}, Mn^{2+} and Cu^{2+} were investigated. Preliminary titrations on 2,2,2-THA alone were used to determine the ligand protonation constants as described in the previous chapter. In the studies described here, a solution containing equimolar concentrations of 2,2,2-THA and the metal ion, plus excess acid, were titrated with standard base. The resulting titration curves are shown in Figure 4.1. The negative values of mmole KOH/mmole metal ion in the Figure 4.1 represent the

base required to titrate any excess of acid added to the solution at the beginning of the titration.

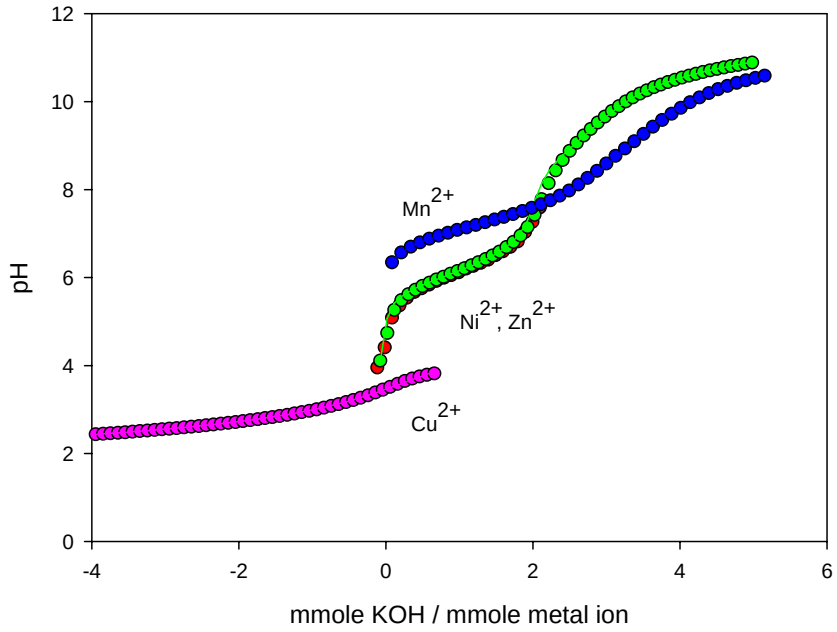

Figure 4.1 Potentiometric titration curves of Ni^{2+} (red), Zn^{2+} (green), Mn^{2+} (blue) and Cu^{2+} (pink) with 2,2,2-THA. The symbols represent the observed data points while the lines represents the least squares fit based on the ligand protonation constants and the stability constants listed in Table 4.2.

The equilibrium constants of the species that form over the investigated pH range and without precipitation were calculated through a non-linear least–squares analysis of the titration data. The calculations included the ligand protonation constants as fixed parameters, while the binding constants for the divalent metal ions with 2,2,2-THA were treated as adjustable parameters. These constants, which are reported in Table 4.2, were used to calculate distribution curves of the varying species as a function of pH.

System	i	j	k	reaction	log β_{ijk}	σ
2,2,2-THA	0	1	1	$L^{3-} + H^{+} \rightleftharpoons HL^{2-}$	10.26	
	0	1	2	$L^{3-} + 2H^{+} \rightleftharpoons H_2L^{-}$	19.68	
	0	1	3	$L^{3-} + 3H^{+} \rightleftharpoons H_3L$	28.15	
Ni-2,2,2-THA	1	1	0	$Ni^{2+} + L^{3-} \rightleftharpoons NiL^{-}$	10.73*	0.14
	1	1	1	$Ni^{2+} + L^{3-} + H^{+} \rightleftharpoons NiLH$	19.10*	0.14
Zn-2,2,2-THA	1	1	-1	$Zn^{2+} + L^{3-} \rightleftharpoons ZnLOH + H^{+}$	-0.56*	0.02
	1	1	0	$Zn^{2+} + L^{3-} \rightleftharpoons ZnL^{-}$	10.13*	0.01
	1	1	1	$Zn^{2+} + L^{3-} + H^{+} \rightleftharpoons ZnLH$	19.13*	0.01
Mn-2,2,2-THA	1	1	-1	$Mn^{2+} + L^{3-} \rightleftharpoons MnLOH + H^{+}$	-1.69*	0.09
	1	1	0	$Mn^{2+} + L^{3-} \rightleftharpoons MnL^{-}$	8.95*	0.12
	1	1	1	$Mn^{2+} + L^{3-} + H^{+} \rightleftharpoons MnLH$	17.06*	0.03
Cu-2,2,2-THA	1	1	1	$Cu^{2+} + L^{3-} + H^{+} \rightleftharpoons CuLH$	23.61*	0.04
	1	1	2	$Cu^{2+} + L^{3-} + 2H^{+} \rightleftharpoons CuLH_2$	27.15*	0.21

Table 4.2 Variable (*) and fixed parameters for least squares refinement of the potentiometric titration data for divalent metal ion with 2,2,2-THA.

4.2.1 The Ni^{2+} system with 2,2,2-THA

The potentiometric titrations of 2,2,2-THA with Ni^{2+} (Figure 4.1) showed an inflection point at 2 equiv of base, with precipitation above pH 8.0. Various models, consisting of different combinations of β_{110}, β_{111} and β_{112}, were used to fit the data. The best fit was obtained for the model that included β_{111} and β_{110}, and the final values of log

β_{111} and log β_{110} are shown in Table 4.2. Proposed structures for the 110 and 111 complexes are shown in Figure 4.2.

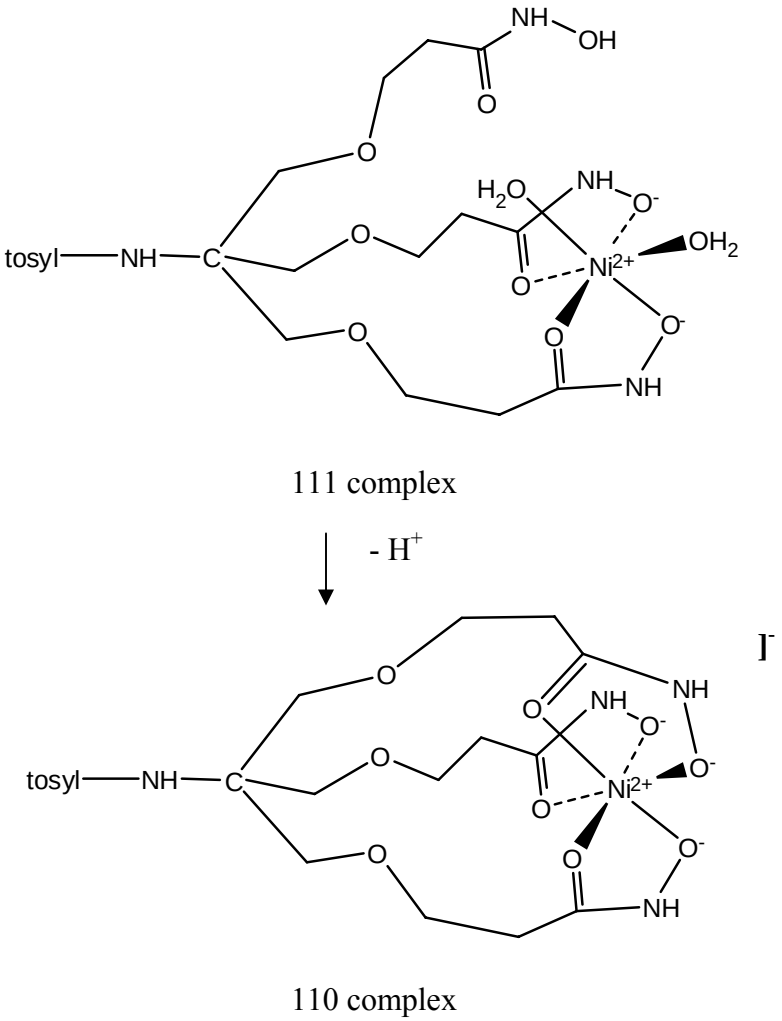

Figure 4.2 Proposed structures of the 111 and 110 complexes of Ni^{2+} and 2,2,2-THA.

Figure 4.3 illustrates the calculated concentrations of the species present at equilibrium for a solution that is 1 mM in both 2,2,2-THA and Ni^{2+} as a function of pH. Two metal complex species exist between pH 5 and 8. The bis(hydroxamate) complex, NiLH, in which two hydroxamate groups bind to the metal, and the tris(hydroxamate)

complex, NiL, in which all three hydroxamate groups bind the metal. The NiLH complex is present at >80% at pH = 6.5-7.5. On increasing pH above 7.5, the concentration of NiLH decreases as the NiL complex begins to form. Precipitation was observed above pH 8.0.

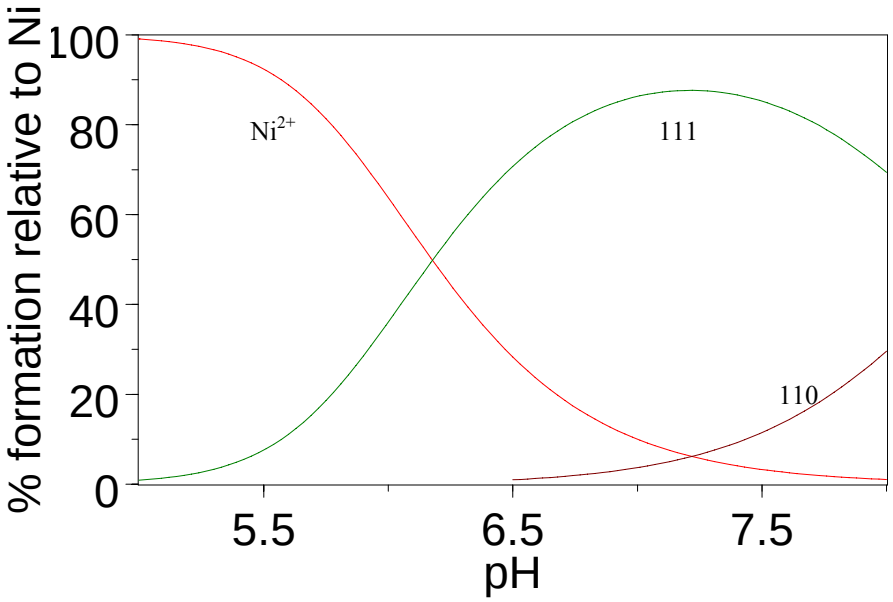

Figure 4.3 Species distribution diagram for 1 mM Ni^{2+} and 1 mM 2,2,2-THA as a function of pH.

4.2.2 The Zn^{2+} system with 2,2,2-THA

In the Zn^{2+} system, just as with the titration of Ni^{2+}, there is an inflection at 2 equiv of base per metal, as shown in Figure 4.1. However, in contrast to the Ni^{2+} titration, there was no precipitation even above pH 10. Various models involving the 110, 111, 112 and 11-1 species were evaluated in the non-linear least square fits of the data. The lowest GOF of 0.006 was obtained for the model consisting of the stability constants for the 110, 111 and 11-1 complexes. Values for β_{111}, β_{110} and $\beta_{11\text{-}1}$ are listed in Table 4.2.

A species distribution diagram for the Zn-2,2,2-THA system is shown in Figure 4.4. The monoprotonated 111 complex was predominant from pH 6 to 9, reaching a maximum of >90% at pH 7.5. From pH 9 to 10.5, the 110 complex is the main species in the solution. A hydrolyzed 11-1 complex is observed at very high pH.

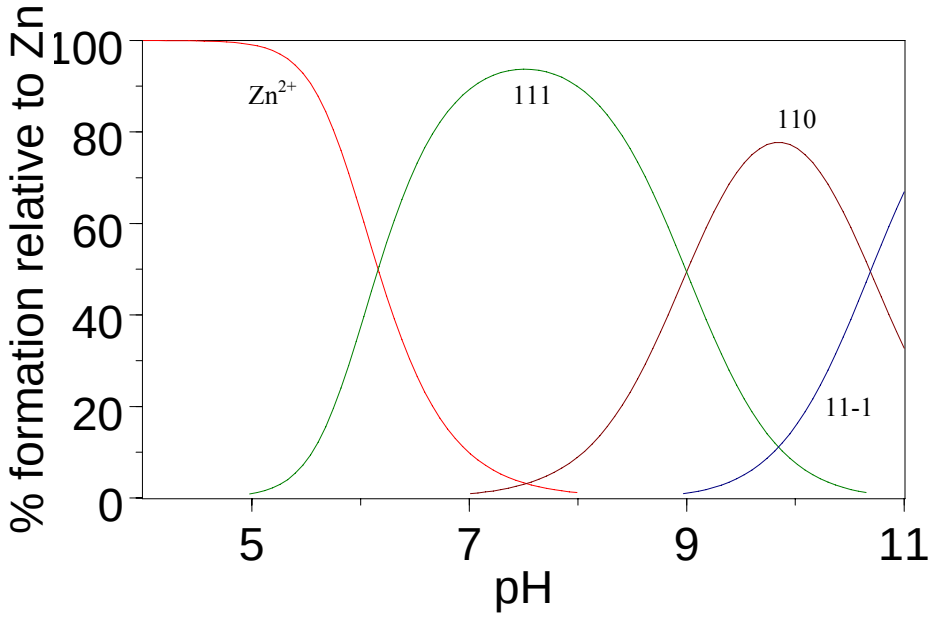

Figure 4.4 Species distribution diagram of 1 mM Zn^{2+} and 1 mM 2,2,2-THA as a function of pH

Proposed structures for the Zn^{2+} complexes with 2,2,2-THA are shown in Figure 4.5. The 11-1 complex could be 5 or 6 coordinate with a dangling hydroxamate or 7-coordinate with an OH^- group bound in addition to all three hydroxamate groups. As discussed in Chapter 3 for the proposed structures of Al^{3+} and Fe^{3+} with 2,2,2-THA, there appears to be some difficulty with the binding of all three hydroxamate groups to the central metal ion. Therefore, the structure with one dangling hydroxamate group is favored, as shown in Figure 4.5.

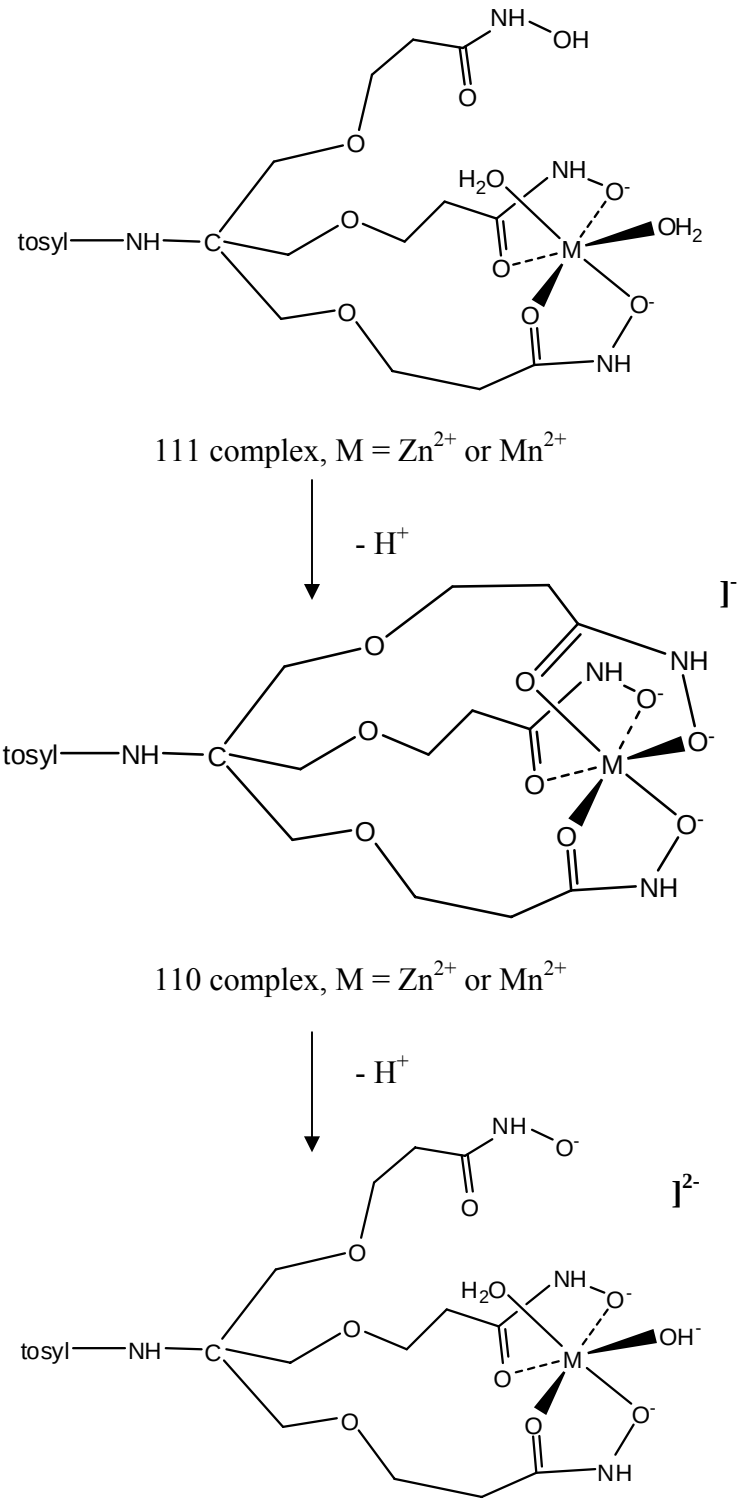

Figure 4.5 Proposed structures of the 110, 111 and 11-1 complexes of Zn^{2+} or Mn^{2+} with 2,2,2-THA.

4.2.3 The Mn^{2+} system with 2,2,2-THA

The titration curve of a 1:1 ratio of Mn^{2+} and 2,2,2-THA is shown in Figure 4.1. In the titration curve of the Mn^{2+} system, the inflection appears at 3 equiv of base, indicating the formation of a MnL complex that involves the release of three protons. In this neutral complex, all three of the hydroxamate groups are deprotonated and bound to the metal ion. There was no precipitation during the Mn^{2+} titrations. The titration data were analyzed by non-linear least squares with fixed values for the ligand protonation constants and adjustable parameters for the metal-ligand complexes as shown in Table 4.2. The data were refined with different models involving five species, the 110, 111, 112, 11-1 and 11-2 complexes. A very low GOF of 0.009 was observed for the model consisting of the 110, 111 and 11-1 complexes. The stability constants of the 110, 111 and 11-1 complexes are shown in Table 4.2. However, due to the low affinity of OH^- with Mn^{2+}, the formation of a 11-1 complex with Mn^{2+} seems unlikely. The release of more than three protons in the Mn^{2+} titration may be due to the oxidation of Mn^{2+} to Mn^{3+}, which has a very strong tendency to hydrolyze.

A speciation diagram for the Mn-2,2,2-THA system is shown in Figure 4.6. The species observed, the 110, 111 and 11-1 complexes, are the same in the Zn^{2+} system. However, the 111 complex accumulates to a maximum of only 60% at pH 7.5. There is a 50:50 mixture of the 110 and 111 complexes at pH 8.2. On increasing the pH above 8.2, the 110 complex reaches about 90% at pH 9.5. The 11-1 complex begins to form at pH 9.0. The proposed structures of the 110, 111 and 11-1 complexes are shown in Figure 4.5.

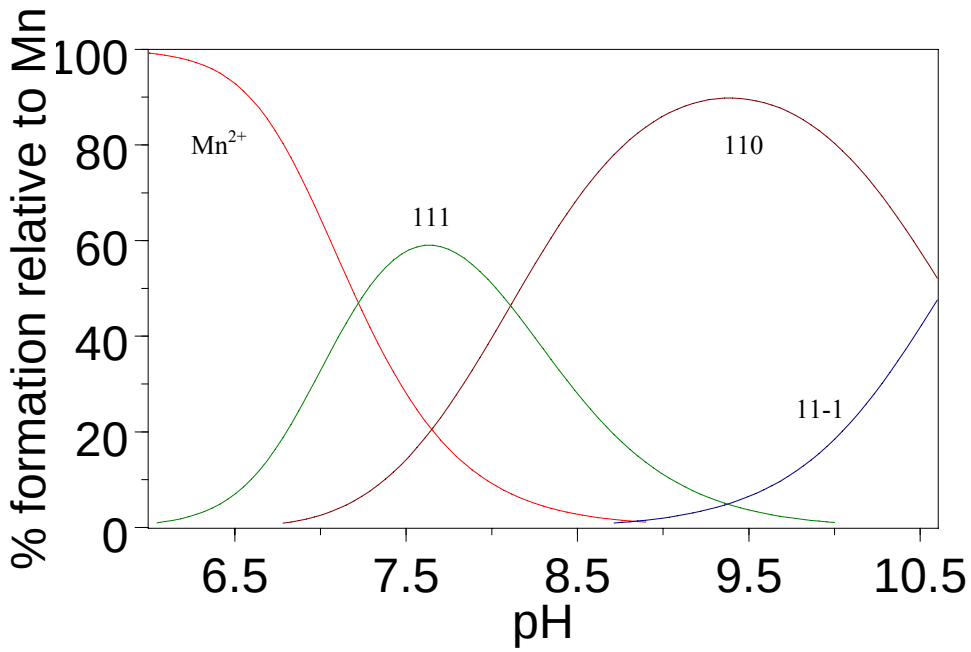

Figure 4.6 Species distribution diagram of 1 mM Mn^{2+} and 1 mM 2,2,2-THA as a function of pH.

4.2.4 The Cu^{2+} system with 2,2,2-THA

Strong acid was added to the Cu^{2+} system because precipitation occurred very quickly in the titration of only Cu^{2+} and 2,2,2-THA. The titration curve of Cu^{2+} with 2,2,2-THA is shown in Figure 4.1. Different models involving the 110, 111 and 112 complexes were used to fit the titration data. The best model included the 111 and 112 species and gave the lowest GOF of 0.012. The stability constants of Cu^{2+}-2,2,2-THA are shown in Table 4.2, with $\log \beta_{112} = 27.15 \pm 0.21$ and $\log \beta_{111}$ 23.61 $\pm$ 0.04.

The species distribution diagram of the Cu-2,2,2-THA system is shown in Figure 4.7. The maximum concentration of the initial deprotonated, monohydroxamate complex is about 15% at pH 3.5-4.0. The formation of the 112 species, with only one coordinated

hydroxamate groups, reflects the high affinity of Cu^{2+} for the hydroxamate functional group. The precipitation of the neutral 111 complex is observed when this species accumulates to about 40% of the total Cu.

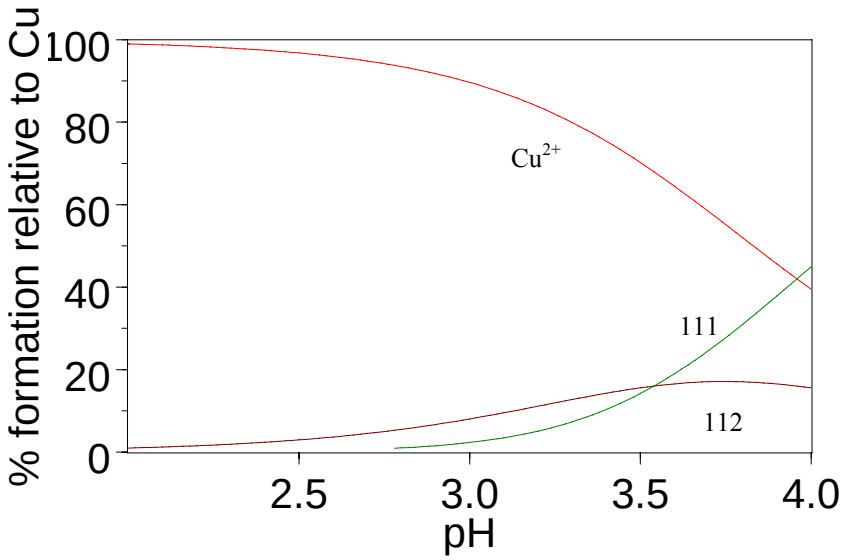

Figure 4.7 Species distribution diagram of 1 mM Cu^{2+} and 1 mM 2,2,2-THA as a function of pH.

The absence of a 110 complex of Cu^{2+} can be attributed to the Jahn-Teller effect associated with this d^9 metal ion, which typically weakens the binding of a pair of trans ligands and favors the formation of tetragonal 6-coordinate or square planar 4-coordinate complexes. In the 111 complex, two hydroxamate groups of 2,2,2-THA can bind with square planar geometry, so there is no barrier to the formation of this complex. In contrast the formation of a 110 complex would require binding to the weak axial coordination sites.

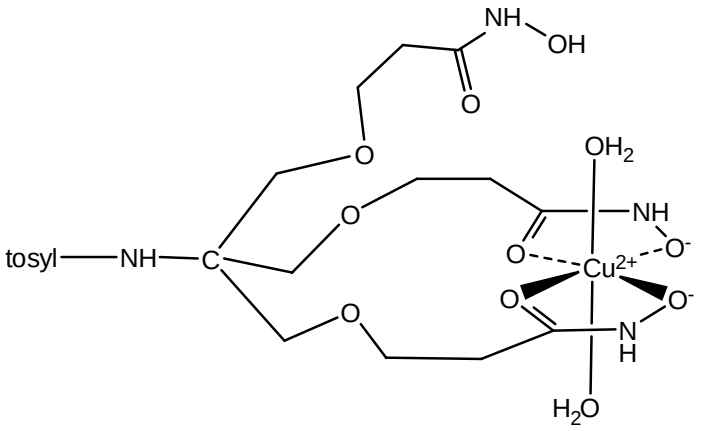

111 complex

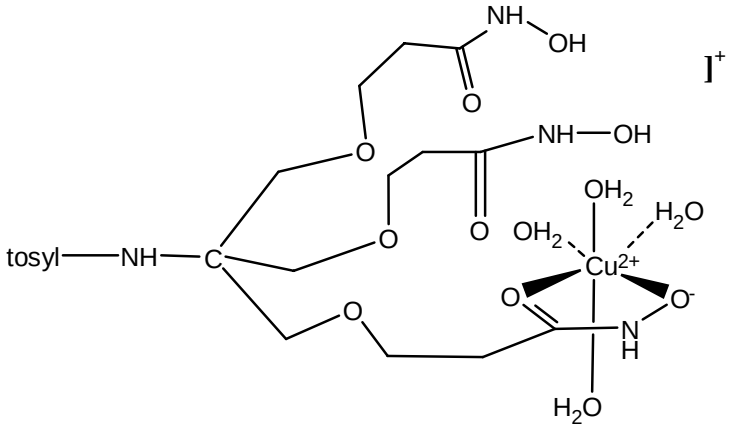

112 complex

Figure 4.8 Propose structures of the 111 and 112 complexes of Cu^{2+} with 2,2,2-THA.

4.3 Divalent metal ions with 2,2-DHA

To understand better the magnitude of the stability constants of divalent metal ions with 2,2,2-THA, the stability constants with 2,2-DHA and 2-HA have also been studied. Potentiometric titrations of Ni^{2+}, Zn^{2+}, Mn^{2+} and Cu^{2+} with 2,2-DHA were

performed at a 1:1 ligand:metal molar ratio. Potentiometric titration curves for the various metal ion-ligand complexes are shown in Figure 4.9.

Generally, it is observed that the divalent metal complexes of 2,2-DHA form in the pH range 4-7, while only Cu^{2+} forms complexes at low pH. The titration data were refined using the program BETA, and the stability constants of Ni^{2+}, Zn^{2+}, Mn^{2+} and Cu^{2+} with 2,2-DHA are tabulated in Table 4.3.

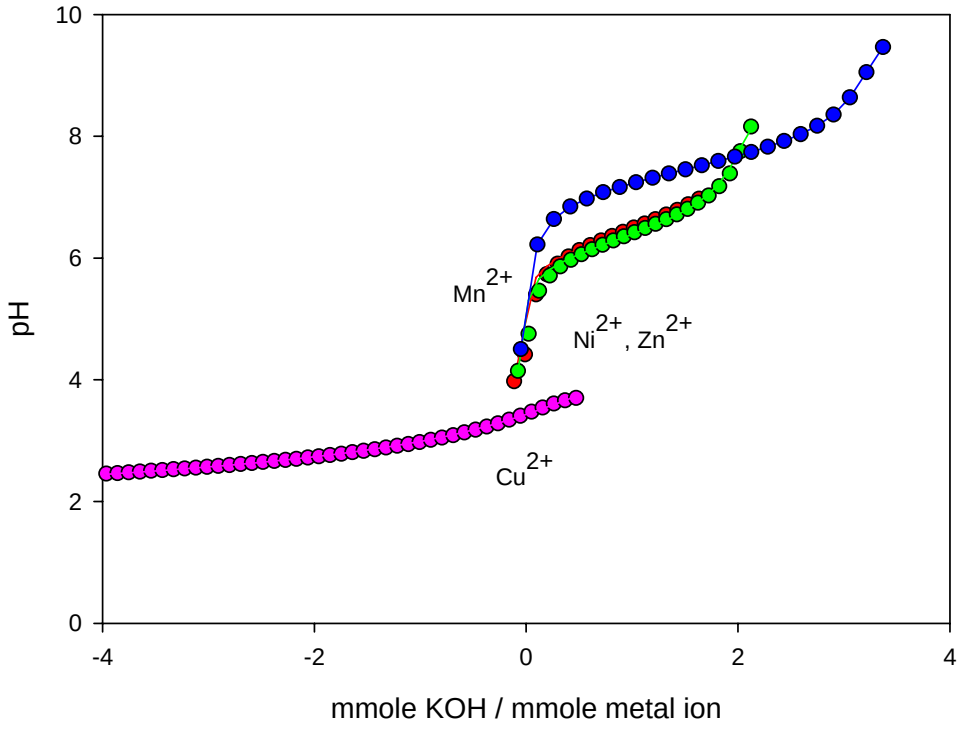

Figure 4.9 Potentiometric titration curves of Ni^{2+} (red), Zn^{2+} (green), Mn^{2+} (blue) and Cu^{2+} (pink) with 2,2-DHA. The symbols represent the observed data points while the lines represents the least squares fit based on the ligand protonation constants and the stability constants listed in Table 4.3.

System	i	j	k	reaction	log β_{ijk}	σ
2,2-DHA	0	1	1	$L^{2-} + H^{+} \rightleftharpoons HL^{-}$	9.80	
	0	1	2	$L^{2-} + 2H^{+} \rightleftharpoons H_2L$	18.49	
Ni-2,2-DHA	1	1	0	$Ni^{2+} + L^{2-} \rightleftharpoons NiL$	9.02*	0.01
Zn-2,2-DHA	1	1	0	$Zn^{2+} + L^{2-} \rightleftharpoons ZnL$	9.18*	0.01
	1	1	-1	$Zn^{2+} + L^{2-} \rightleftharpoons ZnLOH^{-} + H^{+}$	0.35*	0.03
Mn-2,2-DHA	1	1	-1	$Mn^{2+} + L^{2-} \rightleftharpoons MnLOH^{-} + H^{+}$	-0.06*	0.01
	1	1	0	$Mn^{2+} + L^{2-} \rightleftharpoons MnL$	7.15*	0.02
	1	1	1	$Mn^{2+} + L^{2-} + H^{+} \rightleftharpoons MnLH^{+}$	14.03*	0.02
Cu-2,2-DHA	1	1	0	$Cu^{2+} + L^{2-} \rightleftharpoons CuL$	13.97*	0.14
	1	1	1	$Cu^{2+} + L^{2-} + H^{+} \rightleftharpoons CuLH^{+}$	18.07*	0.01

Table 4.3 Variable (*) and fixed parameters for least squares refinement of the potentiometric titration data for divalent metal ions with 2,2-DHA.

.

4.3.1 The Ni^{2+} system with 2,2-DHA

In Figure 4.9, the 1:1 titration system showed one extended buffer region between pH 6 and 8, which terminated with a sharp inflection point at 2 equiv of base per metal. Precipitation occurred above pH 8.2. The position of the inflection was consistent with the formation of the 110 species. The 111 and 11-1 complexes were also tested in various models to fit the data, but there was no indication that these complexes were present. Therefore, only the stability constant of the NiL complex of log $\beta_{110} = 9.02 \pm 0.01$ with GOF = 0.009 was calculated.

Using this value for β_{110}, the species distribution diagram at different pH for Ni^{2+} with 2,2-DHA was determined as shown in Figure 4.10. It shows the formation of the 110 species between pH 5 and 8. The proposed structure of the 110 complex is shown in Figure 4.11.

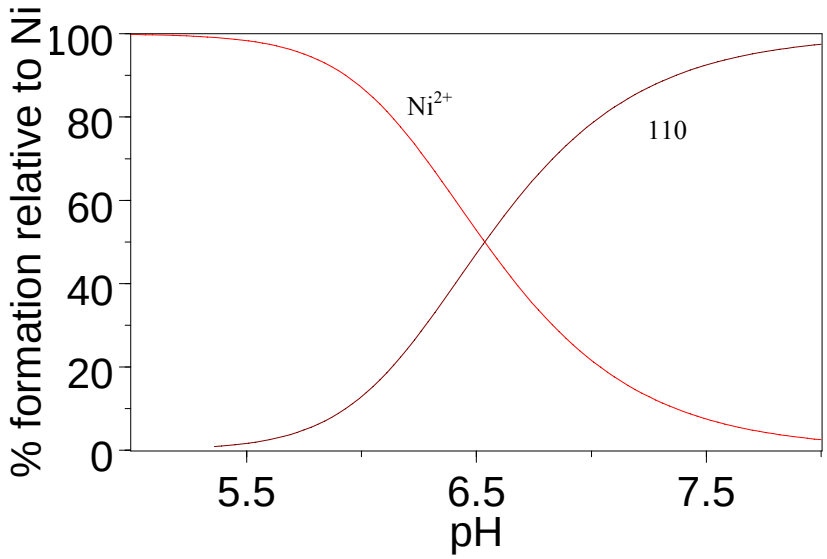

Figure 4.10 Species distribution diagram of 1 mM Ni^{2+} and 1 mM 2,2-DHA as a function of pH.

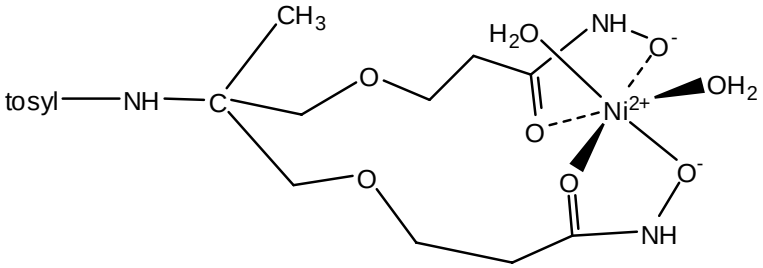

110 complex

Figure 4.11 Proposed structure of the 110 complex of Ni^{2+} with 2,2-DHA.

4.3.2 The Zn^{2+} system with 2,2-DHA

The titration curve of Zn^{2+} with 2,2-DHA is shown in Figure 4.9. The best fit of 0.009 GOF was observed for the model consisting of the 110 and 11-1 complexes, with stability constants of log β_{110} = 9.18 $\pm$ 0.01 and log $\beta_{11\text{-}1}$ = 0.35 $\pm$ 0.03. The addition of a 111 complex did not improve the fit, so this species was excluded from the model. These constants were used to calculate the species distribution diagram shown in Figure 4.12.

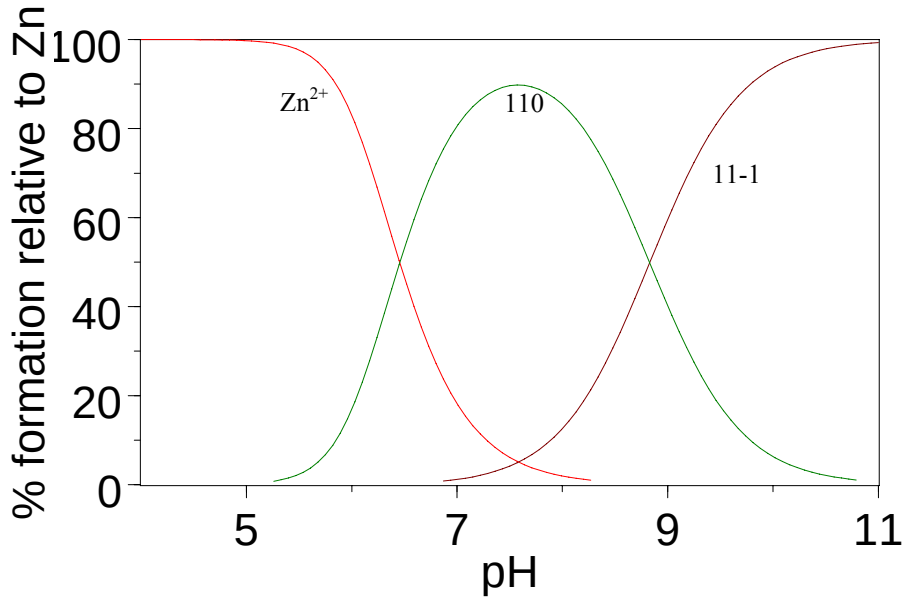

Figure 4.12 Species distribution diagram for 1 mM Zn^{2+} and 1 mM 2,2-DHA as a function of pH.

No complexation occurs below pH 5. The 110 species accumulates to a maximum of 90% at pH 7.5. Above this pH, the 11-1 species begins to form. The proposed structures of the 110 and 11-1 complexes are shown in Figure 4.13. An OH^- was added to an open site of the 110 complex to form the 11-1 complex.

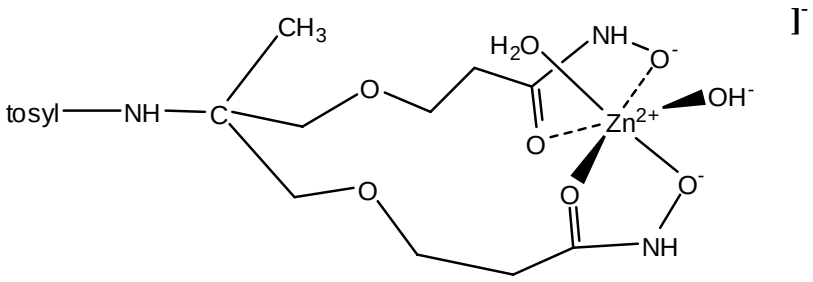

11-1 complex

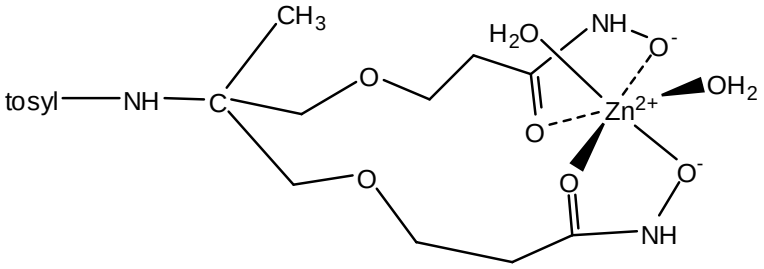

110 complex

Figure 4.13 Proposed structures of the 110 and 11-1 complexes of Zn^{2+} with 2,2-DHA.

4.3.3 The Mn^{2+} system with 2,2-DHA

An inflection at 3.0 equiv of base per metal is observed in the Mn^{2+} system with 2,2-DHA as shown in Figure 4.9, indicating a 11-1 complex is the predominant species at the inflection point. However, the very low affinity of Mn^{2+} for OH^- makes it unlikely that a 11-1 complex would be fully formed at pH 9. As discussed above for the Mn-2,2,2-THA system, we suspect the oxidation of Mn^{2+} to Mn^{3+}, even though the samples were protected from atmospheric oxygen by an argon atmosphere. There is no precipitation during the titration up to pH 10.5 in the manganese titrations. Therefore, non-linear least

squares was utilized to evaluate the stability constant of a 11-1 complex as well as those of the 110 and 111 complexes. The best fit was obtained for the model consisting of the 110, 111 and 11-1 complexes as shown in Table 4.3. A speciation diagram of Mn^{2+} with 2,2-DHA was calculated in the basis of these constant in Figure 4.14.

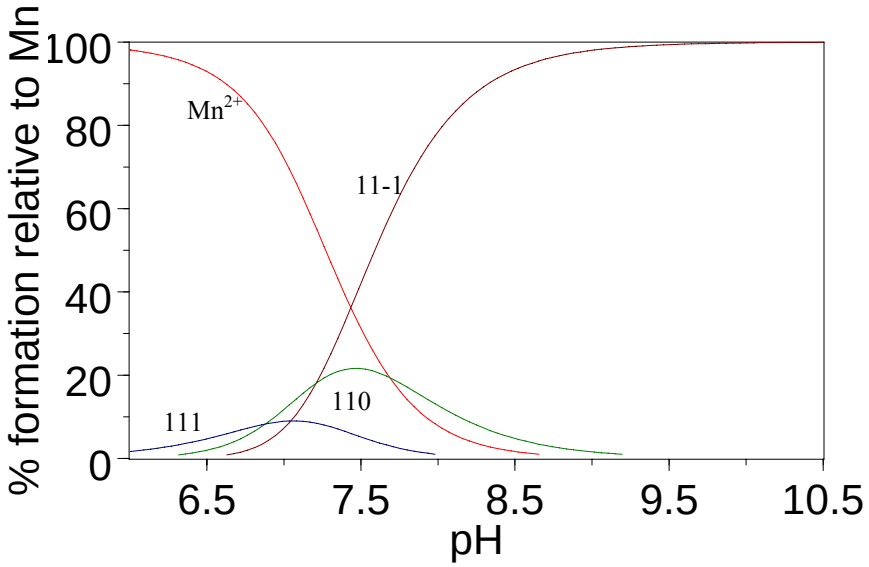

Figure 4.14 Species distribution diagrams for 1 mM Mn^{2+} and 1 mM 2,2-DHA as a function of pH.

Structures for Mn^{2+} complexes that are consistent with the potentiometric data are shown in Figure 4.15. It is odd that Mn^{2+} would hydrolyze at neutral pH to form the 11-1 complex. The hydrolysis pK_a for free Mn^{2+} is 10.9,[20] and complexation by 2,2-DHA should have increased this value. The release of a third proton in the Mn^{2+} titration might be due to oxidation of Mn^{2+} to Mn^{3+}. At this time the source of this "extra" proton is still in doubt, and the structure of the 11-1 complex should be viewed cautiously.

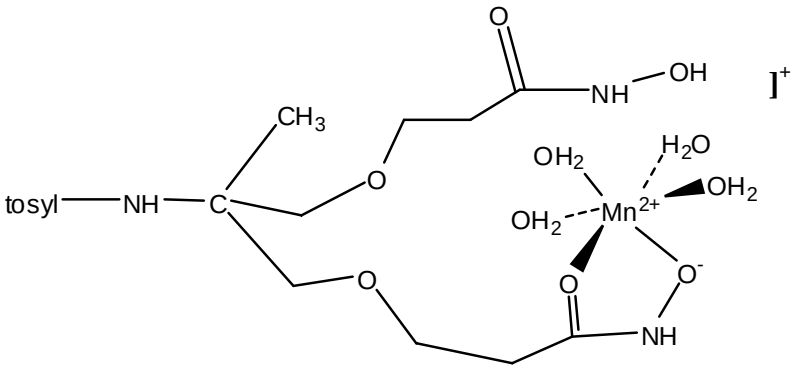

111 complex

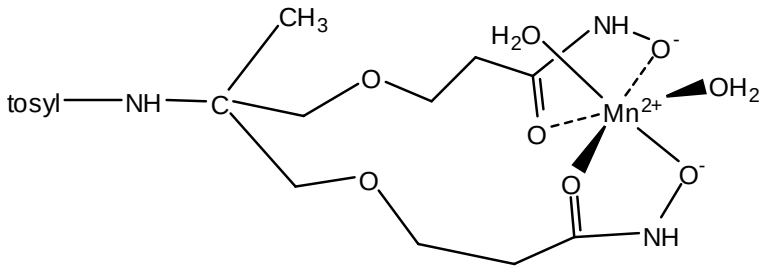

110 complex

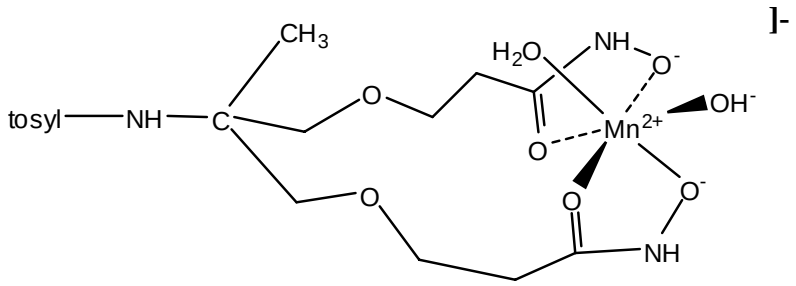

11-1 complex

Figure 4.15 Proposed structures of the 110, 111 and 11-1 complexes of Mn^{2+} with 2,2-DHA.

4.3.4 The Cu^{2+} system with 2,2-DHA

The Cu^{2+} system with 2,2-DHA behaved differently compared to the other divalent metal ions, as shown in Figure 4.9. Because a precipitate appeared as early as pH 3.7, there was a very narrow range of data points that could be used to calculate the stability constants for this system. By adding stock acid, we were able to extend the data to lower pH. The best GOF of 0.005 was observed for the model consisting of the 110 and 111 complexes, with log β_{110} = 13.97 $\pm$ 0.14 and log β_{111} = 18.01 $\pm$ 0.01. These constants have been used to calculate the species distribution diagram in Figure 4.16.

Figure 4.16 shows that the 111 complex is about 5% formed at the beginning of the titration. This complex accumulates to a maximum of 40% at pH 4. The 110 species begins to form at pH 3, but accumulates only to ~30% before precipitation occurs. The proposed structures of the 111 and 110 complexes of Cu^{2+} system are shown in Figure 4.17.

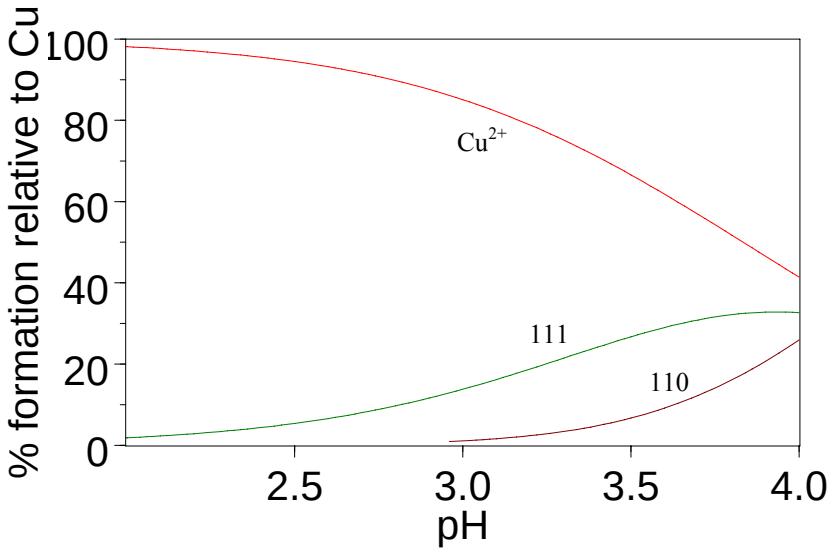

Figure 4.16 Speciation diagram for 1 mM Cu^{2+} and 1 mM 2,2-DHA as a function of pH.

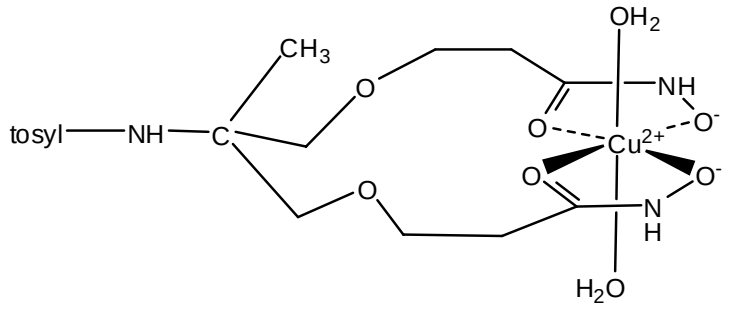

110 complex

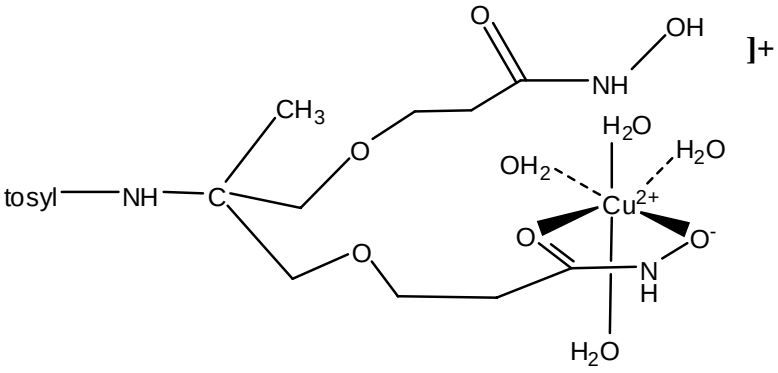

111 complex

Figure 4.17 Proposed structures of the 110 and 111 complexes of Cu^{2+} with 2,2-DHA.

4.4 Comparison of complexation by 2,2,2-THA and 2,2-DHA

The speciation diagrams for 2,2,2-THA with the divalent metal ions consistently show that the predominant complex at neutral pH is the protonated 111 complex, rather than the fully deprotonated 110 complex. The stability of the 111 complex can also be expressed as

$$M^{2+} + HL^{2-} \rightleftharpoons M(HL) \qquad \text{Eq 4.1}$$

with the corresponding equilibrium constant

$$K_{MHL} = \frac{[M(HL)]}{[M^{2+}][HL^{2-}]} \qquad \text{Eq 4.2}$$

This equilibrium constant is not independent of the data reported in Table 4.2. Rather it is a reformulation of the overall β_{ijk} values. Specifically, K_{MHL} can be calculated as

$$K_{MHL} = \beta_{110} / \beta_{011} \qquad \text{Eq 4.3}$$

The advantage of reformulating the binding constant for the protonated form of the complexes of 2,2,2-THA is that the values for K_{MHL} can be compared directly with the β_{110} values for 2,2-DHA. The metal ion is coordinated to two hydroxamate groups in both the M(HL) complexes of 2,2,2-THA and in the 110 complexes of 2,2-DHA, so the binding constants for the two ligands with a given metal ion are expected to be similar to one another. The values for K_{MHL} and the β_{110} values for 2,2-DHA are compared in Table 4.4.

Metal Ion	2,2,2-THA log K(MHL)	2,2-DHA log β_{110}	Δlog K	log β_{120}(AHA)
Mn^{2+}	6.80	7.15	-0.35	6.90
Ni^{2+}	8.84	9.02	-0.18	9.30
Cu^{2+}	13.35	13.97	-0.62	14.06
Zn^{2+}	8.87	9.18	-0.31	9.60

Table 4.4. Comparison of binding affinities for dihydroxamate complexes of 2,2,2-THA and 2,2-DHA. Data on AHA taken from reference 20.

The M(HL) complexes of 2,2,2-THA are consistently less stable than the ML complexes of 2,2-DHA. However, the differences are relatively small, and we feel that the agreement between the stability constants of 2,2,2-THA and 2,2-DHA is quite good.

Table 4.4 also lists the β_{120} values for acetohydroxamic acid. These β_{120} values reflect the chelate effect associated with the formation of a five-membered chelate ring with each bidentate hydroxamate group. The stability constants of the M(HL) complexes of 2,2,2-THA and the 110 complexes of 2,2-DHA also reflect the chelate effect associated with two five-membered hydroxamate chelate rings. In addition, these stability constants will reflect the strain energy associated with the incorporation of the bidentate hydroxamate groups into a larger multidentate ligand. The stability constants for 2,2,2-THA and 2,2-DHA are very similar to the log β_{120} constants for AHA. This is strong evidence that the bis(hydroxamate) complexes of 2,2,2-THA and 2,2-DHA can form with relatively little steric strain.

Although there is no "macrochelate effect" associated with the linkage of two hydroxamates into a tetradentate ligand, it is important to note that for a tetradentate and a bidentate ligand for which log β_{110} (tetradentate) = log β_{120} (bidentate), the tetradentate ligand will be the more effective chelating agent at dilute concentrations. Even when the binding constants are the same, the effective binding affinity of the bidentate ligand will decrease as the square of the ligand concentration, so that dilution will favor binding by the tetradentate ligand.

4.5 Order of stabilities for different metal ions

For a given ligand, the stabilities of the complexes with the divalent first row transition metal ions often show a consistent pattern, which is known as the Irving-Williams order.[21] This order is typically represented as

$$Mn^{2+} < Fe^{2+} < Co^{2+} < Ni^{2+} < Cu^{2+} > Zn^{2+}$$

The position of Zn^{2+} with respect to Co^{2+} and Ni^{2+} is ambiguous. For traditional multidentate ligands such as the amino acids glycine, NTA, and EDTA, or polyamines such as ethylenediamine, diethylenetriamine, or tetraethylenetetraamine, the stability constants for Zn^{2+} are slightly greater than those of Co^{2+} and less than the constants for Ni^{2+}. Thus for these types of ligands, the appropriate description of the order of stabilities would be

$$Mn^{2+} < Fe^{2+} < Co^{2+} \sim Zn^{2+} < Ni^{2+} < Cu^{2+}$$

For both 2,2,2-THA and 2,2-DHA, the order of the experimental stability constants can be represented as

$$Mn^{2+} < Zn^{2+} \sim Ni^{2+} < Cu^{2+}$$

It initially appeared that these ligands were showing an unusually high affinity for Zn^{2+} relative to Ni^{2+}. However, the absolute position of Zn^{2+} in the Irving Williams order

depends on the nature of the ligand. The relative binding affinities for Zn^{2+} and Ni^{2+} for different types of ligands are illustrated by the three linear free energy relationships (LFER) in Figure 4.18. The LFER for the three types of ligands can be described by the linear functions.

N-donors: $\log K (Ni^{2+}) = (1.28 \pm 0.03)\log K (Zn^{2+}) + (0.11 \pm 0.31)$ $\sigma_y = 0.84$ Eq 4.4

N,O-donors: $\log K (Ni^{2+}) = (1.08 \pm 0.02)\log K (Zn^{2+}) + (0.72 \pm 0.20)$ $\sigma_y = 0.62$ Eq 4.5

O-donors: $\log K (Ni^{2+}) = (0.83 \pm 0.02)\log K (Zn^{2+}) + (1.00 \pm 0.14)$ $\sigma_y = 0.43$ Eq 4.6

Using these functions, a log K value of 10.0 for a Zn^{2+} complex would predict log K (Ni^{2+}) values of 12.9 for N-donors and 11.5 for N,O-donors. Thus traditional polyamine and amino acids form more stable complexes with Ni^{2+} than with Zn^{2+}. However, the slope of the LFER for O-donors is clearly smaller than the slopes for either N-donors or N,O-donors, so that a log K of 10.0 for Zn^{2+} predicts a log K of only 9.3 for Ni^{2+}. Thus for hydroxamates, the binding affinities for Zn^{2+} and Ni^{2+} will be similar, with slightly higher values for Zn^{2+}. The results in Table 4.4 are consistent with this LFER prediction.

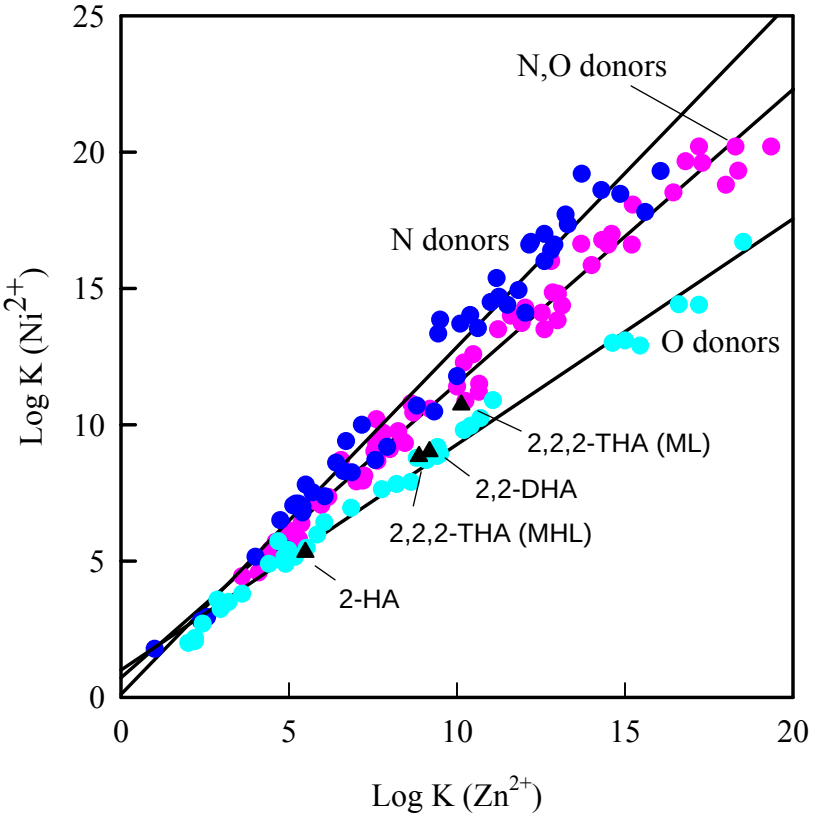

Figure 4.18. Linear free energy relationships for the complexation of Ni^{2+} and Zn^{2+} for three types of ligands: N-donors (aliphatic amines, imidazoles, pyridines), N,O-donors (N-donors linked with carboxylate and phenolate groups), and O-donors (carboxylates, phenols, hydroxamates). Stability constant data were taken from reference 20.

The data for the regression line for O-donors included four hydroxamic acids, for which the average residual between the observed log K and the regression line was only 0.39. Thus literature log K values for hydroxamates fit the O-donor regression line very well. The log K values for the monohydroxamate complexes with 2-HA and the bis(hydroxamate) complexes of 2,2,2-THA and 2,2-DHA are also in excellent agreement

with the regression line for the LFER for O-donor ligands. The log β_{110} value for 2,2,2-THA does not agree as well with the LFER for O-donors. The data point for this constant lies 1.3 log units (~ 3 σ_y) above the regression line. There is no obvious reason why the Ni^{2+} complex of 2,2,2-THA should be unusually stable relative to the Zn^{2+} complex. Due to ligand field stabilization energy, the Ni^{2+} ion has a stronger preference for a regular octahedral geometry. Thus we would have predicted that due to greater steric strain, the Ni^{2+} complex might be *less stable* relative to Zn^{2+}.

There are experimental problems regarding the determination of the β_{110} constant for Ni^{2+}. The potentiometric titration data are terminated by precipitation after only a small fraction of the Ni^{2+} 111 complex has been deprotonated to the 110 complex. The low degree of formation of the 110 complex and the potential errors in pH introduced by incipient precipitation lowers our degree of confidence in the log β_{110} constant for the Ni complex. The LFER would suggest that our value for the Ni^{2+} log β_{110} constant is too high.

Based on the Irving Williams order, one certainly expects Mn^{2+} complexes to be relatively weak, and the data shown in Table 4.4 confirm that Mn^{2+} forms the weakest complexes with both hydroxamate ligands. As shown in Figure 4.18, one can use LFER to make more quantitative predictions of stability constants. Figure 4.19 shows an LFER in which log K values for Zn^{2+} are correlated with log K values for Mn^{2+} for a series of 53 O-donor ligands. The regression line for this LFER is described by the equation

$$\log K\,(Mn^{2+}) = (0.76 \pm 0.01)\log K(Zn^{2+}) + (0.08 \pm 0.10), \quad \sigma_y = 0.42 \qquad \text{Eq 4.7}$$

The filled triangles in Figure 4.19 show the data points for 2,2-DHA, 2,2,2-THA, and the literature values for AHA. The hydroxamate data are in excellent agreement with the LFER for all the data with one exception. Once again, the value for β_{110} for 2,2,2-THA lies well above the regression line, suggesting that the value for Mn^{2+} is too high.

It is also noteworthy that the best fit of the potentiometric data for Mn^{2+} included a 11-1 complex. The equilibrium constant for the binding of an OH^- ligand to the 110 complex to form the 11-1 complex is log K_{OH} = 3.4. The corresponding log K_{OH} value for binding OH^- to the hexaaquo Mn^{2+} ion is only 2.9. Thus the data would appear to indicate that a Mn^{2+} ion already bound to three hydroxamate groups in the 110 complex has a higher affinity for an OH^- ligand than does the hexaaquo Mn^{2+} ion. This is an unreasonable conclusion. As strong ligands coordinate a metal ion, the affinity for adding an OH^- ligand should decrease relative to that of the aquo ion. Indeed, for the Zn^{2+} complex with 2,2,2-THA, the log K_{OH} value is 3.9, compared to a log K_{OH} of 5.0 for the hexaaquo Zn^{2+} ion. The Mn^{2+} complex with 2,2-DHA also appears to show an unusually high tendency to bind an OH^- ligand.

It is well-established in the literature on iron complexes that the coordination of hydroxamate ligands stabilizes higher metal ion oxidation states. For example, the coordination of DFO shifts the reduction potential of Fe^{3+} from +0.77 V to -0.468 V vs NHE.[22] Even though the potentiometric titration samples were kept under an argon atmosphere, we suspect that some oxidation of the Mn^{2+} occurred at higher pH values. The presence of either Mn^{3+} or Mn^{4+} would release additional protons both by binding more tightly to the ligand and by hydrolysis, which would lead to the calculation of higher values for the Mn^{2+} binding constants. The LFER would suggest that the values for

β_{111} for 2,2,2-THA and β_{110} for 2,2-DHA are accurate. We suspect that oxidation at higher pHs has effected the accuracy of β_{110} and $\beta_{11\text{-}1}$ for 2,2,2-THA and $\beta_{11\text{-}1}$ for 2,2-DHA.

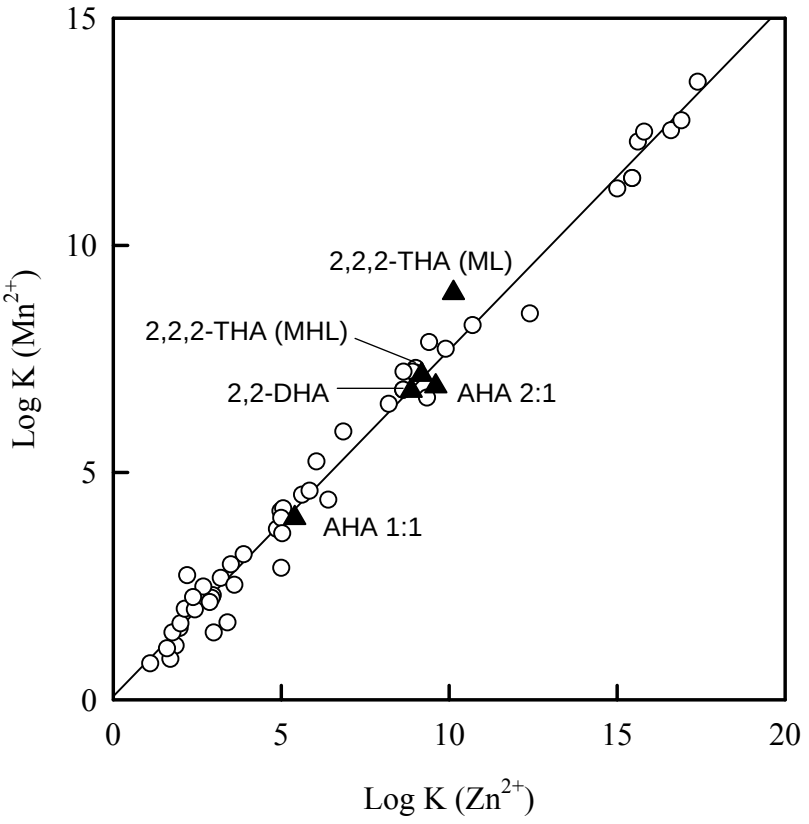

Figure 4.19. Linear free energy relationship for the complexation of Mn^{2+} and Zn^{2+} for O-donors.

4.6 Divalent metal ions with 2-HA

Potentiometric titrations of a 1:1 mixture of Cu^{2+}, Mn^{2+}, Zn^{2+} and Ni^{2+} with 2-HA were performed. The titration curves of all the divalent metal are shown in Figure 4.20. Precipitation occurs for Cu^{2+} at pH 4.0, while precipitation in the Ni^{2+}, Mn^{2+} and Zn^{2+}

systems is observed between pH 7 and 8. Models that included the 110 and 11-1 complexes were considered for the refinement of the titration data, but the results showed that only the 110 species is present in significant concentrations. The values for log β_{110} are listed in Table 4.5.

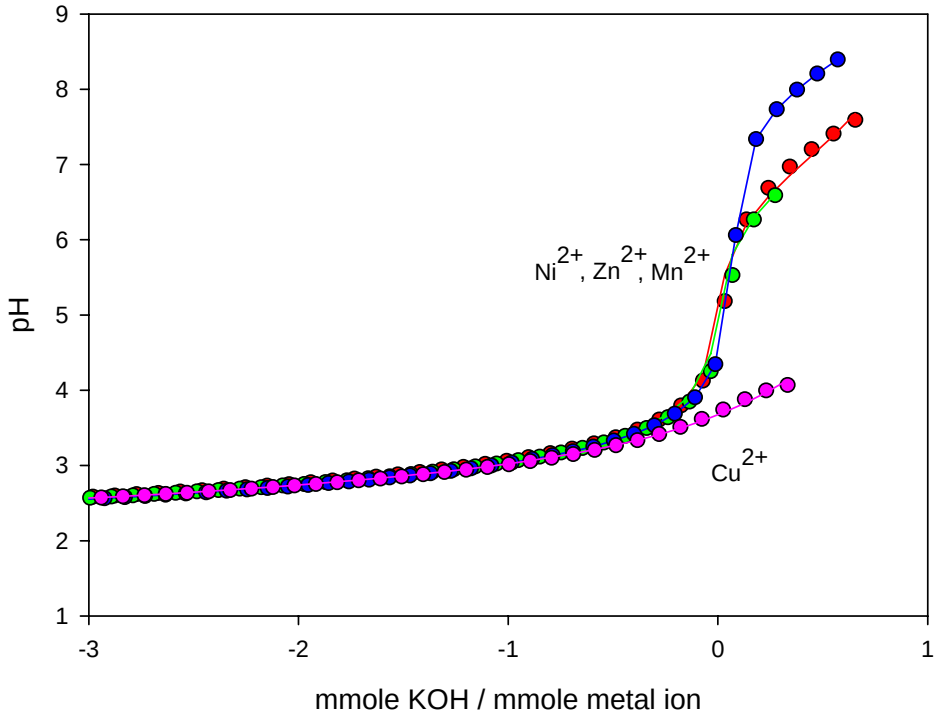

Figure 4.20 Potentiometric titration curves of 1:1 ratios of Ni^{2+} (red), Zn^{2+} (green), Mn^{2+} (blue) and Cu^{2+} (pink) with 2-HA. The symbols represent the observed data points while the lines represent the least squares fits based on the ligand protonation constants and the stability constants listed in Table 4.5.

System	i	j	k	reaction	log β_{ijk}	σ
2-HA	0	1	1	$L^- + H^+ \rightleftharpoons HL$	9.26	
Ni-2-HA	1	1	0	$Ni^{2+} + L^- \rightleftharpoons NiL^+$	5.33*	0.04
Zn-2-HA	1	1	0	$Zn^{2+} + L^- \rightleftharpoons ZnL^+$	5.49*	0.09
Mn-2-HA	1	1	0	$Mn^{2+} + L^- \rightleftharpoons MnL^+$	4.30*	0.10
Cu-2-HA	1	1	0	$Mn^{2+} + L^- \rightleftharpoons MnL^+$	8.26*	0.02

Table 4.5 Variable (*) and fixed parameters for the least squares refinement of the potentiometric titration data for divalent metal ions with 2-HA.

The stability constants of the 110 complexes of Cu^{2+}, Zn^{2+} and Ni^{2+} with AHA and 2-HA are compared in Table 4.6. The binding constants for 2-HA and AHA are essentially identical for Ni^{2+} and Zn^{2+}. 2-HA has a slightly higher affinity for Cu^{2+} than does AHA. The reason for this is not clear. Given the steric bulk of 2-HA, lower binding constants for this ligand might have been expected.

Metal ion	log β_{110} AHA	log β_{110} 2-HA
Ni^{2+}	5.30	5.33
Zn^{2+}	5.40	5.49
Cu^{2+}	7. 9	8.26

Table 4.6 Comparison of log β_{110} values for the monohydroxamates AHA[20] and 2-HA.

The log β_{110} values Cu^{2+}, Mn^{2+}, Zn^{2+} and Ni^{2+} with 2-HA were used to calculate species distribution diagrams as shown in Figure 4.21. For Mn^{2+}, Zn^{2+} and Ni^{2+} with 2-HA, the 110 species begin to form at pH 5, and accumulate to >50% above pH 7 for Zn^{2+}, Ni^{2+} and Mn^{2+} and to > 40% at pH 4 for the 110 complex of Cu^{2+} .

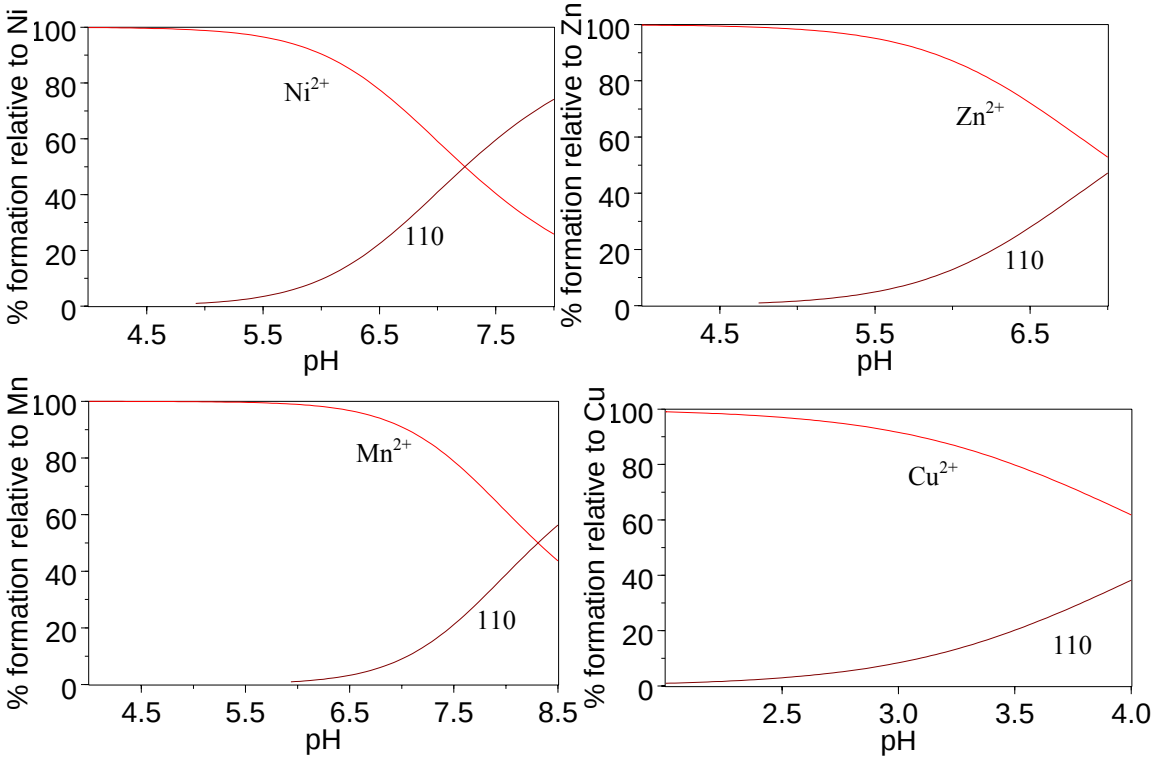

Figure 4.21 Species distribution diagrams of 1 mM Cu^{2+}, Mn^{2+}, Zn^{2+} and Ni^{2+} and 1 mM 2-HA as a function of pH.

The complexation behavior of ligands containing different numbers of hydroxamate groups with Cu^{2+}, Mn^{2+}, Zn^{2+} and Ni^{2+} has been studied. The variation in stability of the metal complexes follow the Irving-William order for 2,2,2-THA, 2,2-DHA and 2-HA, with the order of stability represented as

$$Mn^{2+} < Zn^{2+} \sim Ni^{2+} < Cu^{2+}$$

The results on these studies also give the magnitude of the stability constants of divalent metal ions with a new series of hydroxamic acid ligands compared to trivalent metal ions, for which the order of the stability constants is

$$Mn^{2+} < Zn^{2+} \sim Ni^{2+} < Cu^{2+} < Al^{3+} < Fe^{3+}$$

References

1. Kurzak, B.; Kozlowski, H.; Farkas, E. *Coord. Chem. Rev.* 1992, 114, 169.

2. Crumbliss, A. L. *Coord. Chem. Rev.* 1990, 105, 155.

3. Neilands, J. B. *J. Biol. Chem.* 1995, 270, 2672.

4. Tam, S. S. C.; Lee, D. H. S.; Wang, E. Y.; Munroe, D. G.; Lau, C. Y. *J. Biol. Chem.* 1995, 270, 13948.

5. Marmion,C. J.; Murphy, T.; Docherty, J. R.; Nolan, K. B. *Chem. Commun.* 2000, 1153.

6. Miller, M. J. *Chem. Rev.* 1989, 89, 1563.

7. Botos, I.; Scapozza, L.; Zhang, D.; Liotta L. A.; Meyer, E. F *Proc. Natl. Acad. Sci. USA* 1996, 93, 2749.

8. Arnold, M.; Brown, D. A.; Deeg, O.; Errington, W.; Haase, W.; Herlihy, K.; Temp, T. J.; Nimir, H.; Werner, R. *Inorg. Chem.* 1998, 37, 2920.

9. Pearson, M. A.; Michel, L. O.; Hauusinger, R. P.; Andrew, K. P. *Biochemistry* 1997, 36, 8164.

11. Stemmler, A. J. ; Kampf, J. W.; Kirk , M. L.; Pecoraro,V. L. *J. Am. Chem. Soc.* 1995, 117, 6368.

12. Parker, M. H.; Lunney, E. A.; Ortwine, D. F.; Paviovsky, A. G.; Humblet, C.; Brouillette, C. G. *Biochemistry* 1999, 38, 13592.

13. Scolnick, L. R.; Clements, A. M.; Liao, J.; Crenshaw, L.; Helberg, M.; May, J.; Dean, T. R.; Christianson, D. W. *J. Am. Chem. Soc.* 1997, 119, 850.

14. Gaynor, D.; Starikova, Z. A.; Haase, W.;Nolan, K. B. *J. Chem. Soc*, *Dalton Trans.*

2001, 1578.

15. Pearson, R. G. *J. Chem. Ed.* 1968, 45, 681.

16. Martin, R. B. *Bioinorganic chemistry of magnesium. Metal ions in biological systems* 1990, 26, 1.

17. Evers, A.; Hancock, R. D.; Martell, A. E.; Motekaitis, R. J. *Inorg. Chem.* 1989, 28, 2189.

18. Anderegg, G.; L'Eplattenier, F.; Schwarzenbach, G. *Helv. Chim. Acta* 1963, 46, 100.

19. Farkas, E.; Csoka, H.; Micera, G.; Sanna, D. *J. Inorg. Biochem.* 1995, 60, 45.

20. Martell, A. E.; Smith, R. M. *Critical stability Constants*, Plenum, New York, 1988, vol 6.

21. Irving, H.; Williams, R. J. P. *J. Chem. Soc*. 1953, 3192.

22. Albrecht-Gary, A. M.; Crumbliss, A. L. *Coordination Chemistry of Siderophores: Thermodynamics and Kinetics of Iron Chelation and Release, In:Metal Ions in Biological Systems,* Sigel, A. and Sigel H., Eds, Volume 35, Marcel Dekker, New York, 1998, 239.

Chapter 5

The stability constant of aluminum with gluconic acid

5.1 Introduction

Gluconic acid consists of a six-carbon chain with five hydroxyl groups terminating in a carboxylic acid as shown in Figure 5.1. In acidic aqueous solution, there is an equilibrium between the linear carboxylic acid and the cyclic ester glucono-σ-lactone.[1]

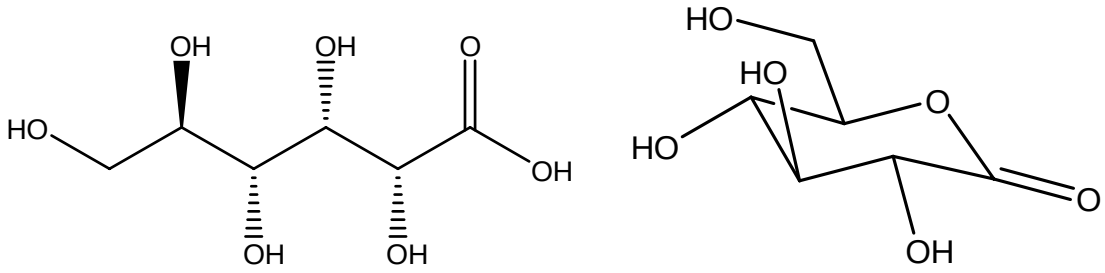

Figure 5.1 The linear and cyclical structures of gluconic acid.[1]

Aqueous Ca-gluconate is the main source of Al^{3+} contamination in TPN solutions. The high level of Al^{3+} in gluconate solutions is due in large part to the fact that gluconate has a relatively high binding affinity for the Al^{3+} ion.[2] Any chelating resin will have to compete against gluconate to remove Al^{3+} from solution, so it is important to have an accurate assessment of the strength of the Al-gluconate binding. Therefore, the complexation Al^{3+} by gluconic acid has been evaluated by a combination of potentiometric and spectrophotometric methods.

5.2 Potentiometric titration of gluconic acid and a 1:3 ratio of Al^{3+}: gluconic acid

Potentiometric titrations were conducted to determine the protonation constant of gluconic acid and the binding constants of aluminum-gluconate. The results are shown in Figure 5.2. In the ligand titration, one proton is released from the carboxylic acid, resulting in a sharp inflection at 1 equiv of base. These titration data were used with the non-linear least squares program BETA to calculate the protonation constant of gluconic acid. The refinement had a GOF of 0.012 for a protonation constant of log K = 3.62 $\pm$ 0.06, which is comparable to the value from the literature.[2]

A 1:3 ratio of Al^{3+} and gluconic acid was titrated in the forward direction by using KOH as titrant, and the titration curve is shown in Figure 5.2. However, there was a serious problem with long equilibration times. In our potentiometric titration studies, we generally used a maximum equilibration time of 10 min for each titration point. As shown in Figure 5.2, only the initial points in the titration reached equilibrium within the allowable 10 min. Data points that did not reach equilibrium are excluded from any calculations, so the forward titrations provide very little data suitable for least squares refinement.

At low pH the equilibrium between the linear and cyclical forms of gluconic acid favors the cyclical form. There was concern that the slow equilibration kinetics might be related to a slow rate of ring opening from the lactone to the linear gluconic acid. Therefore, backward titrations from high pH to low pH were also conducted. In these experiments, the gluconic acid was taken to high pH by the addition of KOH and allowed to equilibrate, which should ensure that all the gluconate was in the linear form. An aliquot of Al^{3+} was added to this solution, which was then titrated with HCl. The

backward titration curve is also shown in Figure 5.2. The system again failed to reach equilibrium for the titration points from pH 10 to pH 4. The lack of equilibration is also indicated by the obvious difference between the forward and reverse titrations, which should be essentially identical. Thus potentiometric titrations using our standard procedures failed to produce any data which could be used to calculate the Al-gluconate binding constants.

Stability constants for Al-gluconate determined by potentiometric titration have been reported.[2] It appears that these workers used much longer equilibration times. We could have repeated the potentiometric titrations using a larger limit for the maximum equilibration time. However, a single titration would have taken many hours, and we were concerned that the inevitable drift in the calibration of the pH electrode would compromise the quality of the data. Therefore, we decided to pursue spectrophotometric studies on Al-gluconate binding.

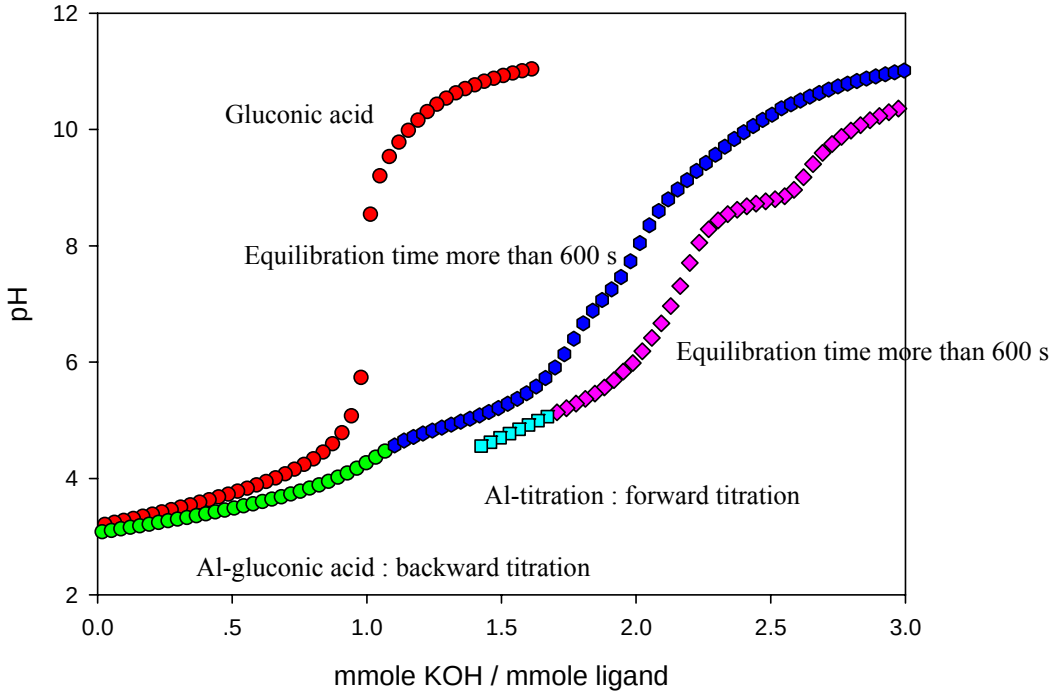

Figure 5.2 Potentiometric titration curves for gluconic acid and both forward and back titrations of a 1:3 ratio of Al^{3+}: gluconic acid.

The Al^{3+} ion, gluconate, and Al-gluconate are all colorless, so some complexiometric indicator is needed for spectrophotometric studies on this system. The chelating agent calcein has been used as a fluorescent probe for aluminum studies.[3] It is a fluorescent molecule with excitation and emission wavelengths of 495 and 515 nm, respectively. Calcein is also used as an indicator for titrations of calcium ions with EDTA,[4] and for fluorometric determinations of ferric ion [5-6] and divalent metal ions such as Fe^{2+}, Cu^{2+}, Co^{2+} and Ni^{2+}.[7-8]

The solution pH of Ca-gluconate in TPN solutions is between pH 5 and 8. We initially planned to follow Al^{3+} binding by fluorescence, but over this pH range, but the differences in the fluorescence spectra of free calcein and the Al-calcein complex is rather small.[3] Due to this limitation, the binding of Al^{3+} to calcein was studied using UV-vis spectroscopy instead of fluorescence.

5.3 Visible spectrophotometric studies of Al-calcein

The objective was to use calcein both as a spectrophotometric indicator and as a competitive chelating agent in the assessment of Al-gluconate binding. Prior to any studies on the Al^{3+} binding affinity for gluconate, it was necessary to unambiguously establish the metal:ligand stoichiometry and binding constant for the Al-calcein complex. A UV-visible titration was carried out by the addition of Al^{3+} to a HEPES-buffered solution (pH 8.0) of calcein. Free calcein has an absorbance peak at λ_{max} = 490 nm, as shown in Figure 5.3. The addition of Al^{3+} results in a decrease in the absorbance and a blue shift in λ_{max}. At low ratios of Al^{3+}:calcein, the spectra exhibit a well-defined isosbestic point at 480 nm. This isosbestic point indicates that only one metal-calcein complex is being formed. The program SPECFIT has been used to fit these data using two models. One model assumed the formation of a 1:1 complex, while the second model assumed the formation of a 1:2 $Al(calcein)_2$ complex.

.

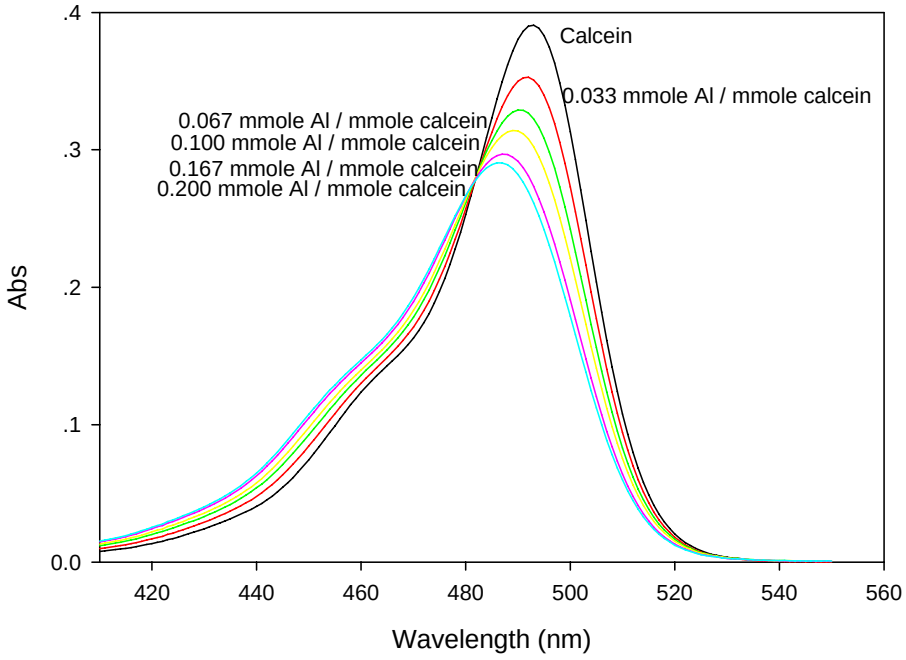

Figure 5.3 Visible spectra from the titration of calcein with Al^{3+} at pH 8.

In the solutions represented by the spectra in Figure 5.3, OH^- functions as a competitive ligand versus the calcein. Thus the aluminum hydrolysis constants were included as fixed parameters in SPECFIT, while the stability constant of either the 110 or 120 complex of Al-calcein was treated as a variable parameter to refine the spectrophotometric titration data. The results for the two models are shown in Table 5.1. A much smaller error of 0.39 was found for the model that included the 120 complex. Additional replicate titrations resulted in an average value of log β_{120}^{*} = 19.70 $\pm$ 0.15. This is an effective binding constant that is valid only at the experimental pH of 8.

Species	1:1 Model	1:2 Model
100	0	0
010	0	0
10-1	-5.46	-5.46
10-2	-10.04	-10.04
10-3	-15.74	-15.74
10-4	-23.49	-23.49
110	14.08± 1.19*	-
120	-	19.75±0.39*

Table 5.1 Variable (*) and fixed parameters in the SPECFIT analysis of the spectrophotometric titration data for Al-calcein.

5.4 Determination of the effective binding constant of Al-calcein by competition with HEDTA

We also measured the stability constant of $Al(calcein)_2$ by competition versus the chelating ligand HEDTA. The samples contained a 1:5 ratio of Al^{3+}:calcein to ensure the formation of the $Al(calcein)_2$ complex. The samples were initially titrated with EDTA in HEPES buffer at pH 8. The results indicated that the addition of approximately 1 mmole EDTA/mmole Al^{3+} resulted in the complete removal of the Al^{3+} from the calcein, which reflects the strong binding of Al^{3+} by EDTA at the experimental pH of 8. Since the

competition equilibrium between calcein and EDTA is shifted so strongly in favor of EDTA, this ligand is a poor choice to use in the determination of an Al-calcein binding constant. Therefore, other ligands having structures similar to EDTA but with lower log β_{110} values were considered, and the ligand HEDTA was selected. The structures for EDTA and HEDTA are shown in Figure 5.4. The log β_{110} values for EDTA and HEDTA are 16.5 and 14.4,[9] respectively.

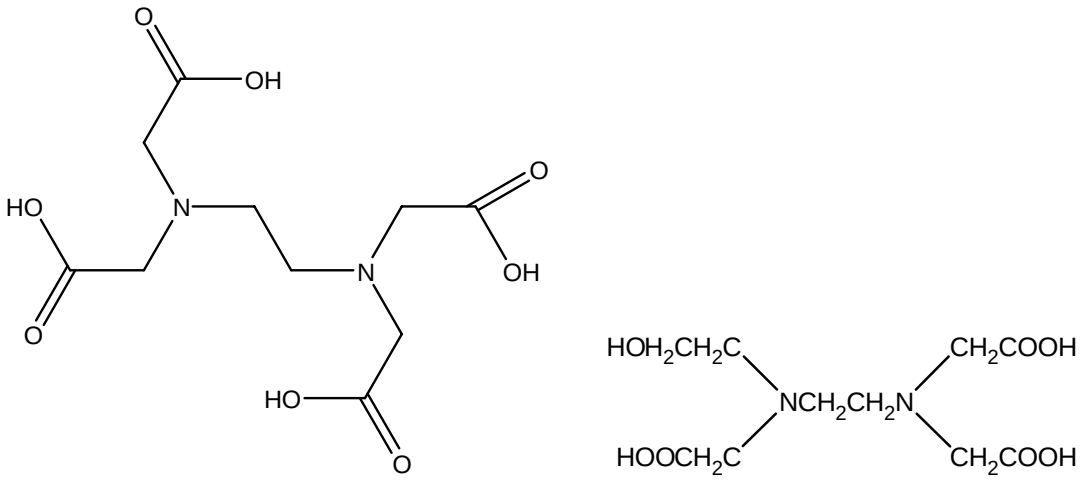

EDTA HEDTA

Figure 5.4 Structures of EDTA and HEDTA.

Two different spectrophotometric methods were used to monitor the titration of Al-calcein with HEDTA. For the spectra shown in Figure 5.5, the spectrophotometric baseline was set with equimolar calcein in both the sample and reference cuvettes. Aluminum was then added to the sample cuvette to give the spectrum marked as Al-calcein. The peak at 490 is negative because the Al(calcien)$_2$ complex has a smaller

absorbance than the free calcein that was used to set the baseline. The addition of aliquots of HEDTA removes Al^{3+} from the $Al(calcein)_2$ complex, and the absorbance moves back toward the calcein vs calcein baseline. Aliquots of HEDTA were added until there is no further change in the absorbance.

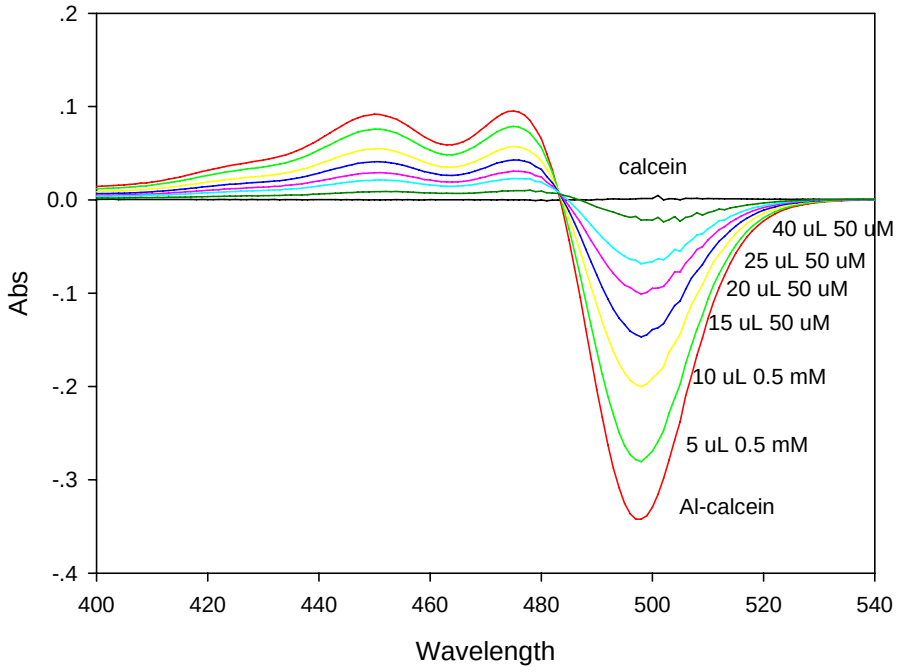

Figure 5.5 HEDTA Titration of Al-calcein using calcein vs calcein as the spectrophotometric baseline.

In the second method, an equilibrated Al-calcein solution was placed in both the sample and reference cuvettes and used to set the spectrophotometric baseline. The sample cuvette was then titrated with HEDTA to generate the family of spectra shown in Figure 5.6. The spectra showed an increasing absorbance with the addition of HEDTA.

The addition of HEDTA removed Al^{3+} from the $Al(calcein)_2$ complex, generating free calcein. Since this free calcein has a higher absorbance than the $Al(calcien)_2$ complex that was used to set the baseline, the absorbance at 490 nm increased. Aliquots of HEDTA were added until there was no further change in the absorbance.

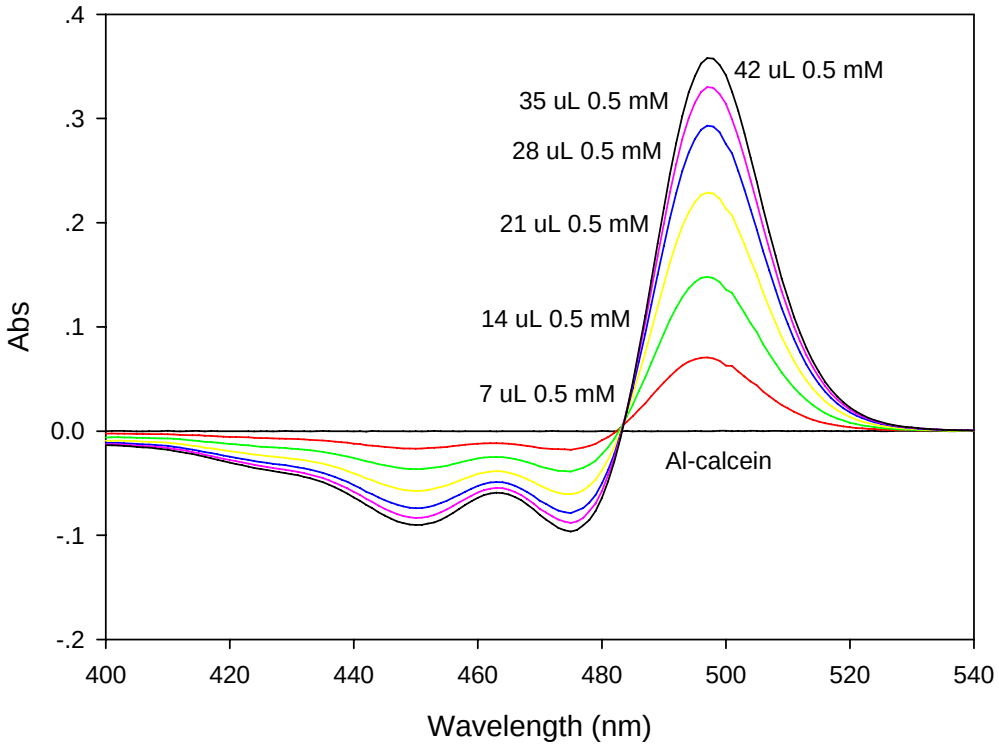

Figure 5.6 HEDTA titration of Al-calcein using Al-calcein vs Al-calcein as the spectrophotometric baseline.

The data from Figure 5.5 were used to prepare a plot of absorbance vs mmole HEDTA/mmole Al^{3+}. The spectra cover a range 0 to 4 mmole HEDTA/mmole Al^{3+}, as shown in Figure 5.7.

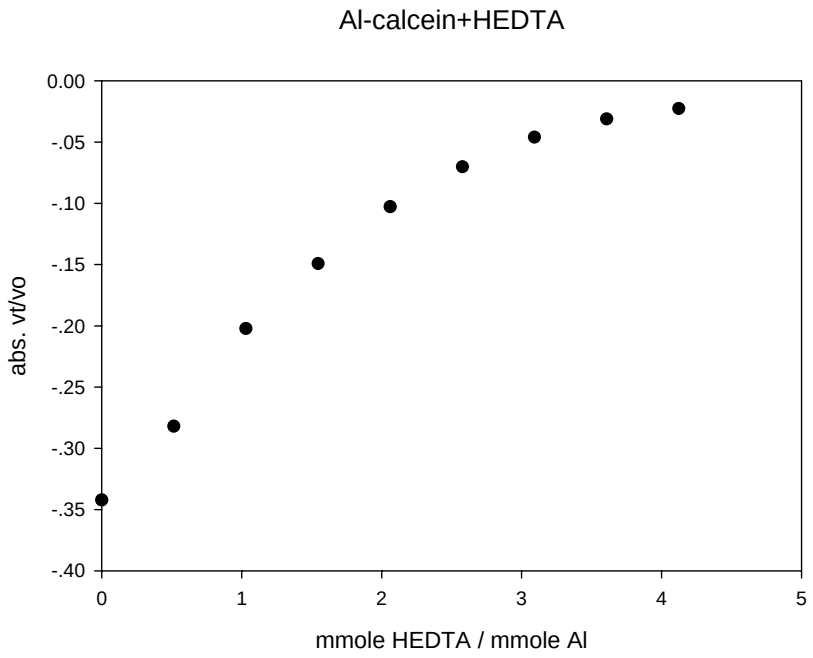

Figure 5.7 Plot of absorbance vs mmole HEDTA/mmole Al^{3+} for an HEDTA titration of $Al(calcein)_2$.

The exchange constant for the competition between calcein and HEDTA for Al^{3+} is shown in Equation 5.1. The $Al(calcein)_2$ complex reacts with HEDTA to form Al-HEDTA and release free calcein.

$$Al(Cal)_2 + HEDTA^{3-} \rightleftharpoons \text{Al-HEDTA} + 2Cal \qquad \text{Eq 5.1}$$

The exchange constant, K_X, represents the ratio of the effective binding constants for Al-HEDTA and $Al(calcein)_2$ at the experimental pH 8, as shown in Equation 5.2.

$$K_X = \frac{[Al(HEDTA)][Cal]^2}{[Al(Cal)_2][HEDTA]} = \frac{\beta_{110}(Al-HEDTA)}{\beta^*_{120}(Al-Calcein)} \qquad \text{Eq 5.2}$$

where β_{120}^* is the effective binding constant for calcein at pH 8.

The mass balance equations for total aluminum, HEDTA, and calcein that describe the exchange experiments are shown below.

$$[Al]_{tot} = [Al(Cal)_2] + \alpha_{ML}[Al\text{-}HEDTA] \qquad \text{Eq 5.3}$$

$$[HEDTA]_{tot} = \alpha_L [HEDTA^{3-}] + \alpha_{ML}[Al\text{-}HEDTA] \qquad \text{Eq 5.4}$$

$$[Cal]_{tot} = 2[Al(Cal)_2] + [Cal] \qquad \text{Eq 5.5}$$

where the α_L term in Equation 5.4 is defined as

$$\alpha_L = 1 + K_1[H] + K_1K_2[H]^2 + K_1K_2K_3[H]^3 \qquad \text{Eq 5.6}$$

The Ks in the α_L term are the known protonation constants for HEDTA,[10] and this term accounts for the different protonated forms of free HEDTA present in the solution at pH 8. The α_{ML} term is defined as

$$\alpha_{ML} = 1 + \frac{K_{ML}^{OH}}{[H]} \qquad \text{Eq 5.7}$$

and

$$K_{ML}^{OH} = \frac{[ML(OH)][H]}{[ML]} \qquad \text{Eq 5.8}$$

The absorbance spectra in Figure 5.5 and 5.6 can be used to determine the concentration of Al(HEDTA) and $Al(Cal)_2$ at each point in the titration. Once these concentrations are known, the concentrations of free HEDTA and free calcein can be obtained from the mass balance equations. This provides all the concentrations needed to

calculate K_X. The values of K_x and the known β_{110} value for HEDTA have been used with Equation 2 to calculate the β_{120}^* for the $Al(Cal)_2$ complex to be log β_{120}^* = 19.83 $\pm$ 0.16 for pH 8.0. This result is in excellent agreement with the value of log β^*_{120} = 19.70 that was obtained by competition with OH^- in the absence of HEDTA.

5.5 Determination of the effective binding constant of Al-gluconate by competition with calcein

A competition study of Al-gluconate with calcein has been performed, in which aliquots of gluconate were added to a 1:10 ratio of Al-calcein solution at pH 8. In these experiments calcein was used in both cuvettes to set the spectrophotometric baseline. Aluminum was added and allowed to equilibrate, which produced the spectrum marked as Al-calcein in Figure 5.8. This solution was then titrated with gluconate to generate the other spectra in Figure 5.8. The formation of the Al-gluconate complex and the release free calcein caused an increase in the absorbance. The absorbances as a function of the mmole gluconate/mmole Al^{3+} in these studies is shown in Figure 5.9.

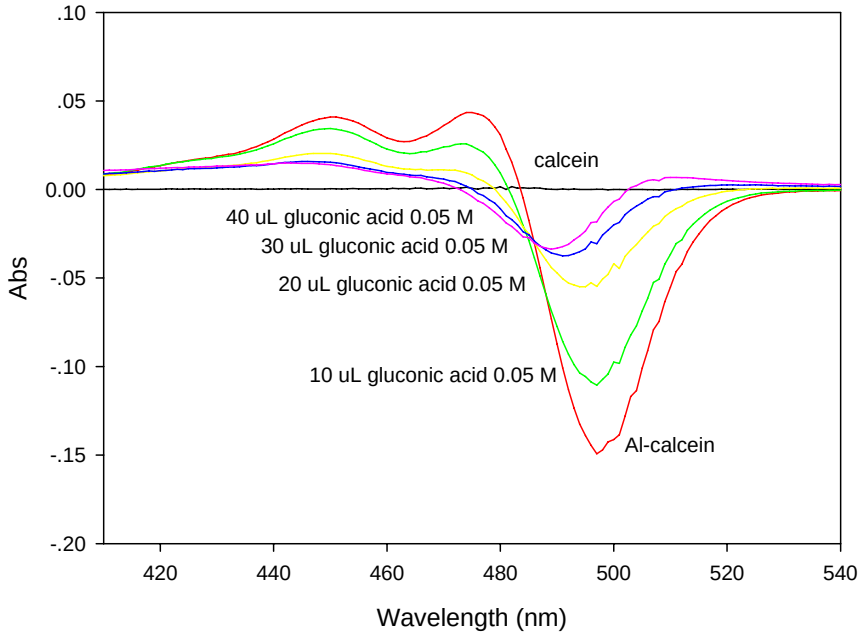

Figure 5.8 Gluconate titration of Al-calcein using calcein vs calcein to set the spectrophotometric baseline.

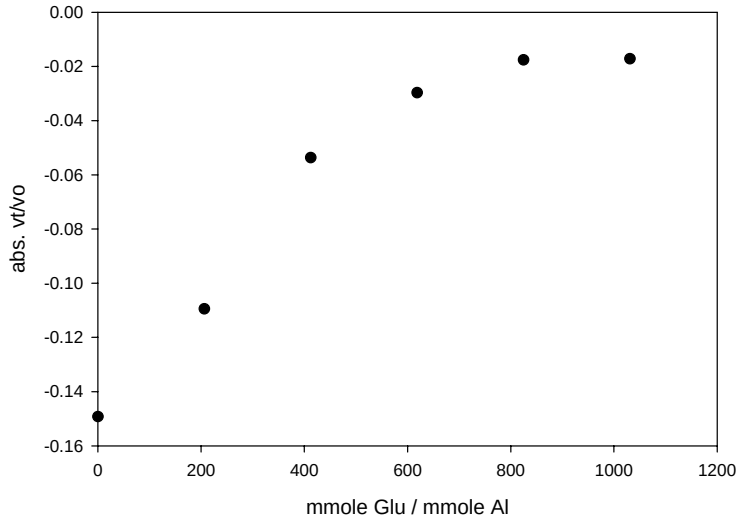

Figure 5.9 Plot of absorbance vs mmole gluconate/mmole Al^{3+} for the titration of Al-calcein with gluconate.

As with the HEDTA competition studies with Al-calcein, the exchange constant, K_x, represents the ratio of the effective binding constant for Al-gluconate and Al-calcein at the experimental pH 8 as shown in Equations 5.9 and 5.10.

$$Al(Cal)_2 + Gluconate \rightleftharpoons Al(Gluconate) + 2Cal \qquad \text{Eq 5.9}$$

$$K_X = \frac{[Al(glu)][Cal]^2}{[Al(Cal)_2][glu]} = \frac{\beta^*_{110}(Al-gluconate)}{\beta^*_{120}(Al-calcein)} \qquad \text{Eq 5.10}$$

The β values in Equation 5.10 are both effective binding constants that are valid only at the experimental pH of 8. The appropriate mass balance equations for total aluminum, total gluconate, and total calcein are

$$[Al]_{tot} = [Al(Cal)_2] + [Al\text{-}Gluconate] \qquad \text{Eq 5.11}$$

$$[Glu]_{tot} = \alpha_L [Gluconate] + [Al\text{-}Gluconate] \qquad \text{Eq 5.12}$$

$$[Cal]_{tot} = [Al(Cal)_2] + [Cal] \qquad \text{Eq 5.13}$$

where the α_L function in Equation 12 represents the protonation of gluconate and is defined as

$$\alpha_L = 1 + K_1[H] \qquad \text{Eq 5.14}$$

Equation 5.11 shows that the total concentrations of Al^{3+} is the sum of the concentrations of the $Al(calcein)_2$ and Al(gluconate) complexes. These concentrations were determined from the absorbance spectra of the competition experiments. The concentrations of free gluconate and free calcein were determined from the mass balance

equations. These concentrations were used to calculate a value of K_X for each spectrum. These values of K_x and the log β_{120}^* for $Al(Cal)_2$ determined as described above have been used to calculate values for β_{110}^* for the Al-gluconate complex. The average value was log $\beta_{110}^* = 13.96 \pm 0.09$.

The formal stability constants shown below for the Al-gluconate system have been reported by Motekaitis and Martell.[2]

$$\beta_{110} = \frac{[Al(glu)^{2+}]}{[Al^{3+}][glu^-]} = 10^{1.98} \qquad \text{Eq 5.15}$$

$$\beta_{11-1} = \frac{[Al(H_{-1}glu)^{+}][H^+]}{[Al^{3+}][glu^-]} = 10^{-0.89} \qquad \text{Eq 5.16}$$

$$\beta_{11-3} = \frac{[Al(H_{-3}glu)^{-}][H^+]^3}{[Al^{3+}][glu^-]} = 10^{-10.18} \qquad \text{Eq 5.17}$$

Motekaitis and Martell[2] did not report an experimental potentiometric titration curve for Al-gluconate. Therefore, the constants in Equations 5.15-5.17 were used with the program HySys to simulate the titration of a 1:3 ratio of Al^{3+}: gluconate, and the result is shown in Figure 5.10. The plot shows an inflection at 2 mmole base/mmole ligand. Since there are three moles of ligand per mole of Al^{3+}, this would correspond to six mmoles of H^+ per mmole of Al^{3+}. These can be accounted for as 3 mmoles of H^+ from the ligand and the release of 3 mmoles of H^+ due to the formation of the $Al(H_{-3}glu)^-$ complex. The curve in Figure 5.10 is similar to the forward titration curve in Figure 5.2, except that the experimental curve indicates the loss of additional H^+ ions above pH 8. This presumably reflects the hydrolysis of the $Al(H_{-3}glu)^-$ complex to $Al(OH)_4^-$.

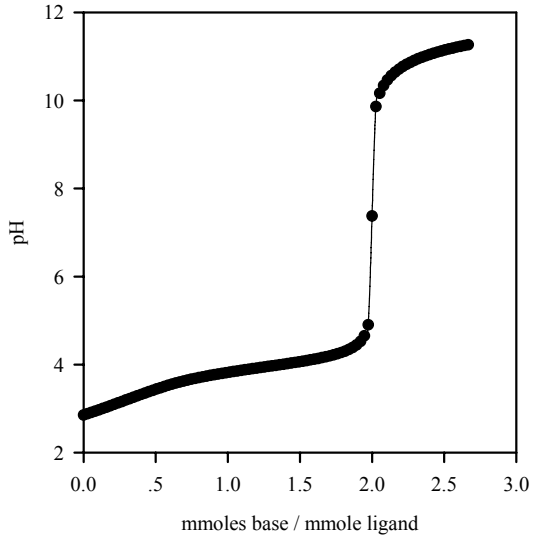

Figure 5.10 Simulated titration curve for a 1:3 ratio of Al^{3+}: gluconate based on the equilibrium constants reported by Motekaitis and Martell.[2]

The constants in Equations 5.15-5.17 have also been used to calculate the speciation of Al^{3+} in a 1:3 Al^{3+}:gluconate solution as a function of pH, as shown in Figure 5.11.

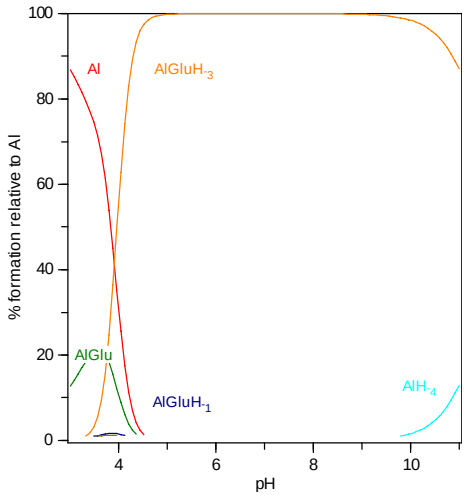

Figure 5.11 Species distribution diagram for a mixture of 2 mM Al^{3+} and 6 mM gluconate as a function of pH.

This analysis of the literature data established that at the experimental pH of 8 used in our spectrophotometric studies, the Al-gluconate would have been present entirely as the $Al(H_{-3}glu)^-$ complex. Therefore, an effective binding constant for gluconate at pH 8 can be calculated by using this hydrogen ion concentration with Equation 5.17, as shown below.

$$\beta^*_{110} = \frac{[Al-glu]}{[Al][glu]} = \frac{\beta_{11-3}}{[H^+]^3} = \frac{10^{-10.18}}{(10^{-8})^3} = 10^{13.82} \qquad \text{Eq 5.18}$$

This value of $10^{13.82}$ for the effective binding constant of Al-gluconate at pH 8 that is based on formal binding constants from the literature[2] compares very well with the experimental value of $10^{13.96}$ determine from our spectroscopic studies.

5.6 Potentiometric titration of Ca^{2+} with 2,2,2-THA and species distribution calculations for mixtures of 2,2,2-THA and calcium gluconate

The ability of 2,2,2-THA to remove Al^{3+} from clinical solutions of $Ca(gluconate)_2$ can be evaluated from speciation calculations for a mixture of 2,2,2-THA and gluconic acid. Commercial calcium gluconate contains 0.23 M Ca^{2+}, 0.46 M gluconic acid and 187 μM Al^{3+}. The binding constants of Ca^{2+} with both 2,2,2-THA and gluconate are needed for the speciation calculations. The Ca-gluconate binding constant of log β_{110} = 1.21 has been reported.[10]

A binding constant for Ca^{2+} with 2,2,2-THA has been determined by potentiometric titration. The potentiometric titration curve of Ca^{2+} with 2,2,2-THA is shown in Figure 5.12. Different models involving the 110, 111 and 11-1 complexes were

tested to fit the titration data. The model consisting of the 110 and 111 complexes gave the lowest GOF of 0.003. The stability constants of Ca-2,2,2-THA were determined to be log β_{110} = 3.71 $\pm$ 0.12 and log β_{111} = 13.34 $\pm$ 0.03.

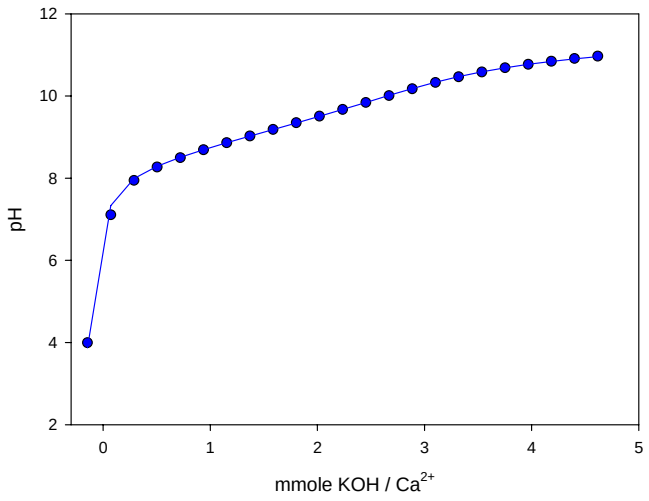

Figure 5.12 Potentiometric titration curve of Ca^{2+} with 2,2,2-THA. The symbols represent the observed data points while the line represents the least squares fit based on the ligand protonation constants and the stability constants, listed in Table 5.2.

System	i	j	k	reaction	log β_{ijk}	σ
2,2,2-THA	0	1	1	$L^{3-} + H^{+} = HL^{2-}$	10.26	
	0	1	2	$L^{3-} + 2H^{+} = H_2L^{-}$	19.68	
	0	1	3	$L^{3-} + 3H^{+} = H_3L$	28.15	
Ca-2,2,2-THA	1	1	1	$Ca^{2+} + L^{3-} + H^{+} = CaLH$	13.34 *	0.03
	1	1	0	$Ca^{2+} + L^{3-} = CaL^{-}$	3.71 *	0.12

Table 5.2 Variable (*) and fixed parameters for the least square refinement of the potentiometric titration data for Ca-2,2,2-THA.

These constants were used to calculate the speciation distribution shown in Figure 5.13 for the distribution of Al^{3+} in a solution of 2,2,2-THA and commercial $Ca(gluconate)_2$. These calculations included the protonation constants of 2,2,2-THA and gluconic acid, and the binding constants of Al-gluconic acid, Al-2,2,2-THA, Ca-gluconic acid and Ca-2,2,2-THA. At low pH, the 111 complex of Al-2,2,2-THA was predominant. Between pH 5 and 9, the 110 complex of Al-2,2,2-THA became the main species. The 11-3 complex of gluconate became the predominant species only above pH 9. These results show the strong binding of Al-2,2,2-THA at pH 2-10 in a mixture with $Ca(glu)_2$ and indicate that 2,2,2-THA should be able to completely sequester the Al^{3+} in commercial Ca-gluconate solutions.

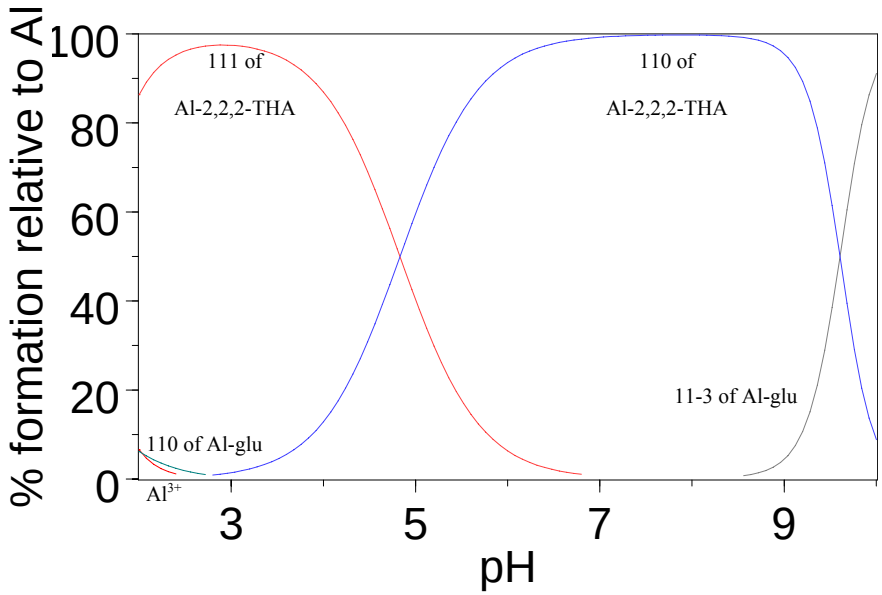

Figure 5.13 Species distribution diagram of 187 µM Al^{3+} in a mixture of 0.1 M 2,2,2-THA and 0.23 M $Ca(gluconate)_2$.

References

1. http://encyclopedia.thefreedictionary.com/gluconic+acid.

2. Motekaitis, R. J.; Martell, A. E. *Inorg. Chem*. 1984, 23, 18.

3. Li, H. B.; Feng, C. *Fresenius J. Anal. Chem*. 2000, 368, 501.

4. Chiv, C. K. V.; Haynes, D. H. *Biophys. J.* 1977, 18, 3.

5. Thomas, F.; Serratrice, G.; Bėguin, C.; Aman, E. S.; Pierre, J. L., Fontecave, M.; Laulhere, J. P. *J. Biol. Chem.* 1999, 274, 13375.

6. Ali, A.; Zhang, Q.; Dai, J.; Huang, X. *Biometals* 2003, 16, 285.

7. Brever, W.; Epsztejn, S.; Millgram, P.; Cahantchik, I. Z. *Am. J. Physiol.* 1995, 268, C1354.

8. http://probes.invitrogen.com/servlets/structure?item=481

9. Aikens, D. A.; Bahbah, F. J. *Anal. Chem.* 1967, 39, 646.

10. Martell, A.E.; Smith, R.M. NIST *Critical stability constants of metal complexes*, NIST Standard Reference Database 46, Version 5.0, 1998.

Chapter 6

Binding properties of hydroxamate ligands immobilized on a polystyrene resin

6.1 Introduction

Immobilization of chelating agents onto solid matrices has been known since 1948.[1] Because of the high selectivity offered by multidentate ligands toward metal ions, immobilized chelate-based absorbents have gained popularity in industry.[2] One type of application involves immobilized metal affinity chromatography. For example, a cation exchanger equilibrated with Al^{3+} ions was used to fractionate RNA,[3] while 8-hydroxyquinoline, covalently attached to an agarose support and complexed with Zn^{2+} ions, was used to isolate metalloproteins.[4] Chelex, a chelating resin with iminodiacetate groups, was utilized as a model for the surface of microbes and to study the adsorption of silicic acid to the aluminum ion.[5-6] Furthermore, iminodiacetic acid is the chelating agent of choice for covalent attachment either to a soft gel matrix such as cross-linked agarose[7] or to silica[8] for the complexation of borderline Lewis metal ions such as Cu^{2+}, Ni^{2+} or Zn^{2+}.

Chelating resins are ion exchange resins containing groups which are also able to complex metal ions, so that their sorption mechanism is primarily through chelation instead of simple ion exchange. A suitable resin enriched with a metal-chelating agent for chemical and biological applications should possess a high capacity for, and a favorable selectivity toward, the target metal ion, combined with high stability and rapid exchange kinetics. Most commercial resins exhibit a high capacity but poor selectivity.[2] As a result, studies on new functional groups are needed to develop a chelating resin that can remove traces of a hard metal ion such as Al^{3+} from clinical solutions.

As mentioned in Chapter 1, the primary clinical treatment for high levels of Al^{3+} ion has been chelation therapy with the trihydroxamate ligand desferrioxamine (DFO).

There are several research groups interested in the immobilization of specific chelators for hard metal ions on solid supports.[9-12] We have covalently linked 2,2,2-THA to a polystyrene resin and studied the ability of this resin to remove Al^{3+} from solutions. The final target will be removal of Al^{3+} contamination from commercial Ca-gluconate solutions.

6.2 Loading of 2,2,2-THA on the resin

A potentiometric titration of ~25 mg of resin containing covalently linked 2,2,2-THA is shown in Figure 6.1. The titration curve reflects the total protons that were titrated with KOH. This includes the sulfonic acid groups (-SO_3H), carboxylic groups (-COOH) and hydroxamic acid groups that are bound to resin. In principle, the sulfonic acid and carboxylic acid should not be present in the 2,2,2-THA resin. Free –SO_3H groups indicate an incomplete loading of the 2,2,2-THA onto the resin, and any –CO_2H groups would reflect the hydrolysis of hydroxamic acid groups. Both factors would decrease the chelating efficiency of the 2,2,2-THA resin.

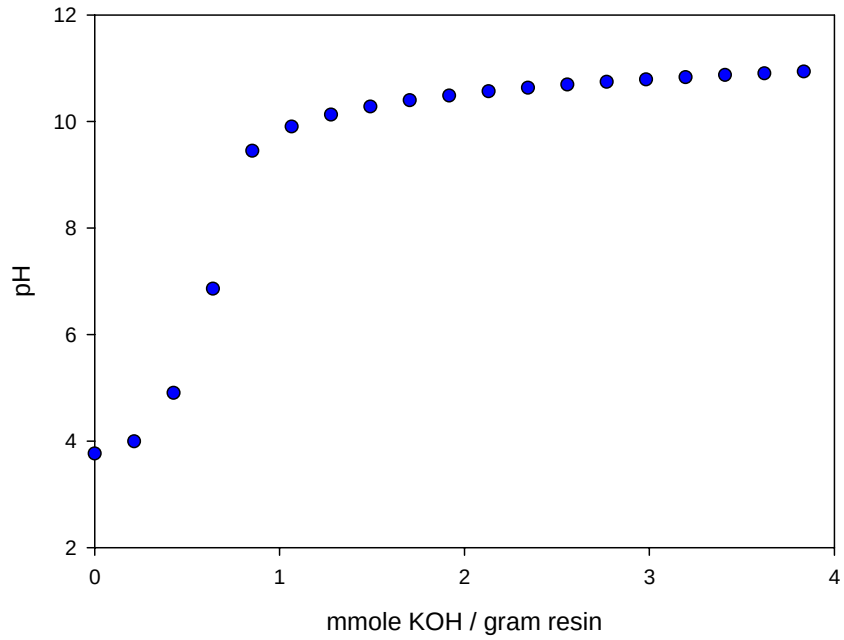

Figure 6.1 Potentiometric titration of the 2,2,2- THA resin.

The titration curve in Figure 6.1 shows a sharp inflection at 0.6 mmole KOH/gram resin, which reflects a total loading of sulfonated/carboxylate groups on the 2,2,2-THA resin of about 0.6 mmol/gram resin. The titration data beyond the inflection were analyzed to determine the apparent protonation constants for the immobilized hydroxamate groups. Three hydroxamate protonation constants were used as adjustable parameters in a least square refinement of the potentiometric titration data past the inflection. The mmoles of ligand bound to the resin was manually varied in these calculations. The best fit, with a GOF of only 0.0046, was obtained for a ligand loading of 0.30 mmole ligand/gram resin. An element analysis of the resin showed 1.14 mmole of nitrogen/gram resin. Since there are four nitrogen atoms per ligand molecule, the

elemental analysis corresponds to a ligand loading of 0.29 mmole ligand/gram resin, which is in good agreement with the results from the potentiometric titration.

The small number of mmoles of ligand associated with the titration sample size of 25 mg samples of resin made it difficult to study this system potentiometrically. Rather than use more resin, we shifted to spectroscopic studies of aluminum binding using the colorimetric indicator ferron. In addition, spectrophotometric studies are not directly affected by the presence of the unreacted $-SO_3H$ groups on the resin.

6.3 Spectroscopic studies of Al-ferron with EDTA

The UV-vis spectra of free ferron and a 1:1 ratio Al^{3+}:ferron are shown in Figure 6.2. Ferron has an absorbance maximum at 434 nm (ε = 1,267 M^{-1} cm^{-1}). The binding of Al^{3+} shifts this peak to 364 nm (ε = 3,267 M^{-1} cm^{-1}). Thus the visible spectra can be used to monitor the binding of Al^{3+} to ferron.

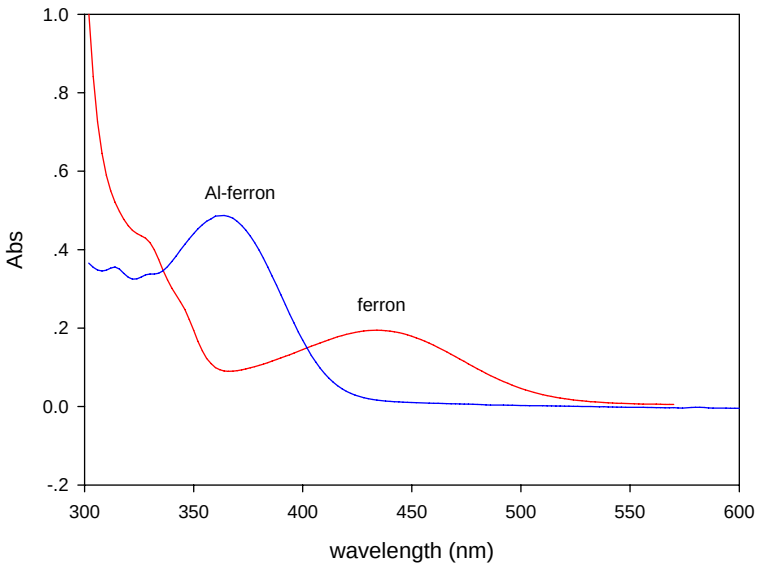

Figure 6.2 UV-vis spectra of ferron and a 1:1 ratio of Al and ferron at pH 5.

The strong chelating agent EDTA was added to the Al-ferron solution. As expected, the EDTA easily removed the Al^{3+} from the ferron and resulted in a smooth transition from the Al-ferron spectrum to the spectrum of free ferron, as shown in Figure 6.3. The removal of Al^{3+} from Al-ferron by EDTA took approximately 10 min, with an isosbestic point at 405 nm, as shown in Figure 6.3.

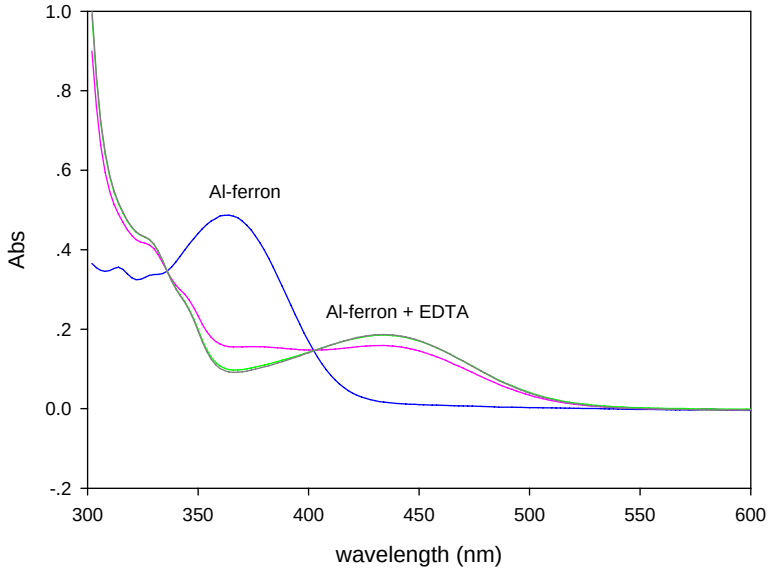

Figure 6.3 Kinetic studies on the transfer of Al^{3+} from ferron to EDTA (total time = 10 min).

6.4 Spectroscopic studies of ferron with the 2,2,2-THA resin

When the 2,2,2-THA resin was mixed with a solution of ferron, there was an increase in the absorbance below 350 nm that did not match the spectra of Al-ferron or free ferron, as shown in Figure 6.4. Fortunately, the characteristic band of ferron at 434 nm does not change upon addition of the resin. Since no Al^{3+} was involved in these

experiments, the changes below 350 nm were not related to Al-complexation. Thus in subsequent experiments on the exchange of Al^{3+} between ferron and the 2,2,2-THA resin, the absorbance changes below 350 nm have been ignored.

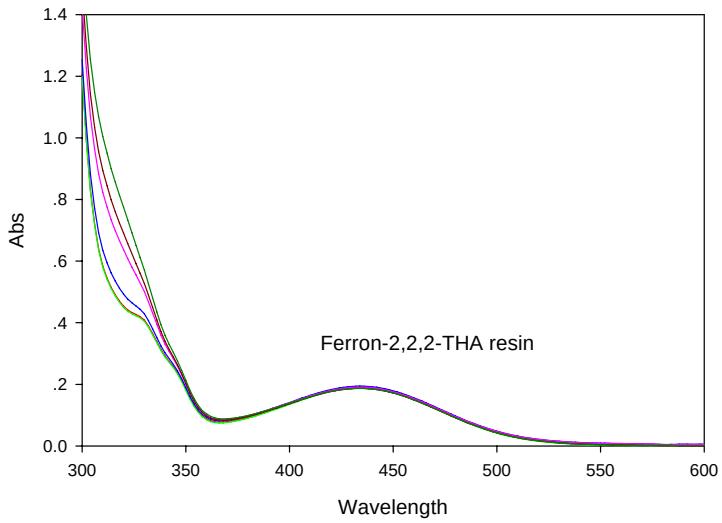

Figure 6.4 Spectra of a mixture of ferron and the 2,2,2-THA resin as a function of contact time, from t = 0 to t = 3 hrs.

6.5 Spectroscopic studies of Al-ferron with the 2,2,2-THA resin

A 1:1 mixture of 150 µM Al^{3+} and the chelating agent ferron was prepared and allowed to equilibrate, and then 20-25 mg of the 2,2,2-THA resin was added to the solution. The removal of Al^{3+} from the Al-ferron complex by the resin was indicated by the decrease in the absorbance band of the Al-ferron complex at 364 nm and the increase in the absorbance band of free ferron at 434 nm, as shown in Figure 6.5.

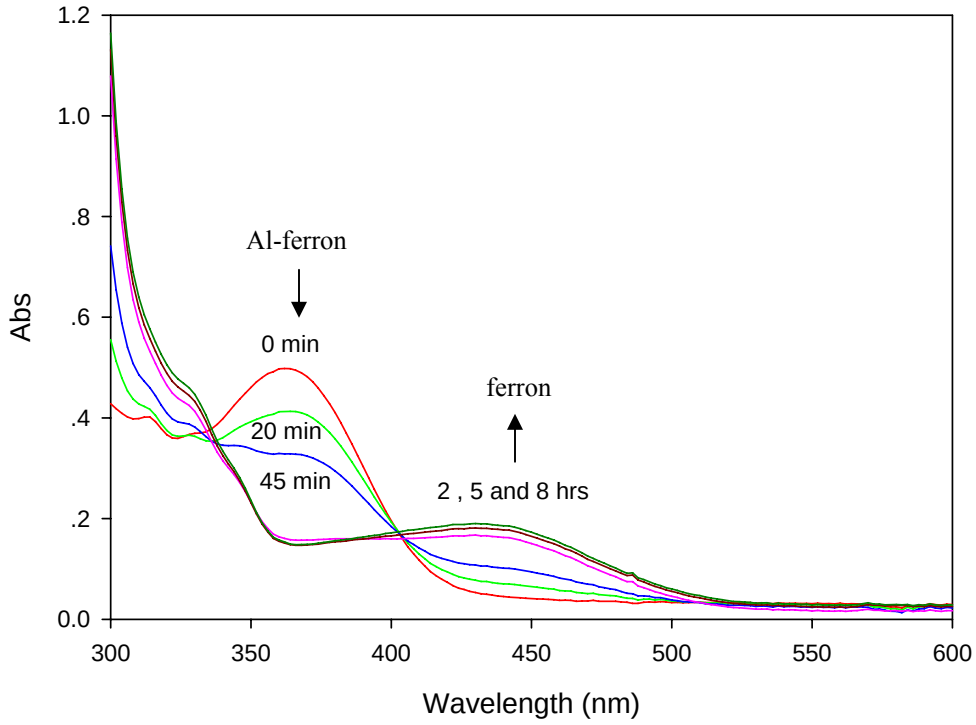

Figure 6.5 The removal of Al^{3+} from ferron by the 2,2,2-THA resin.

The final absorbance in Figure 6.5 represents an equilibrium distribution of the Al^{3+} between ferron and the resin. The fraction of Al^{3+} bound to the resin was calculated by comparing the final absorbance spectrum to that of the Al-ferron complex (Figure 6.2) and the mixture of resin and ferron with no Al^{3+} (Figure 6.4). The results showed that 78% of the Al^{3+} was bound to the 2,2,2-THA resin and only 22% was bound to ferron. An equilibrium model for the mixture of resin, Al^{3+} and ferron was constructed within the speciation software HySys. The model included literature values for protonation and Al-binding constants for ferron from the literature[13] and Al^{3+} hydrolysis constants[14] as fixed parameters. An effective "concentration" for the immobilized 2,2,2-THA was calculated

by dividing the total mmoles of 2,2,2-THA on the resin by the total sample volume. The three protonation constants for free 2,2,2-THA described in Chapter 3 were used as fixed parameters. A single binding constant for the immobilized ligand was entered as β_{110} and was manually varied until the speciation calculation matched the distribution of 78% Al-resin and 22% Al-ferron at pH 5. The result was log β_{110} = 19.18 for Al^{3+} binding to the immobilized form of 2,2,2-THA.

The predicted speciation of the mixture of resin and ferron as a function of pH is shown in Figure 6.6. The results indicate that the resin should bind essentially 100% of the Al^{3+} between pH 6 and 9. Above pH 9, hydrolysis to form $Al(OH)_4^-$ begins to compete with binding to the resin. The speciation calculations below pH 5 should be interpreted cautiously, since it was not possible to include a 111 complex of the immobilized 2,2,2-THA in these calculations.

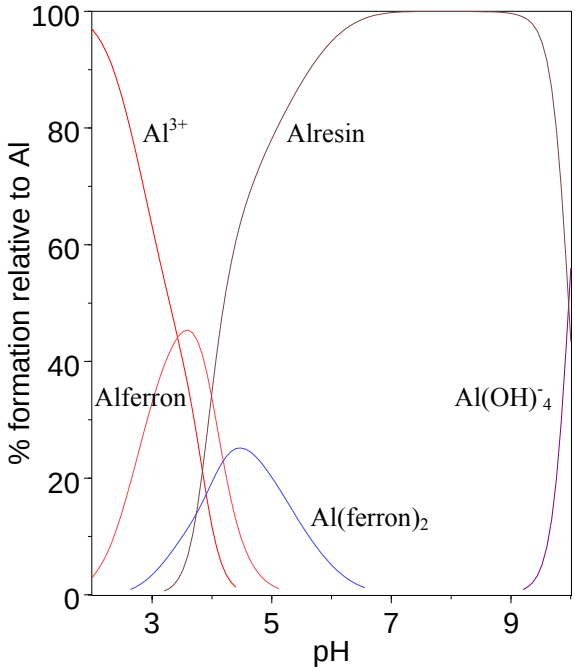

Figure 6.6 Species distribution diagram of Al^{3+} in a solution of ferron and the 2,2,2-THA-resin at pH 2-10.

Another method used to study the binding of Al^{3+} to the 2,2,2-THA resin was atomic absorption spectrometry (AAS) performed in the Yokel laboratory at the University of Kentucky Medical center. This method was used to directly measure the concentration Al^{3+} in a solution in equilibrium with a suspension of the resin. In these experiments, the chelating agent EGTA (ethyleneglycolbis(2-aminoethylether)-N,N,N'N'-tetraacetic acid) was used in competition with the resin to give a reasonable distribution of the Al^{3+} between the resin and the aqueous phase. These experiments gave a value of $\log \beta_{110} = 19.0$ as the apparent binding constant for the immobilized 2,2,2-THA, which is in excellent agreement with the value from the spectrophotometric competition studies with ferron.

The goal of these studies is to remove Al^{3+} from the commercial solutions of Ca^{2+} gluconate that are used to prepare TPN solutions, so it is necessary to study the chelating resin in competition with gluconate solutions. Atomic absorption spectrometry was also used to study the removal of Al^{3+} from solutions of calcium gluconate. The results showed that the immobilized 2,2,2-THA did not bind the Al^{3+} strongly enough to completely remove this ion from the gluconate solution.

Figure 5.13 showed the results of speciation calculations for Al^{3+} in a calcium gluconate solution based on the values of $\log \beta_{111} = 26.27$ and $\log \beta_{110} = 21.44$ for Al^{3+} binding to the free 2,2,2-THA molecule. This speciation calculation clearly showed that 2,2,2-THA should be capable to removing Al^{3+} from gluconate solutions. However, the immobilized 2,2,2-THA shows a smaller Al binding constant of $\log \beta_{110} = 19$. This decrease of 2.4 log units in the binding affinity for the immobilized ligand seriously diminishes the ability of the resin to remove Al^{3+} from the gluconate solutions.

References

1. Meinhardt, J. E. *Science* 1948, 110, 387.

2. Sahni, S. K.; Reedijk, J. *Coord. Chem. Rev.* 1984, 59, 1.

3. Shankar, V.; Joshi, P. N. *J. Chromatogr.* 1974, 90, 99.

4. Everson, R. J.; Parker, H. E. *Bioinorg. Chem*. 1974, 4, 15.

5. Zachariou, M.; Hearn, M. T. *Biochemistry* 1996, 35, 202.

6. Aramaki, Y.; Yokoyama, T.; Okaue, Y.; Watanabe, K. *Chemical Geology* 2004, 212, 339.

7. Porath, J. *J. Mol. Recognit*. 1990, 3, 123.

8. Wirth, H. J.; Unger, K. K.; Hearn, M. T. W. *Anal. Biochem*. 1993, 208, 16.

9. Anthone, S.; Ambrus, C. M.; Kohli, R.; Min, I.; Anthone, R.; Stadler, A.; Stadler, I.; Vladutiu, A. *J. Am. Soc. Nephrol*. 1995, 6, 1271.

10. Ambrus, C.M.; Stadler, I.; Toumbis, C. A.; Constantine, A.; Stadler, A.; Anthone, S.; Anthone, R.; DeAlarcon, P.; Deshpande, G.; Conway, J.; Vladutiu, A. O.; Ambrus, J. L. *J. Med. (Westbury, New York)* 1999, 30, 211.

11. Breuer, W.; Ronson, A.; Slotki, I. N.; Abramov, A.; Hershko, C.; Cabantchik, Z. I. *Blood* 2000, 95, 2975.

12. Yehuda, Z.; Hadar, Y.; Chen, Y. *J. Plant. Nutrit.* 2003, 26, 2043.

13. Goto, K.; Taguchi, S.; Miyabe, K.; Haruyama, K. *Talanta* 1982, 29, 569.

14. Baes, C. F.; Mesmer, R. E. *The hydrolysis of cations*, Wiley and Sons, New York, 1967.

Chapter 7

Conclusions

A high percentage of premature neonates require intravenous feeding or total parenteral nutrition (TPN). These infants are at high risk of Al^{3+} toxicity because some of the TPN component solutions, in particular the Ca-gluconate solution, are contaminated with Al^{3+}. Therefore, we have conducted studies on a chelating resin with a new hydroxamate ligand that could be used in an in-line filter to remove Al^{3+} from Ca gluconate solutions.

The complexation of Al^{3+} with a new series of hydroxamate ligands, 2-HA, 2,2-DHA and 2,2,2-THA, was studied by potentiometric titration. At lower pH, both 2,2,2-THA and 2,2-DHA form bis(hydroxamate) complexes. The stability constants of these bis(hydroxamate) complexes were consistent with literature data on other dihydroxamate ligands. At higher pH, the third arm of 2,2,2-THA deprotonates and coordinates to form the tris(hydroxamate) complex of Al^{3+}. Spectrophotometric studies on the complexation of Fe^{3+} with 2,2,2-THA also showed the formation of bis(hydroxamate) and tris(hydroxamate) complexes.

A linear free energy relation (LFER) was plotted to compare the binding constants of bis(hydroxamate) and tris(hydroxamate) complexes with Al^{3+} and Fe^{3+}. For the bis(hydroxamate) complexes, the stability constants of both metal ions are consistent with other dihydroxamate ligands. The stability constants for the tris(hydroxamate) complex of 2,2,2-DHA also fell on the regression line of the LFER, indicating the same binding mode for both Al^{3+} and Fe^{3+}. However, the stability constants for Fe^{3+} and Al^{3+} with 2,2,2-THA are significantly lower than those for DFO. This suggests that steric stain hinders the formation of the tris(hydroxamate) complexes of 2,2,2-THA with both metal ions. Therefore, future studies will evaluate variations in the structure of 2,2,2-THA to

reduce the steric stain.

The selectivity of these hydroxamate ligands for trivalent ions relative to divalent metal ions was evaluated by measuring the binding constants of 2,2,2-THA and 2,2-DHA with a series of divalent metal ions. The results indicate that 2,2,2-THA is very selective for trivalent metal ions over divalent metal ions. Thus we should be able to target trivalent metal ions such as Al^{3+} with little interfere from divalent metal ions.

To evaluate the ability of 2,2,2-THA to remove Al^{3+} from commercial Ca-gluconate solutions, the binding constants of Al-gluconate and Ca-2,2,2-THA were also measured. Potentiometric titration samples of Al-gluconate required very long equilibration times. Because of concerns about the long-term stability of the pH electrode calibration, a new spectrophotometric method using the ligand calcein was developed to study this system. This method gave a Al-gluconate binding constant that agreed with literature data on this system. The binding of Ca by 2,2,2-THA was studied by potentiometric titration, and the results confirmed the low affinity of 2,2,2-THA for Ca^{2+} compared to Al^{3+}, indicating very good selectivity for Al^{3+} over Ca^{2+}. These binding constants were incorporated into speciation calculations, which indicated that free 2,2,2-THA should be able to remove Al^{3+} from a commercial solution of Ca-gluconate.

A new chelating resin was prepared by linking 2,2,2-THA to a polystyrene resin, and the ability of this resin to reduce the Al^{3+} contamination in a Ca-gluconate solution was evaluated. It appears that the Al stability constant of 2,2,2-THA bound to the resin is about 1.4 log units less than that of the free ligand. This decrease in the binding constant shifts the competition for Al^{3+} in the Ca-gluconate solution, so that this proposed resin is less effective than expected. Therefore, future studies are planned to produce new resins

that avoid this loss in stability by using longer tethers to link the ligand to the resin.